CHAPTER 9

RELATIONSHIP BETWEEN STRUCTURE AND MECHANICAL PROPERTIES IN PA6 REINFORCED NANOCOMPOSITES

In this chapter an attempt is made to explain the mechanical properties of PA6 - reinforced MFCs relating them to their structure. As in previous studies with the pure polyamides in this thesis, WAXS and SAXS from synchrotron were extensively used as analytical techniques complemented by ^{13}C solid state NMR. From the four composite types whose mechanical properties were considered in Chapter 8, the UDP MFCs were selected for further investigations because of the following reasons. First, these composites displayed the best mechanical properties within the whole studied range of HDPE/PA6/YP concentrations. Second, the micromechanics of the UDP lamina obeys simple additive models such as the rule of mixtures, RM, which allows the calculation of theoretical values of longitudinal Young's modulus, E_1 and longitudinal stress, $\sigma_{1\max}$, that can afterwards be compared to the experimental ones. Third, the fact that the UDP systems are reinforced by long, parallel PA6 micro- and nanosized fibrils makes them very suitable to study by X-ray scattering with 2D detection. Last but not least, the effect of the compatibilizer upon the tensile properties was most clear in UDP MFCs.

In Chapter 3 and 4 it was established that the crystalline structure of PA6 has an important influence upon its mechanical properties. That is why the investigations on the relationship between the structure and mechanical properties of MFCs were started with determining the crystalline modification in the PA6 reinforcing phase. It became clear that in PA6 the two polymorphs α and γ always co-exist, being in various relations depending on the concrete conditions. That is why the structural investigations started by studying the polymorphism of PA6 in the final UDP MFC.

9.1. Crystalline structure of the PA6 reinforcing phase

A qualitative evaluation was first made by ^{13}C CP-MAS NMR spectra of some HDPE/PA6/YP MFCs at 20°C (Figure 9.1). In both non-compatibilized (Fig. 9.1 a) and compatibilized (Fig. 9.1 b) MFCs there exist resonance lines above 40 ppm characterizing the carbon nuclei next to the amide N atom in α-PA6. The same signal appears in stronger field in the γ PA6 polymorph, which indicates that in both compatibilized and non-compatibilized MFCs the PA6 is predominantly in α crystalline modification.

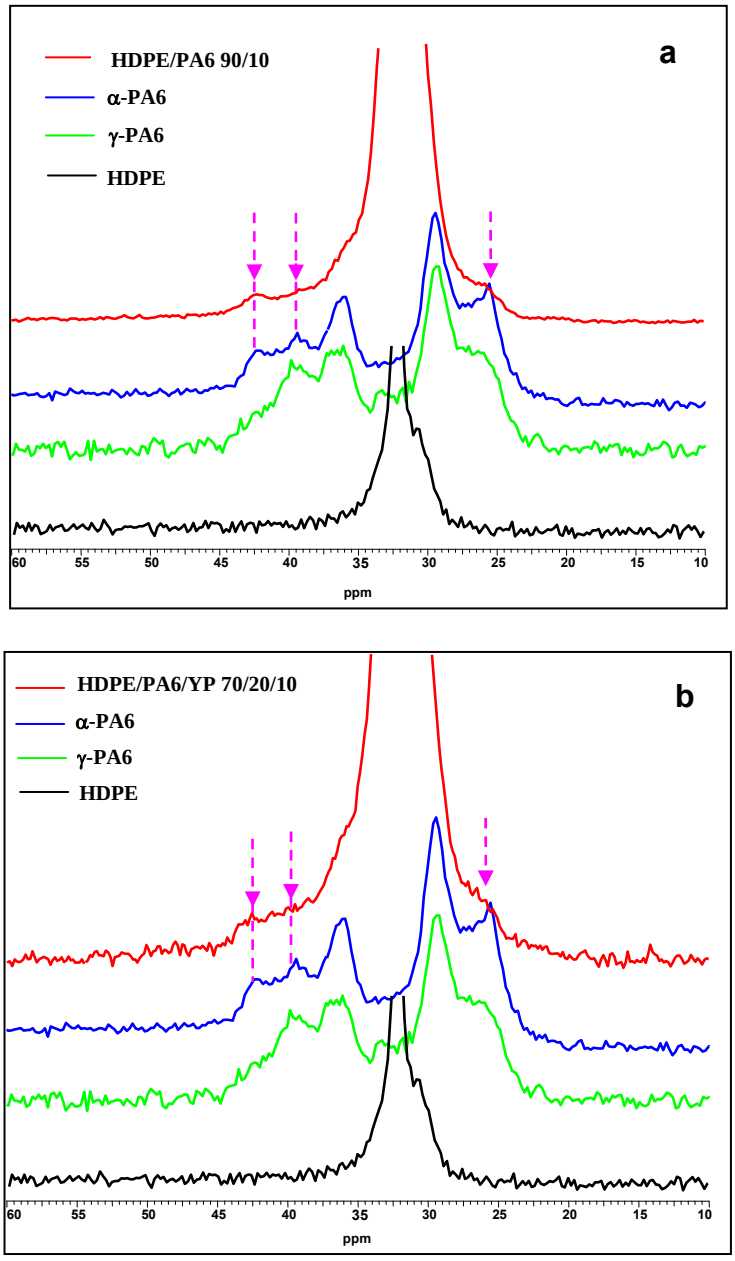

Figure 9.1 CP-MAS ^{13}C NMR spectra of two HDPE/PA6/YP MFCs at 20°C: (a)non-compatibilized 90/10/0 and b – compatibilized 70/20/10 system. To enable comparison, the figures contain also the traces of neat HDPE, α- and γ PA6.

For quantification of the polymorph content, the synchrotron WAXS patterns of the MFCs were used. As seen from Figure 7.6, the 2D WAXS at 30°C display the existence of oriented crystalline material. However, it was quite difficult to evaluate the crystalline structure of PA6 in the MFC at 30°C because of the overlapping of too many reflections appearing in the 18-24° 2θ range: (200) and (002/202) of α monoclinic PA6; (001) and (200) of γ pseudo hexagonal PA6 and (110) and (200) reflections of orthorhombic HDPE. Thus, we used the WAXS patterns at 160°C where the HDPE matrix is molten

applying the following data processing (Figure 9.2). First, the image was calibrated, background corrected and sector integrated between the dashed lines (from 60 to 120° in respect to the horizontal fiber axis). This cut will supposedly reveal the scattering of the above-mentioned planes of the oriented PA6 plus the amorphous halos of HDPE and PA6. To eliminate the latter, additional sector integration was performed of the same image within the solid lines (from -30 to 30°) and subtracted from the first one. This procedure was denoted as Method I Image Integration. The resulting curve was treated with peak-fitting software as described in the Experimental part. The fit for the 80/20/0 MFC is presented in Figure 9.3 (a).

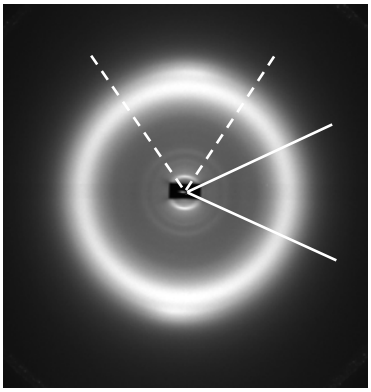

Figure 9.2 2D WAXS pattern at 160°C of the 80/20/0 MFC system explaining he integration routines. The solid lines denote the interval between -30 and 30° in respect to the horizontal fiber axis and the dashed lines from 60 to120°. The fiber axis is horizontal

Judging from Figure 9.2 it can be supposed that PA6 is in its α-crystalline modification. Thus, fits with two Gaussian peaks for monoclinic α-PA6 were made initially.

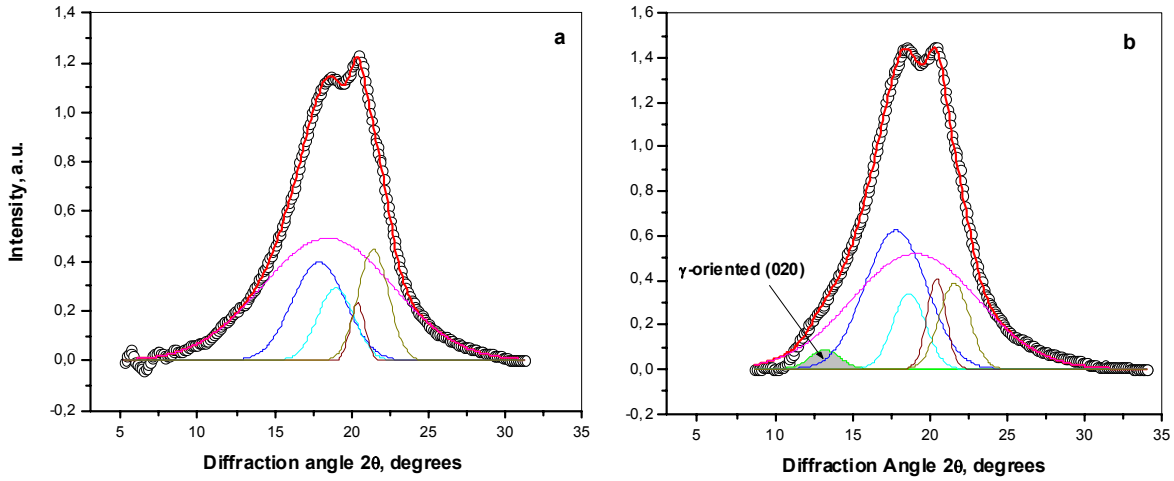

Figure 9.3 WAXS pattern at 160°C of PA6 phase in UDP MFC 80/20/0 after elective subtraction of the HDPE pattern according to: a- method I; b – method II.

Better fits were obtained when two additional peaks for the γ form were introduced, which was in good agreement with the previously established co-existence of the two polymorphs. Thus, the presence of oriented γ PA6 was assumed at 160°C. If this is true, however, a scattering for 0k0 reflections should appear at the meridian (*i.e.*, along the horizontal fiber axis), which cannot be assessed by Method I. Therefore, another procedure for image integration was applied to verify the presence of 0k0 reflections: after calibration and background correction, the image was integrated within the whole range of scattering angles; then, sector integration was performed from -15° to 15° azimuthal angles; finally, subtraction of the second integration curve from the first one was made. The fit of the resulting curve is shown in Figure 9.3 b. There is a small scattering peak (ca. 2%) at 2θ = 13.5°, which can be attributed to the (020) plane of the oriented γ PA6. It should be mentioned, however, that in the second integration procedure a part of the HDPE halo cannot be eliminated thus complicating the treatment of the WAXS data. For this reason, Method I was applied further on to process the rest of the WAXS images collected at 160°C taking into account that the real γ form content would be slightly higher. Table 9.1 summarizes the data from peak-fitting for all HDPE/PA6/YP UDP MFCs at 160°C.

Table 9.1 PA6 polymorph content in various HDPE/PA6/YP MFCs at 160°C

Composition HDPE/PA6/YP wt. %	Vol. fract. of PA6, V_f	α - form %	γ- form , %	γ/α	ECI, %
90/10/0	0.084	21.2	22.7	1.07	43.9
80/20/0	0.171	30.7	12.3	0.40	43.0
70/20/10	0.171	24.0	22.2	0.93	46.2
75/20/5	0.171	23.9	19.5	0.82	43.4
77.5/20/2.5	0.171	29.9	18.0	0.60	47.9
65/30/5	0.261	27.7	13.5	0.49	41.2
0/100/0* or	-	24.0	24.0	1.00	48.0

Notes:
ECI = equatorial crystallinity index. ECI = αECI + γECI; αECI = α(200) + α(002/202);
γECI = γ(001) + γ(200)
*Value taken from Chapter 3, figure 3.6 (b).

Table 9.1 gives information about the degree of crystallinity and its polymorph content. In all compositions PA6 represents a mixture of the two polymorphs. The content of the α-polymorph is the biggest in the 80/20/0 composite and the smallest (approximately 1:1) in 70/20/10 and 90/10/0

systems. The degree of crystallinity of the PA6 fibrils varies in the range from 41 to 48% and corresponds, in general, to the ECI of the neat oriented PA6 at the same temperature.

The crystalline structure of PA6 is important but it is not the only factor influencing the effectiveness of the reinforcement. It was shown in the previous chapter that all UDP systems possess better tensile properties as compared to HDPE, *i.e.*, the long PA6 fibrils effectively reinforce the matrix. Furthermore, the difference between the real E_1 and $\sigma_{1\max}$ values and those calculated according to the rule of the mixture was in favor of the former only in the absence or at very low concentrations of YP. In other words, without YP the reinforcement in the UDP MFCs cannot be attributed only to the simple presence of the fibrous PA6 phase but to some additional interaction, most probably physical, since it is better expressed in the non-compatibilized systems.

Based on the general scheme of MFC preparation (Chapter 2), it can be supposed that after the matrix isotropization stage the final composite will contain fibrilar reinforcement phase embedded in a fully isotropic matrix. The fibrilar morphology of UDP MFCs was undoubtedly proved by SEM in Chapter 7. The first examination of the 2D SAXS patterns in the same chapter showed that the UDP MFCs contains oriented material whose orientation coincides with the draw direction. It can be supposed that this material is PA6, which maintains its fibrilar morphology during the isotropization stage. However, the respective small-angle scattering appears very close to the beamstop with long spacings above 200 Å, which is much larger than the L_B values of the PA6 – typically between 60 and 80 Å. Consequently, it can only be a fraction of the HDPE matrix material crystallized upon the oriented PA6 fibrils thus forming a transcrystalline layer (TCL) at the interface. This TCL certainly affects the mechanical properties of the respective HDPE/PA6/YP composites.

9.2. Transcrystallization in fibril reinforced composites – a brief overview

In general, the mechanical properties of fiber-reinforced polymer composites are dependent upon the following three factors: (1) strength and modulus of the fiber, (2) strength and modulus of the matrix, and (3) effectiveness of the transfer of stress between fiber and matrix [1]. The last factor is closely related to the nature of interactions at fiber/matrix interface that could be realized by either chemical bonds or through boundary layers. In fibrous composites, formation of columnar crystalline layers with limited thickness composed of matrix material that grows upon the fiber is frequently observed. This phenomenon was called transcrystallinity [2,3]. The studies on transcrystallinity in conventional

polymer composites are vast. In their recent review on the subject Quan et al [4] discuss a number of issues related to the formation and growth of transcrystalline layers (TCL): crystallinity of the matrix, mismatch of thermal coefficients of the fiber and the matrix, epitaxy between the fiber and the matrix, surface toughness, thermal conductivity, treatment of fiber, etc. Processing conditions such as cooling rate, temperature, interfacial stress were also found to be important. Irrespective of the numerous existing studies performed in a great variety of fiber/matrix systems, the formation and growth mechanisms of transcrystallinity are not yet fully understood [4]. The reports about the influence of transcrystallinity and the formation of transcrystalline layers upon the mechanical properties of the conventional polymer composites are quite controversial – from clear improvement through no effect or even a strong negative effect. This is an indication that the transcrystallinity phenomenon is probably too specific for each fiber/matrix system and do not allow for generalizations. Nevertheless, there exist an agreement in the literature that in conventional composites the orientation distribution of the polymer chains in the transcrystalline layer will determine the nature and extent of its effect on the properties of the composite material [5].

There exist a limited number of studies on the occurrence of transcrystallinity in MFCs. Li et al. [6-8] studied the crystal morphology of PET/iPP in-situ MFC, prepared by a slit extrusion-hot stretching-quenching process, and found that transcrystallinity occurred around the PET in-situ microfibrils. The authors propose different nucleation mechanisms related to the external field applied to explain this form of crystallization. MFCs obtained in-situ from LDPE matrix reinforced by PET microfibrils (PET/LDPE = 1:1)[9] were processed under industrially relevant conditions via injection molding. By means of TEM the formation of transcrystalline layers of LDPE matrix on the surface of the PET microfibrils was observed. In these layers the crystalline lamellae were aligned parallel to each other and were placed perpendicularly to the fibril surfaces. This was in contrast to the bulk matrix where the lamellae were quasi - randomly arranged. An interesting observation was made in PET/PA12 MFCs [10,11]. The PET microfibrils were not only effective nuclei for the PA12 molecules, but also caused their reorientation by 90° with respect to their initial direction: from parallel to the main chain direction of PET molecules in the oriented precursor to perpendicular in the MFCs. Such crystallization with reorientation was reported for the first time. It can be concluded that although transcrystallization is observed in some MFC systems, as yet this phenomenon is far from being completely understood and its relation to the mechanical properties of the MFCs is not clearly outlined.

In general, synchrotron WAXS and SAXS are usually employed for structural investigations of transcrystallinity. However, it should be noted that its study in MFC systems is not a straightforward procedure. It is due to the fact that the reinforcing phase here is not an inorganic material (e.g. CF, GF). Both the matrix and the reinforcements in the MFC (as in this work) can be semicrystalline polymers with similar crystallographic characteristics. Moreover, the nature of the MFCs requires that the reinforcement should have higher melting temperature, thus it will be problematic to eliminate the reflections of the reinforcements and study the nanostructure of the matrix. Therefore, it is necessary to investigate transcrystallinity in each particular combination of matrix and reinforcing polymers.

9.3. Transcrystallization of HDPE in the presence of oriented PA6

To study the transcrystallization of the matrix in the HDPE/PA6/YP UDP MFCs synchrotron WAXS and SAXS were used. The conditions common for all experiments are given in Chapter 2. Some specific details about image processing will be explained in the course of the present discussion.

9.3.1. 2D WAXS analysis

The visual inspection of the 2DWAXS patterns of UDP MFCs (Figure 7.6) shows the co- existence of isotropic Debye rings and crystalline reflections oriented parallel to the draw direction. To separate the contribution of the isotropic and oriented crystalline fractions and to study their origin, the following procedure was adapted [12]. The 2D WAXS patterns were first corrected for the incident beam intensity and then the empty chamber scattering was subtracted. It was assumed that the total scattered intensity could be separated into two contributions: (i) the isotropic contribution from the amorphous chains and the unoriented crystals, being directly proportional to the azimuthally independent component of the total scattered intensity and (ii) the oriented contribution from all oriented (with varying degree of orientation) scatterers calculated by subtracting the azimuthally independent component from the total scattered intensity. To determine the azimuthally independent intensity and to perform the said subtraction, a subroutine incorporated into the POLAR 2.7.1 X-ray software was used [13]. Figure 9.4 exemplifies this treatment for the 80/20/0 (a) and 70/20/10 (b) HDPE/PA6/YP UDP MFCs showing the starting real 2D WAXS patterns (left), the computer-generated isotropic part of the scattered intensity (center) and the resulting 2D WAXS images of the oriented part after subtraction (right).

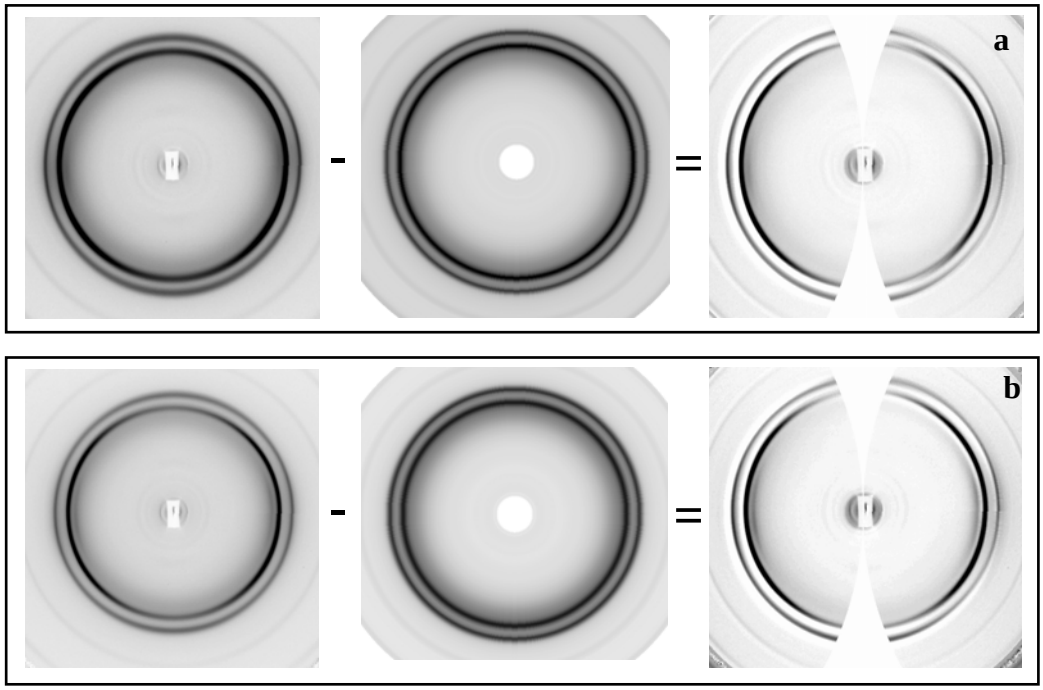

Figure 9.4 Example of the analysis of the WAXS patterns at 30°C of UDP MFCs: Left – total scattered intensity; Center: calculated isotropic intensity; Right: oriented scattered intensity. (a) - 80/20/0 and (b) - 70/20/10. The fiber axis is vertical.

Subtracting the isotropic crystalline and amorphous fractions allows the outlining of the oriented crystalline reflections that are otherwise undetectable. Together with the expected oriented PA6 reflections in the right images in Figure 9.4, one observes also clear reflections of the oriented matrix. The two weak equatorial arcs belong to the (200) and (002/202) planes of PA6 and the other two, more intense equatorial reflections belong to the (110) and (200) planes of orthorhombic unit cell of HDPE. This is an indication for epitaxial crystallization of matrix material upon the reinforcing fiber, whereby the chain direction in the matrix crystals coincides with that in the reinforcing PA6 fibrils. Judging from Figure 9.4, this observation is valid for both selected samples – non-compatibilized (a) and compatibilized (b). Figure 9.5 shows the 3D images of the real WAXS patterns before treatment (left) and of the oriented scattering after subtracting (right) of the same two MFCs. The white arrows indicate the position of the α-PA6 (200) reflection. This representation shows better the anisotropy of the HDPE (110) and (200) diffractions.

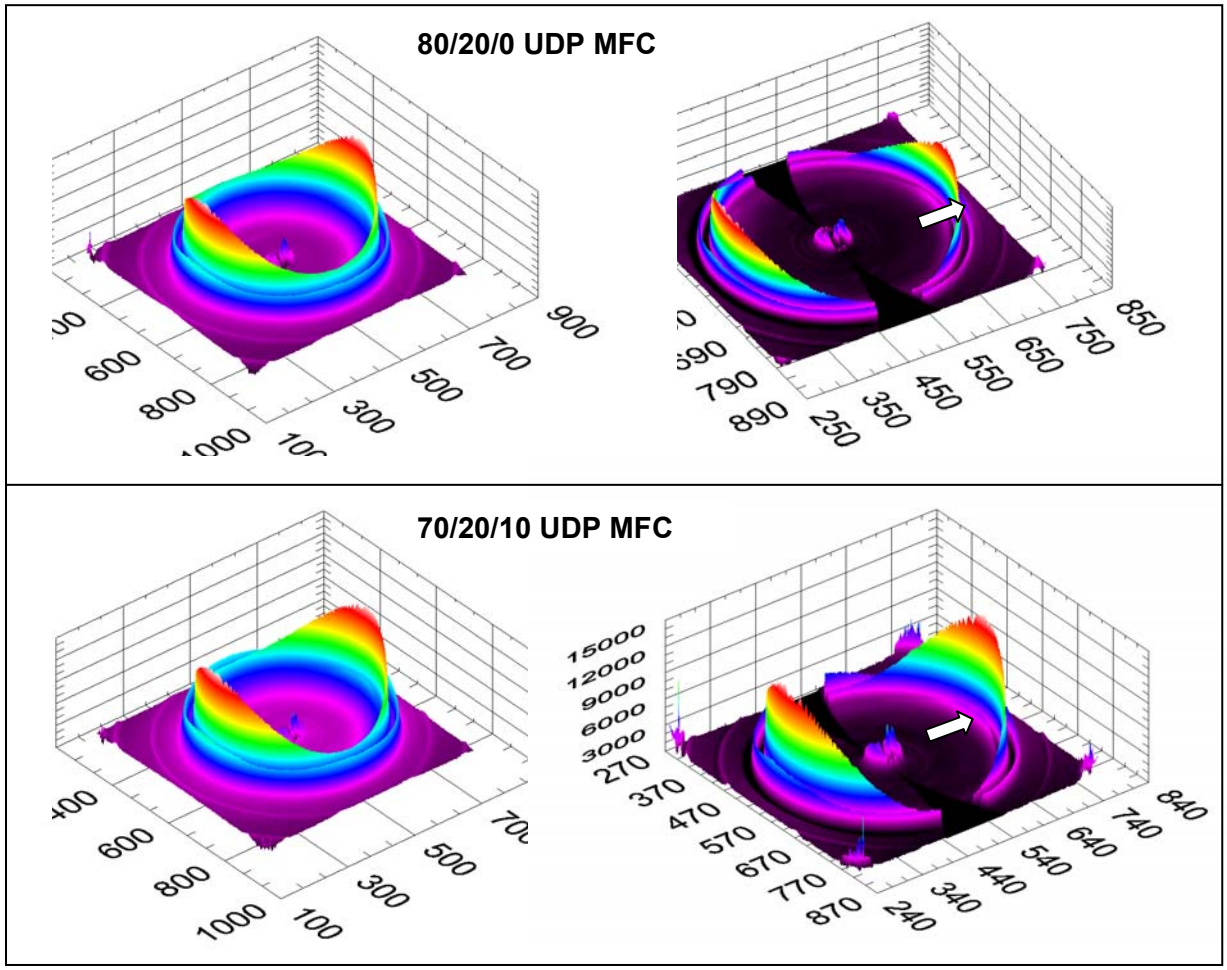

Figure 9.5 3D WAXS patterns of UDP MFCs before (left) and after (fight) the subtraction of the azimuthally independent component of the total scattered intensity. The white arrows point at the (200) reflection of α PA6.

For a quantitative evaluation of oriented and isotropic parts of the total scattered intensities, the respective 2D WAXS patterns were integrated in the 0-180° range to get the 1D WAXS profiles, which were afterwards fitted by Gaussian peaks. The results from peak-fitting applied in the 80/20/0 MFC sample are presented in Figure 9.6 (a) and (b). The deconvolution of the integral profile of the oriented part clearly shows the (110), (200) and (210) contributions of the HDPE (Fig. 9.6 a, the shaded reflections)) and also the four crystalline reflections of α- and γ PA6. The peak-fitting of the isotropic part displayed crystalline reflections (110), (200) and (210) of the HDPE matrix only and the amorphous halos of PA6 and HDPE, respectively (Figure 9.6, b). Based on the angular position of the reflections, the d-spacings (d_{hkl}) of the corresponding planes were calculated. Similar treatment was performed with the 2D WAXS images of all PA6 reinforced UDP MFCs collected at 30°C. A quantitative evaluation of the peak-fitting results for two representative MFCs - without (80/20/0) and with compatibilization (70/20/10), as well as data for d-spacings are given in Table 9.2.

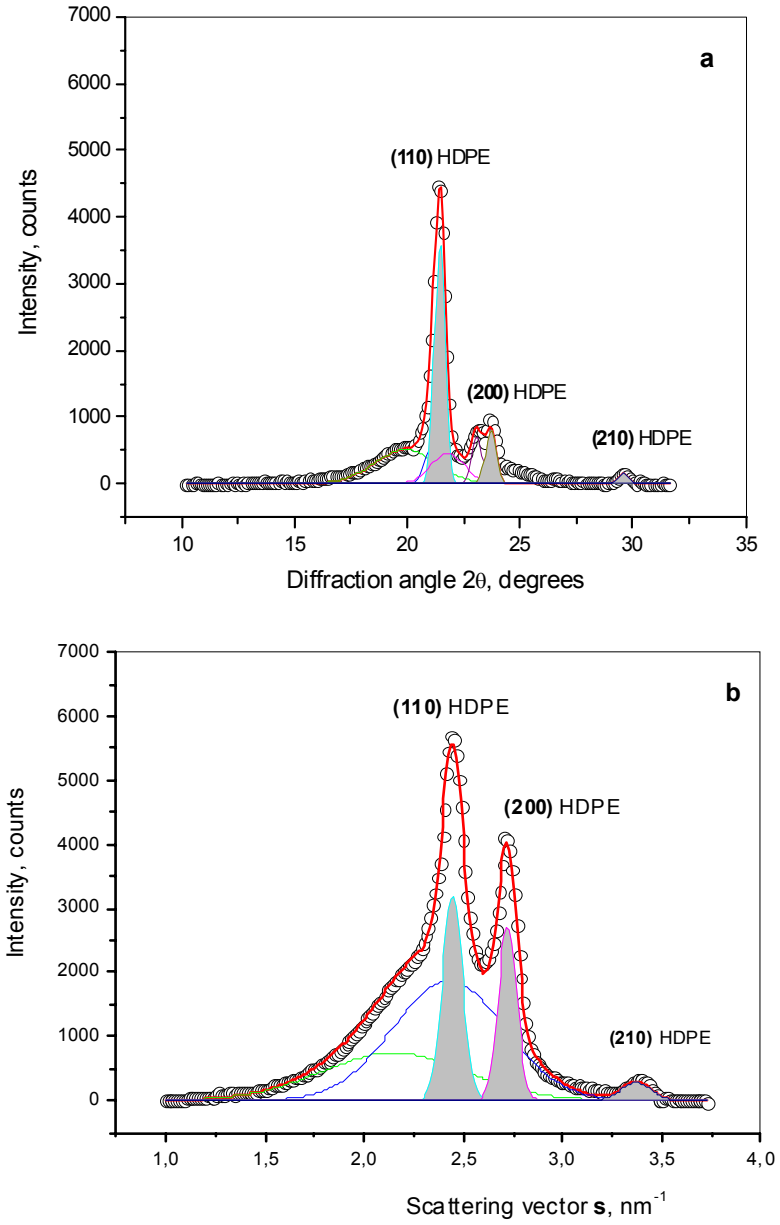

Figure 9.6 1D WAXS profiles of the 80/20/0 HDPE/PA6/YP UDP MFC exemplifying the peak-fitting of the oriented scattering (a) and of the isotropic WAXS scattering (b). The pattern in (a) was obtained after subtracting of (b) from the initial WAXS pattern with the total scattered intensity.

From Figure 9.6 and Table 9.2 it can be seen that a significant part of the HDPE matrix is able to crystallize oriented along the PA6 fiber thus forming a transcrystalline layer in such a way that the chain directions of the two polymers coincide. The rest of the matrix, situated in the bulk, crystallizes isotropically. The relation between the content of the PA6 fibrils and the oriented part of the HDPE matrix (the crystalline fraction) is almost 1.0:1.0 in the 70/20/10 MFC and 1.3:1.0 in the 80/20/0 system. This means that in the presence of compatibilizer a larger part of the HDPE is included in the

transcrystalline layer without changing considerably its crystallographic characteristics. Based on the d-spacing values it can be concluded that the HDPE unit cell is slightly larger in the bulk, as compared to that in the transcrystalline layer.

Table 9.2 Results from the deconvolution of the oriented and isotropic part of 2D WAXS patterns of selected HDPE/PA6/YP UDP MFC

WAXS Reflections	HDPE/PA6/YP					
	80/20/0			70/20/10		
	2θ, deg.	Content, %	d_{hkl}, Á	2θ, deg.	Content, %	d_{hkl}, Á
Oriented part of WAXS intensity						
(200) – α PA6	19.90	28.5	4.34	19.92	28.7	4.34
(001) – γ PA6	21.05	6.6	4.11	21.35	7.6	4.07
(110) – HDPE	21.44	34.9	4.03	21.33	38.2	4.05
(200) – γ PA6	21.79	13.7	3.97	21.66	7.6	3.99
(002)/(202) – α PA6	23.09	6.9	3.75	22.99	6.9	3.76
(200) – HDPE	23.69	7.9	3.65	23.74	9.1	3.65
(210) – HDPE	29.61	1.5	2.94	29.50	1.9	2.95
PA6 fraction, %		55.7			50.8	
HDPE fraction, %		44.3			49.2	
Isotropic part of WAXS intensity						
(110) – HDPE	21.13	14.6	4.09	20.97	9.8	4.12
(200) – HDPE	23.56	11.4	3.67	23.48	12.6	3.69
(210) – HDPE	29.29	1.9	2.96	29.24	1.3	2.97

Notes: - In the isotropic part of the WAXS intensity the crystalline reflections are only included. The difference to 100% will give the content of the amorphous HDPE and amorphous PA6.
- d_{hkl} is the d-spacing of the respective crystalline plane.

9.3.2. 2D SAXS analysis

Figure 9.7 represents the SAXS patterns of two HDPE/PA6/YP UDP MFC compositions: without compatibilizer (1) – 80/20/0 and with compatibilizer (2) - 70/20/10 at different temperatures. The SAXS images of the starting composites (1a and 2a) are almost the same: in both there exists isotropic scattering showing the formation of randomly distributed lamellar structures and equatorial scattering maxima attributable to lamellar crystals oriented parallel to the fiber direction. The isotropic ring and the oriented maxima appear at almost the same scattering angle, quite different than that of the pure

PA6. This is another confirmation that the MFCs contain two different kinds of HDPE matrix material: one that crystallized isotropically in the bulk and other that crystallized oriented along the PA6 fiber. Without a special treatment there is no way to observe at the same time the HDPE and PA6 scattering in patterns 1(a) and 2 (a) because of the strong differences in the scattering intensities. Heating at 160°C eliminates the HDPE scattering and reveals the oriented PA6 reflections (Images 1b and 2b).

Cooling back to 30°C causes that the HDPE matrix recrystallizes which takes place in a different way in the two MFCs under investigation.

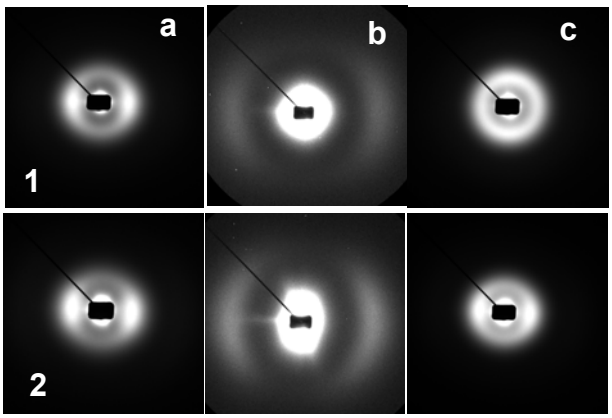

Figure 9.7 2D SAXS images of two HDPE/PA6/YP UDP MFC with compositions: 1 - 80/20/0; 2 - 70/20/10; at different temperatures: (a) - pattern of starting MFC at 30°C; (b) - pattern at 160°C, heated in the beam; (c)- pattern at 30°C after heating at 160°C.

It should be noted that while the oriented scattering in the pattern of the 70/20/10 MFC maintains the equatorial orientation (Fig.9.7, 2c), that of the 80/20/0 system rotates by 90° and appears at the meridian (Fig.9.7, 1c). Isotropic scattering was also present in the two patterns. This reorientation is better observed if azimuthal cuts of the above patterns are performed (Figure 9.8). The curve of the non-compatibilized sample (Figure 9.8 a) clearly shows that after recrystallization the peak of intensity is not at 0° (*i.e.,* along the fiber axis) but at -90 or 90°. In the compatibilized sample (b) the azimuthal distribution of scattered intensity remains the same at the three temperatures studied. It is noteworthy that this reorientation of the lamella that takes place in the non-compatibilized samples is not accompanied by chain direction reorientation, *i.e.*, the chain direction of PA6 and that of the oriented HDPE fraction continue to coincide, as in the starting image at 30°C. A proof for this statements is the analysis of the WAXS pattern of the 80/20/0 MFC at 30°C after heating to 160°C (Figure 9.9).

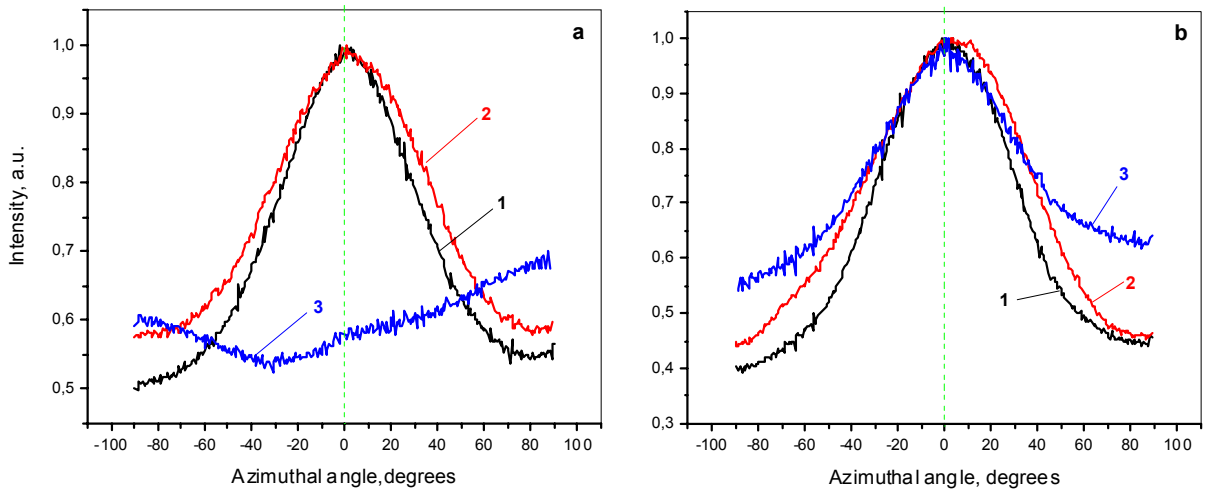

Figure 9.8 Azimuthal distribution of the scattered intensity in the 2D SAXS images of two HDPE/PA6/YP UDP MFCs: (a) 80/20/0; (b) 70/20/10. 1 – initial MFC at 30°C; 2- in beam heating at 160°C; 3 – at 30°C after heating to 160°C The dashed line indicates the fiber direction.

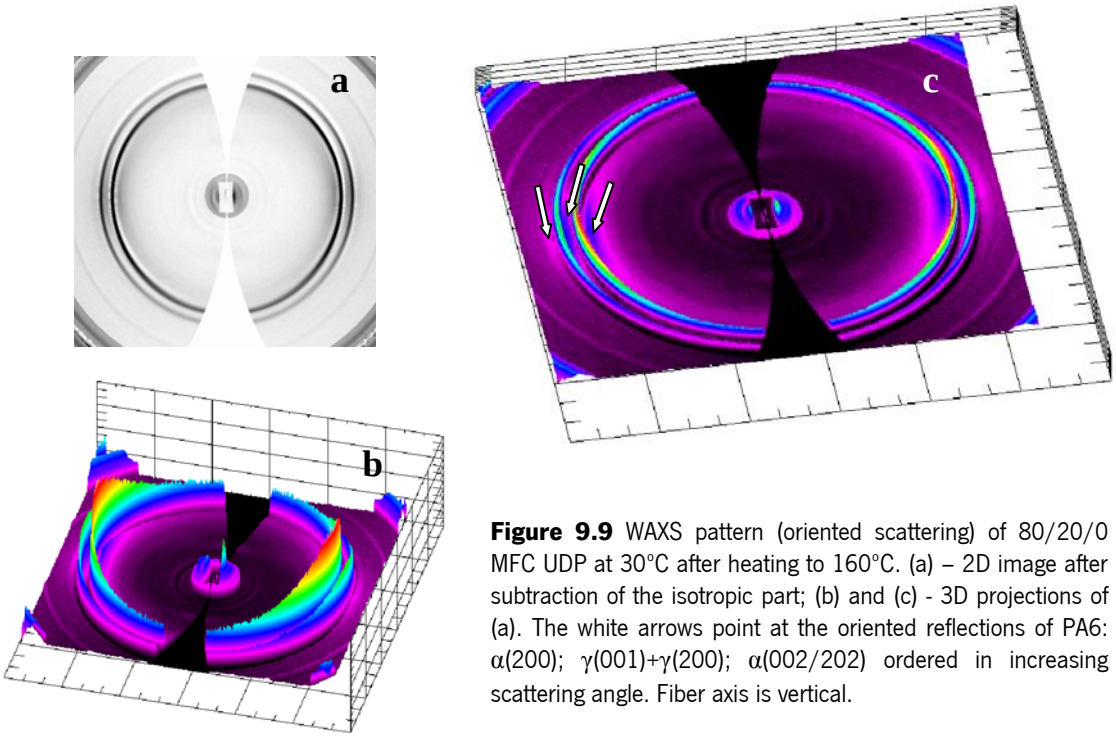

Figure 9.9 WAXS pattern (oriented scattering) of 80/20/0 MFC UDP at 30°C after heating to 160°C. (a) – 2D image after subtraction of the isotropic part; (b) and (c) - 3D projections of (a). The white arrows point at the oriented reflections of PA6: α(200); γ(001)+γ(200); α(002/202) ordered in increasing scattering angle. Fiber axis is vertical.

After subtraction of the isotropic part from the total scattering the resultant image (Fig. 9.9 a) shows that orientation of the PA6 and HDPE crystalline reflection is in the same direction, *i.e.*, there is no reorientation of the HDPE crystallites. The 3D projection (b) gives a better representation of the azimuthal intensity distribution in the HDPE reflections. Figure 9.9 c is a different view of the same 3D

projection and allows the distinction of both PA6 and HDPE oriented crystalline reflections. They all are oriented in the same way.

The 80/20/0 composition was not the only one showing reorientation of the lamellae and keeping the crystallite orientation in the same direction. Figure 9.10 displays the SAXS images of other HDPE/PA6/YP UDP MFCs: at 30°C (a), heating in the beam at 160°C (b) and at 30°C after heating at 160°C (c). Considering the images at 30°C after heating at 160°C it can be concluded that in the absence of compatibilizer (1 c) or when small amounts of it are used (2 c), in addition to the randomly crystallized bulk matrix, HDPE lamellae also recrystalize perpendicular to the fiber direction forming a transcrystalline layer. In the MFCs with higher amount of compatibilizer (above 2.5%), the point-like reflections of the oriented matrix material maintain their initial orientation along the fiber direction (Figure 9.10, 3c and 4c). As recently reported [14], this could be explained as resulting from some fixation of the transcrystalline layer by means of chemical bonds across the fiber – matrix interface.

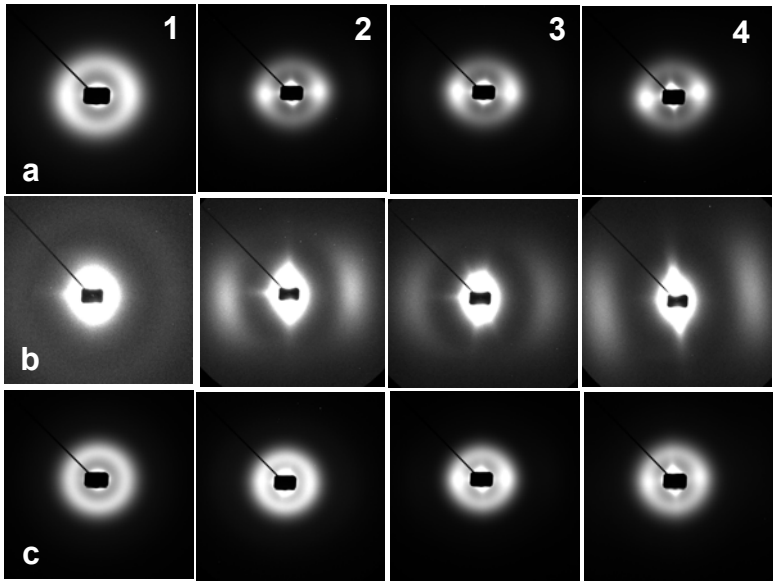

Figure 9.10 2D SAXS images of different HDPE/PA6/YP UDP MFC: 1 - 90/10/0; 2 - 77.5/20/2.5; 3- 75/20/5; 4 - 65/30/5 (w.%); at different temperatures: (a)- patterns of starting MFC at 30°C; (b)- patterns at 160°C in the beam; (c)- patterns at 30°C after heating at 160°C.

To obtain values about the long spacings, integrations were performed of all SAXS patterns of the initial UPD MFCs at 30°C after background correction. Similarly to what was done with the WAXS images (Figure 9.2), in order to separate the oriented from the isotropic scattering, cuts in equatorial and meridional directions were made and the respective curves subtracted. The 1D profiles so obtained are compared in the stacked plot in Figure 9.11. All curves display clearly two long spacings: one in the

range of 80-90 Å attributed to the PA6 and other, larger (>200 Å) and much more intense, belonging to the HDPE matrix. Comparing samples 2-5 that contain the same amount of PA6 with the amount of compatibilizer increasing in this order, it can be seen that the PA6 L_B values remain basically the same. The L_B values of HDPE, however, decrease with the increase of the YP content (Table 9.3). It should be noted that the integration method discussed above does not allow any distinction of how these changes develop in the oriented or in the isotropic HDPE fraction.

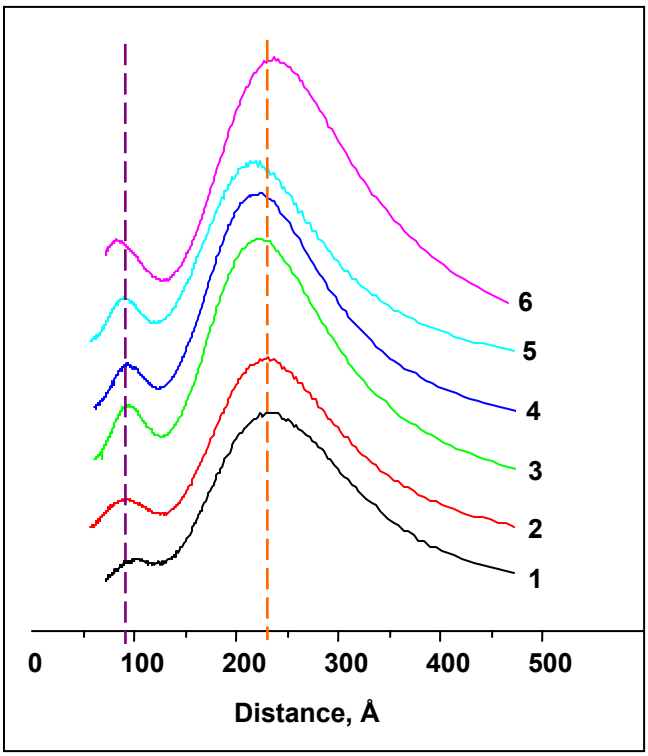

Figure 9.11 1D SAXS patterns of all HDPE/PA6/YP UDP MFCs at 30°C: 1 - 90/10/0; 2 – 80/20/0: 3 - 77.5/20/2.5; 4 - 75/20/5; 5 - 70/20/10 and 6 - 65/30/5.

To make a distinction between the two fractions of HDPE, the deconvolution procedure applied by Somani et al [15] was used. Figure 9.12 (a) shows a pattern of the total scattering of the 75/20/5 MFC composition at 30°C. The deconvoluted 2D image of the isotropic intensity pattern is presented in 9.12 (b), and the resulting image obtained after (a) – (b) subtraction, corresponding to the oriented scatterers is shown in Fig. 9.12 (c). As seen from the latter, the said procedure not only separates the two HDPE components, but also reveals clearly the oriented PA6 fraction located along the equator.

In Figure 9.13 a 3D visualization of the initial pattern (a) and that of the oriented scattering (b) for the same 75/20/5 composition is given. Image (b) shows better the PA6 contribution to the oriented part of the scattering, pointed by the arrows.

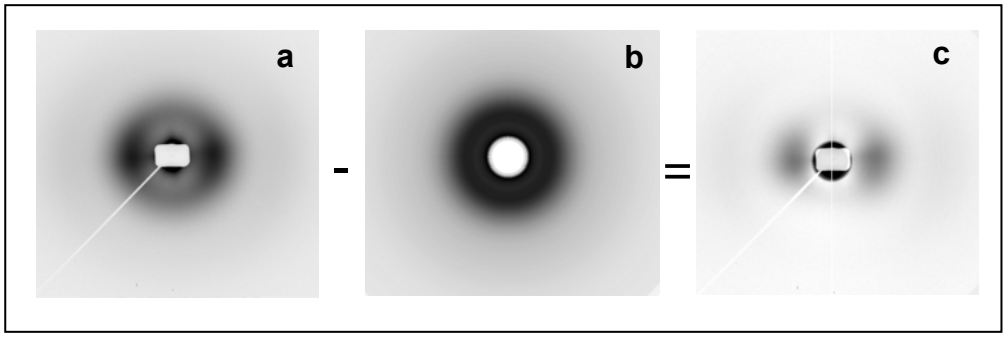

Figure 9.12 Deconvolution procedure of the SAXS pattern of the 75/20/5 UDP MFC. (a) – original SAXS image; (b) intensity pattern of the isotropic scattering; (c) intensity pattern of the oriented scatterers obtained by subtraction (a) – (b) [12].The fiber axis is horizontal.

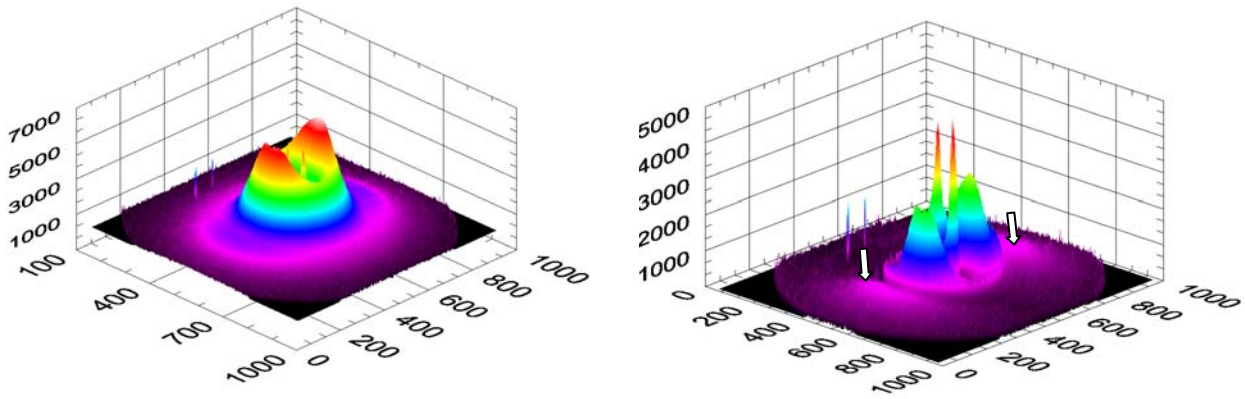

Figure 9.13 3D SAXS patterns of UDP MFCs before (left) and after (fight) the subtraction of the azimuthally independent component of the total scattered intensity. The white arrows indicate the scattering of the PA6 reinforcing phase.

Table 9.3 Long spacing values of the HDPE/PA6/YP UDP composites at 30ºC without (L_B) and with (L_B^*) deconvolution.

Nº	HDPE/PA6/YP composition	L_B, Å		L_B*, Å		
		PA6	HDPE total	HDPE-iso	HDPE-orient.	PA6 orient.
1	90/10/0	100.5	223	224	222	95
2	80/20/0	90	229	225	222	86
				(231)	(225)	
3	77.5/20/2.5	94	221	224	211	91
4	75/20/5	94	220	224	213	92
5	70/20/10	87	215	225	210	88
				(245)	(214)	
6	65/30/5	82	236	223	231	77

Note: The values in parentheses were obtained after recrystallization of the HDPE by in beam heating to 160°C followed by cooling down to 30°C.

Table 9.3 contains the HDPE and PA6 L_B values determined from the scattering maxima of all isotropic and oriented images after deconvolution. It can be seen that in the absence of compatibilizer, there are no significant differences between the long spacings values of HDPE lamellae located in the bulk (isotropic) and those of the oriented HDPE lamellae in the transcrystalline layer (oriented). Introducing YP compatibilizer results in smaller long period in the oriented HDPE, while that of the bulk matrix fraction remains as in the non-compatibilized compositions. Only in the 65/30/5 MFC the distance between the oriented HDPE lamellae is bigger than that of the isotropic fraction. Most probably, this could be explained as a result of a higher amount of PA6 in this composition. As regards the PA6 L_B values, they vary in the 77-95 Å interval. Those obtained after deconvolution are slightly lower but, in our opinion, they should be considered more correct. It is noteworthy that the PA6 long period of 77 Å in the 65/30/5 composition is the closest to the value of the neat oriented PA6 (Chapter 3). On the other hand, in the 90/10/0 composition the respective value is 95 Å.

As mentioned above, after recrystallization, the HDPE fraction in the non-compatibilized and compatibilized samples orients in different ways – in the first case the scattering maxima appeared on the meridian, while in the second maintained their position on the equator. To find out if there is a difference in the HDPE long periods, deconvolution of the 2D SAXS patterns of two selected samples was performed – 80/20/0 and 70/20/10 (Table 9.3, the data in parentheses). It would be expected that if there is any change, it should be in the long spacing values of the oriented HDPE which undergoes reorientation. However, a significant increase of the L_B values of the isotropic HDPE – both in the presence and in the absence of compatibilizer – was actually observed. At this point this experimental fact is not well understood.

9.4. Idealized Model of the PA6 reinforced UDP MFC

The goal of this subsection is to summarize the structural data from the extensive characterization done on the HDPE/PA6/YP UDP composites by means of SEM, NMR, synchrotron WAXS and SAXS and to explain the mechanical properties of these materials. Figure 9.14 gives an idealized model that can be used to explain the experimental data obtained so far.

As it was established by SEM, the reinforcing PA6 component maintains its orientation during the stage of selective matrix isotropization. The preferred polymorph is α PA6 (solid state NMR) whose exact content may vary. As concluded from the X-ray data analysis, the HDPE matrix does not become

completely isotropic in either the compatibilized or non-compatibilized MFCs, as concluded from the X-ray data analysis. The HDPE lamellar structure is of two types. The predominant type corresponds to isotropic bulk lamellae presented in the cartoons in Figure 9.14 by the disordered rectangles placed chaotically in respect to the PA6 fibrils. The second type, found in lower amount, is made of oriented HDPE material, crystallized just upon the PA6 fiber thus forming a transcrystalline layer, in which the lamellae are oriented along the fibrils and the chain direction of the two materials coincide (the shaded patterned rectangles in (a) and (c)). In the presence of compatibilizer the oriented HDPE fraction is approximately equal to that of the PA6 component (1:1 by volume). In the non-compatibilized samples, the ratio between the oriented HDPE and PA6 is 1.0:1.3. The transcrystalline layer behaves differently in these two cases. Thus, when there is no YP, heating to 160°C and cooling back to 30°C (no pressure applied) leads to reorientation of the HDPE lamellae in such a way that they become perpendicular to the PA6 fibrils maintaining the chain direction orientation (the shaded rectangles in (b)). Some correlation in the direction parallel to fiber axis is also maintained (the dashed line in cartoon (b)).

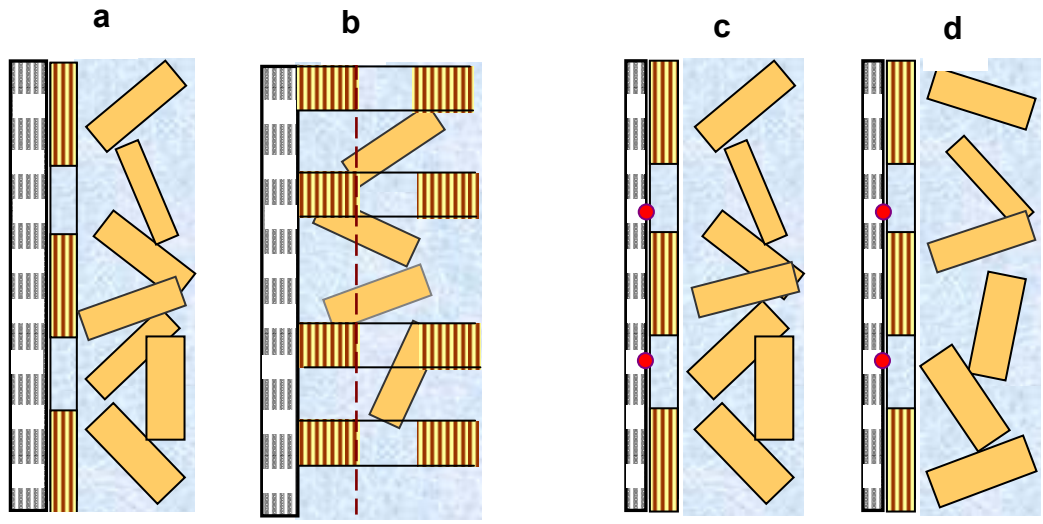

Figure 9.14 Structural models of non-compatibilized ((a) and (b)) and compatibilized ((c) and (d)) HDPE/PA6/YP UDP MFCs. (a) and (c) depict the structure of the as-prepared MFCs, (b) and (d) visualize the structure after the heating-cooling cycle in the absence of pressure. The red points represent the chemical bonds between the PA6 and Yparex. The vertical solid lines indicate the chain direction. The dashed line in (b) sketches out the maintenance of some correlation of lamellae parallel to PA6 fibers.

The above cooling-heating cycle does not change the structure of HDPE in TCL in compatibilized samples (Figure 9.13, c and d). It can be supposed that this is due to the existence of chemical bonds (imide linkages) resulting from the chemical reaction between PA6 amide groups the carbonyls groups of the maleic anhydyde functionality of YP according to a known scheme (Figure 1.9). These linkages

are included in the amorphous PA6 and YP and are given by red points in cartoons (c) and (d). They fix the transcrystalline layer upon the PA6 fibril and no matter how many heating-cooling cycles are performed the orientation of HDPE in transcrystalline layer remains the same. It can be also supposed that in the compatibilized samples it is exactly the HDPE from YP that is mostly included in the transcrystalline layer.

Having in mind the SEM (Figure 7.1, images 2c and 3c) and WAXS data (Table 9.2), it is possible to quantify the transcrystalline layer in both types of MFCs. The calculations are based on the idealization that the fibrils are cylindrical and uniformly coated by coaxial transcrystalline layer of HDPE. Figure 9.15 gives a schematic view of the cross-sections in two selected UDP MFCs.

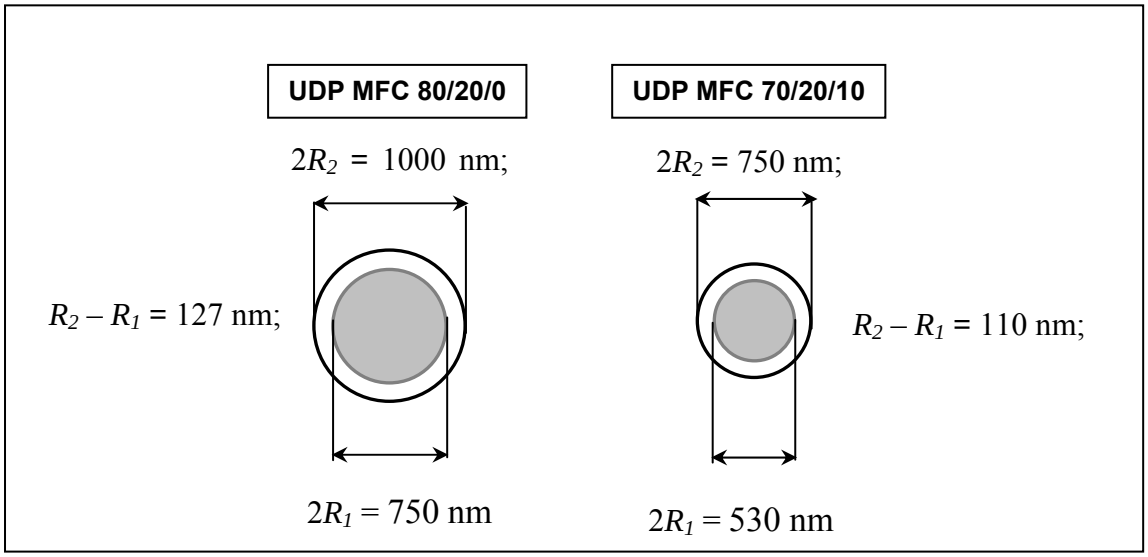

Figure 9.15 Schematic presentation of the fiber cross-sections of 80/20/0 and 70/20/10 UDP MFCs

We can write:

$$V_f = \pi.R_1^2.L \quad (1)$$

$$V_{TCL} = \pi.L.(R_2^2 - R_1^2) \quad (2)$$

Here V_f is the volume fraction of the crystalline oriented PA6, V_{TCL} is the volume fraction of the crystalline oriented HDPE in the TCL, R_1 is the real PA6 fiber radius, R_2 the visible by SEM fiber radius (PA6 + TCL) and L is the fiber length.

In the compatibilized 70/20/10 MFC $V_f = V_{TCL}$ (Table 9.2). Combining Eq. 1 and Eq. 2 it can be seen that $R_2 = 1.414.R_1$. The average thickness of TCL is $R_2 - R_1 = 0.414.R_1$. Similar calculations for the 80/20/0 MFC where $V_f = 1.257.V_{TCL}$ (Table 9.2) lead to a TCL thickness $R_2 - R_1 = 0.340.R_1$. Since the average visible diameter $2R_2$ of the reinforcing fibers in the 80/20/0 MFC was found to be ca. 1000 nm and in the 70/20/10 – of ca. 750 nm, it is easy to find out that the TCL thickness in the non-compatibilized and compatibilized samples will be of 127 nm and 110 nm, respectively. The real PA6 fibril diameter $2R_1$ will be 750 nm and 530 nm, respectively.

Summarizing, the formation of transcrystalline layers (TCL) is common feature for all HDPE/PA6/YP MFCs studied in this work. There is no significant difference between the TCL thicknesses in the compatibilized and non-compatibilized MFCs discussed above. In the 80/20/0 sample the formation of TCL can be attributed to physical interactions at the matrix-fibril interface. In the 70/20/10 system it should be a result of chemical reactions between the maleic anhydride of YP and the amide groups of PA6. It can be expected that in the latter case the TCL will include polyolefin phase from the YP compatibilizer, which is different from the bulk matrix HDPE. This could be one of the possible explanations of the inferior mechanical properties of the compatibilized samples and mostly of the 70/20/10 where the compatibilizer concentration is the highest. On the other hand, the differences in the PA6 fibril characteristics, *e.g.*, diameter, length and aspect ratio will also influence the mechanical properties. At this point the relative importance of all these factors is not clear. Studying the structure of HDPE/PA12 UDP MFCs is supposed to shed more light on this subject.

9.5 References

1. Saiello S, Kenny J, Nicolais L, *J Mater Sci* **25**:3493 (1990).
2. Jenckel K, Tcege E, Hinrichs W, *Kolloid Z* **129**:19 (1952).
3. Misra A, Deopura BL, Xavier SF, Hartley FD, Peters RH, *Angew Makromol Chem* **113**:113 (1983).
4. Quan H, Li Z-M, Yang M-B, Huang R, *Comp Sci Technol* **65:**999 (2005).
5. Nuriel H, Klein N, Marom G. *Compos Sci Technol* **59**:1685 (1999).

6. Li ZM, Yang W, Li LB, Xie BH, Huang R and Yang MB, *J Polym Sci Part B: Polym Phys* **42**:374 (2004)

7. Li ZM, Li BL, Shen KZ, Yang W, Huang R and Yang MB, *Macromol Rapid Commun* **25**:553 (2004)

8. Li ZM, Li LB, Shen KZ, Yang MB, Huang R, *J Polym Sci Part B: Polym Phys* **42**:4095 (2004).

9. Friedrich K, Ueda E, Kamo H, Evstatiev M, Krasteva B and Fakirov S, *J Mater Sci* **37**: 4299 (2002)

10. Fakirov S, Stribeck N, Apostolov AA., Denchev Z, Krasteva B, Evstatiev M and Friedrich K. *J. Macromol Sci – Phys* **B40**:935 (2001)

11. Sapoundjieva D, Denchev Z, Evstatiev M, Fakirov S, Stribeck N and Stamm M, *J Mater Sci* **34**:3063 (1999).

12. Nogales A, Hsiao BS, Somani RH, Srinivas S, Tsou AH, Balta-Calleja FJ, Ezquerra TA, *Polymer* **42** :5247 (2001).

13. Software developed by Stonybrook Technology and Applied Research Inc. NY, USA.

14. Denchev Z, Oliveira MJ, Mano JF, Viana JC, and Funari SS, *J Macromol Sci – Phys* **B43**:163 (2004).

15. Somani RH, Hsiao BS, Nogales A, Srinivas S, Tsou AH, Sics I, Baltá-Calleja FJ, Ezquerra, TA, *Macromolecules*, **33**:9385 (2000).

CHAPTER 10

STRUCTURE DEVELOPMENT IN POLYAMIDE 12 REINFORCED COMPOSITES

Employing the same methodology as in Chapter 7, SEM and X-ray scattering techniques were used to prove the fibrillar morphology of the reinforcing phase in PA12 containing MFCs. Systems with various lengths, diameters and alignment of the reinforcing PA12 fibrils were prepared and investigated, namely UDP, CPC, MRB and NOM. Comparison was made with the respective PA6 containing MFCs and some conclusions were drawn about the possible interactions at the matrix-fibril interface.

10.1. SEM investigations – proofs for fibrillar morphology of MFCs

Figure 10.1 displays SEM images of PA12-containing materials after the extruder die (column 1), after the first haul-off unit (column 2) and of the final MFC UDP (column 3). It is noteworthy that even after the extruder die the PA12 component is somewhat oriented – instead of spheres, as it was in the case of PA6 reinforcing ((Chapter 7, Fig.1-6a), here one observes cylindrical structures better expressed at lower Yparex concentrations (Figure 10.1; 1-2a, 4-5a). Comparing the micrographs in column 1, it may be concluded that the diameters of the PA12 entities decrease with the increase of the compatibilizer concentration – from 1.5 – 2.0 μm in the 90/10/0 and 80/20/0 blends to 0.5 – 1.0 μm in the 70/20/10 blend. Another observation is that increasing the compatibilizer content results in improved adhesion at the HDPE/PA12 interface. In the blends without (1a, 2a) or with less compatibilizer (5a) it seems that the PA12 entities are disentangled from the matrix indicating adhesive failure during the cryogenic fracture. Samples 3a, 4a, and 6a that contain 5-10% Yparex show cohesive fracture in the PA12 reinforcing elements without separation of the latter from the matrix. In sample 6a this effects is the strongest - it is possible to see how the PA12 elements are anchored to the HDPE matrix. The 6a micrograph suggests also a better adhesion between the PA12/HDPE phases as compared to the respective PA6 - containing system (Figure 7.1, 6a). As expected, when the materials pass through the first haul-off unit, the diameters of the PA12 entities decrease in all compositions in average by 30 - 40%. This is an indirect indication that an additional orientation of the PA12 phase was induced at this stage.

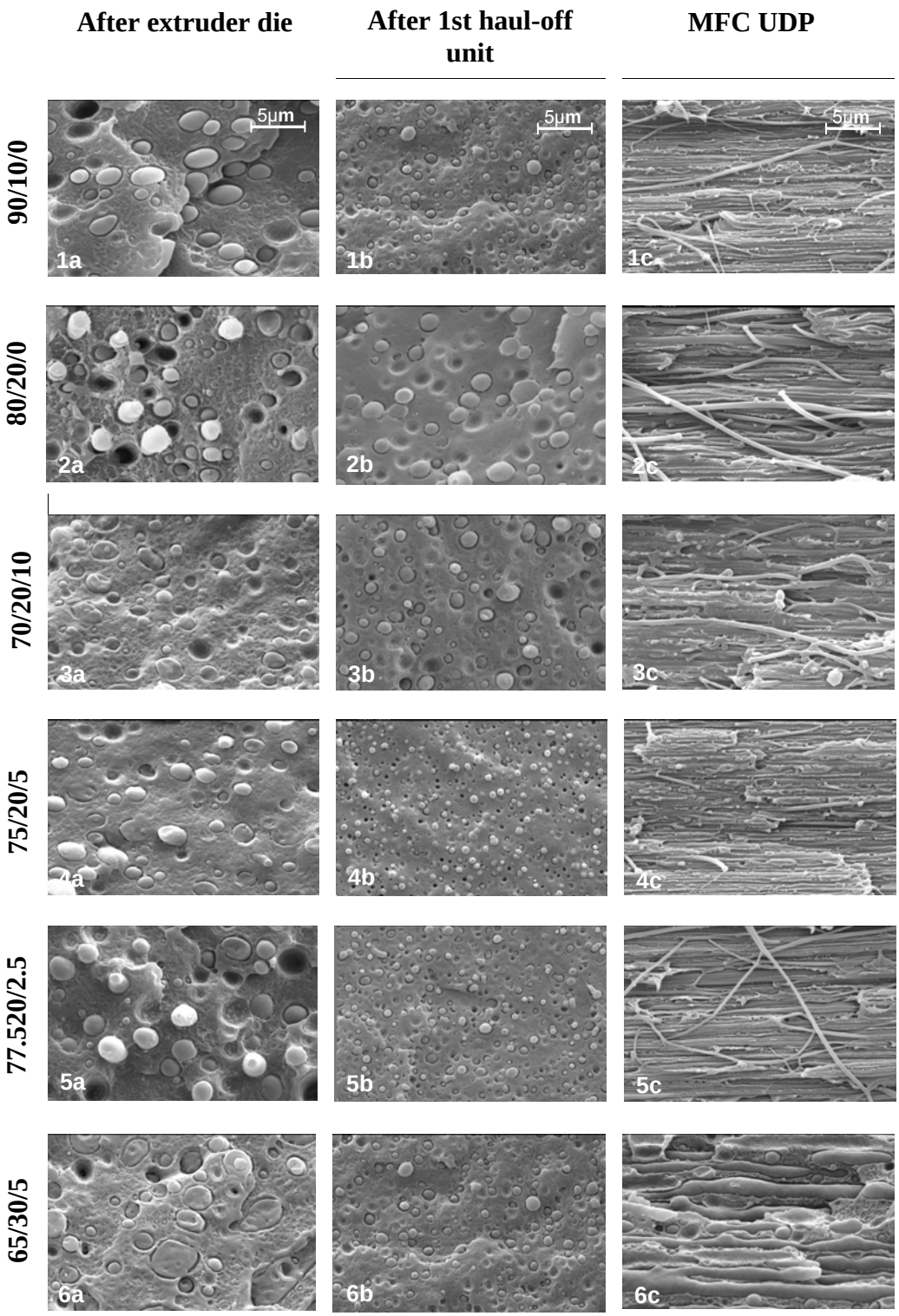

Figure 10.1 SEM images of cryogenic fractured surfaces of various HDPE/PA12/YP materials (compositions given in wt. %) during the stages of the MFCs preparation: non-oriented blend after the extruder die (1-6 a); slightly oriented blends after the first haul-off unit (1-6 b): MFC UDP. fractured in the direction of the fiber (1-6 c).

The fibrils' orientation and morphology could be observed only in the final MFCs after fracturing the specimens in a direction parallel to the fibrils (Figure 10.1, 1 - 6c). The finest fibrils, with diameters

of 0.3-0.5 nm, are observed in the compatibilized MFCs (images 3c - 5c). These images show clearly the above-mentioned improved adhesion in the presence of compatibilizer. The fibrils look like being "cemented" into the HDPE matrix, which is not the case in images (1c, 2c) where the fibrils are smoother and are, apparently, separated from the matrix.

As in the case of PA6-reinfoced composites, the SEM data in Figure 10.1 were used to obtain an estimate of the fibrils' length and aspect ratio. Thus, in non-compatibilized PA12 UDP MFCs the maximal length of the reinforcing fibrils is in the range between 40 and 80 μm and with YP – from 15 to *ca.* 40 μm. This would give aspect ratios of 90-110 and 30-80, respectively.

The direct observation by SEM of the oriented cables obtained after the second haul-off unit that are the precursors for MFC preparation was not straightforward. Because of the low cable diameter (below 1 mm) and the hardness of the cables, it was difficult to prepare fractured samples of good quality. However, selected samples were observed by transmission electron microscopy (TEM) using a Zeiss 902A microscope. The observations were done on ultrathin sections (*ca.* 70 nm) cut at about -130°C with a Leica FC6 ultramicrotome equipped with diamond knife. Before the observation, the sections were stained with ruthenium tetraoxide. Figure 10.2 shows the micrograph of the 77.5/20/2.5 oriented cable.

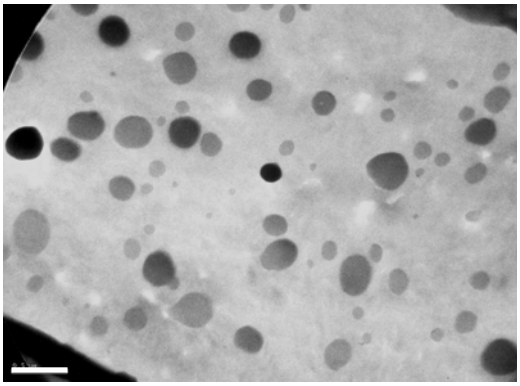

Figure 10.2 TEM image of 77.5/20/2.5 HDPE/PA12/YP oriented precursor obtained after the second haul-off unit. The white bar corresponds to 500 nm.

The above figure shows that the PA12 reinforcing phase is well distributed within the HDPE matrix. The fibrils' diameters vary in the 100-400 nm range, *i.e.* they are somewhat thinner than the fibrils in the final MFC.

Furthermore, the influence of the length and alignment of the reinforcing fibrils (UDP, CPC and MRB) or spheres (NOM) on the composite morphology was studied in all six HDPE/PA12 compositions. The two more representative cases, namely systems without compatibilizer (80/20/0) and with 5% compatibilizer (65/30/5) are presented in Figure 10.3. It can be seen that, irrespective of the reinforcement geometry and orientation, in the compatibilized samples (images 1-4b) the reinforcing entities are better embedded and fixed within the matrix as compared to the non-compatibilized samples (1-4a). In addition to this, in the presence of Yparex the diameters of the PA12 fibrils (MFCs) or spheres (NOM) are smaller.

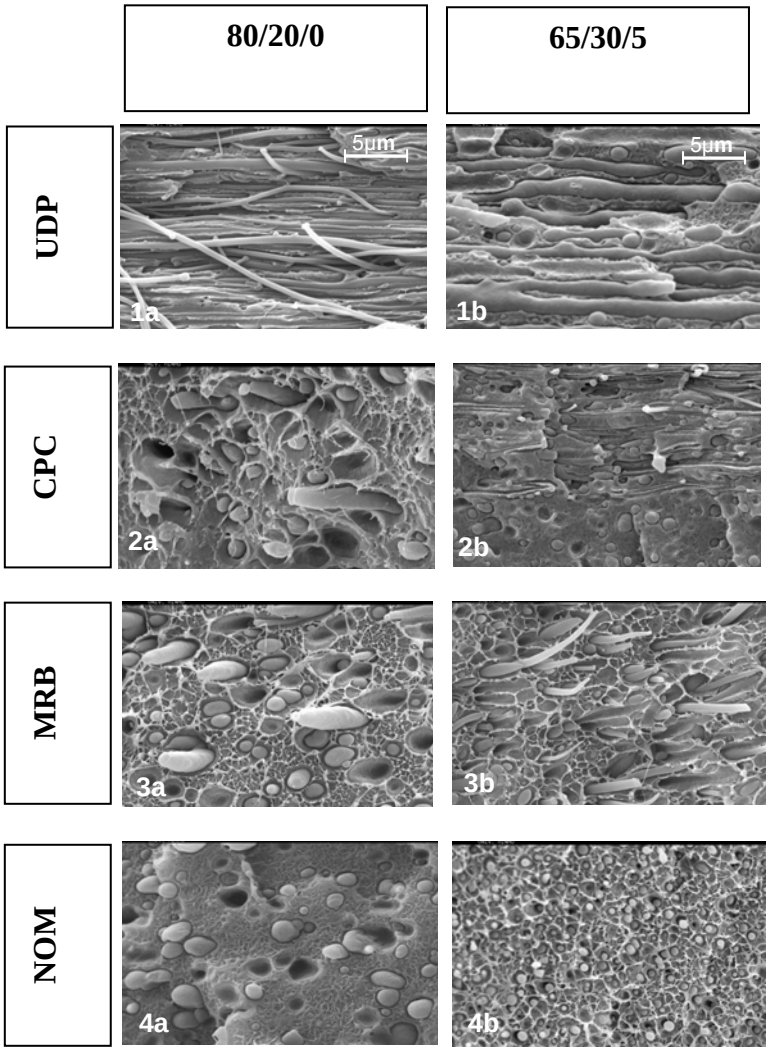

Figure 10.3 SEM images of fractured surface of various composites obtained from two HDPE/PA12/YP compositions (1-4a: 80/20/0 wt.%; 1-4 b: 65/30/5 wt.%). UDP MFC, specimen fractured in the fibrils direction; CPC MFC; MRB MFC; NOM – non–oriented HDPE/PA12/YP mixtures.

The influence of compatibilizer on the PA12 composite morphology is further revealed in Figure 10.4. All images were obtained after selective extraction of the HDPE matrix. As expected, in all MFCs (images 1-3 a) the PA12 reinforcing fibrils are clearly observable, their diameters being between 0.4 – 0.8 μm (1a and 3a) and in the 0.25 – 0.5 μm range for the sample with the largest concentration of compatibilizer (2a). The images after selective dissolution of samples obtained at the extruder die (Figure 10.4, 1b, 3b) prove the above-mentioned PA12 component orientation. Instead of spheres, observed in the case of the respective PA6 reinforced samples (Chapter 7, Figure 7.3 b), one observes here dendrite structures containing oriented stem entities of considerable thickness – from 1-2 (compatibilized) to 3-4 μm (non-compatibilized).

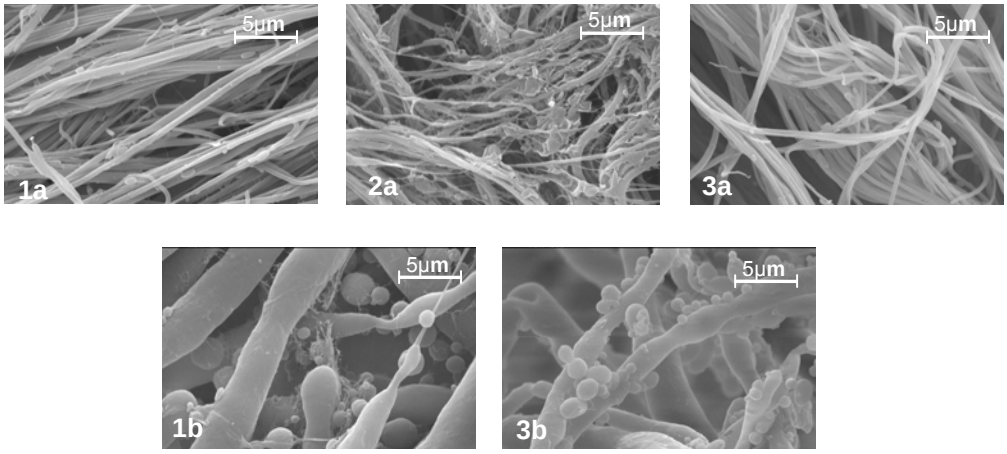

Figure 10.4 SEM images of various HDPE/PA12/YP samples after selective extraction of the matrix (a – final MFCs; b – non-oriented blends after the die exit) with the following compositions (wt. %): 1 - 80/20/0; 2 - 70/20/10; 3 - 65/30/5.

This means that even at the stage of melt blending the two reinforcing polyamides create different morphologies that will probably have different influence on the mechanical behaviour of the respective MFCs.

10.2. X-Ray analyses – WAXS and SAXS

In this preliminary X-ray study the same approach was used as in the case of HDPE/PA6 systems (Chapter 7). First, the oriented precursors were analyzed, modelling their transformation into composites by in-beam heating. Then, the respective MFCs obtained at real processing conditions were studied. Figure 10.5 displays representative 2D WAXS patterns of HDPE/PA12/YP oriented precursors.

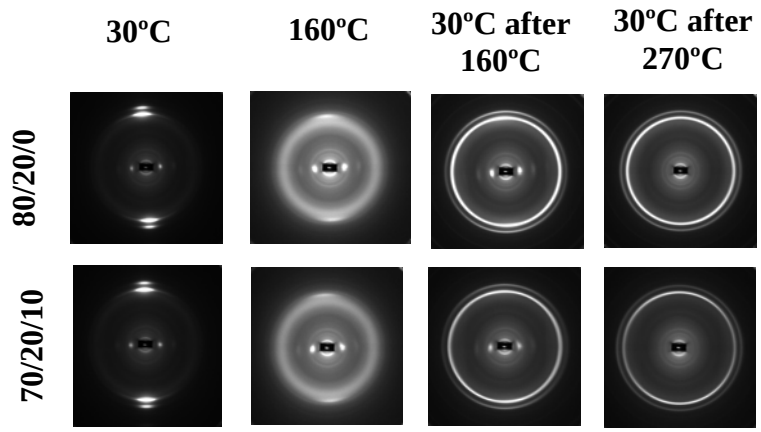

Figure 10.5 2D WAXS patterns of HDPE/PA12/YP oriented cables taken at various temperatures. DD is horizontal

The images at 30°C are typical of samples with fiber symmetry and high degree of orientation. The almost point-like equatorial reflections of the HDPE planes (110) – internal and (200) – external, are superimposed with the equatorial PA12 reflections characterising its (001) and (200) planes (DD is horizontal). Unlike the HDPE/PA6 oriented cables, the presence of oriented PA12 here is clearly observable. Judging from the meridional point-like reflections ascribed to the (0k0) planes of oriented γ polyamide polymorph it can be concluded that PA12 is in its oriented γ crystalline form. The (0k0) reflections remain at 160°C and after cooling down to 30°C indicating that under these conditions the PA12 is still in γ-oriented form. The presence of Debye rings should be related with isotropization of HDPE. After heating to 270°C, both HDPE and PA12 melt and the subsequent pattern at 30°C reveals an isotropic sample. The disappearance of the meridional (0k0) reflections in these patterns is one more proof for the PA12 isotropization.

Additional information about the structure development during the MFC preparation may be obtained from the respective SAXS patterns (Figure 10.6).

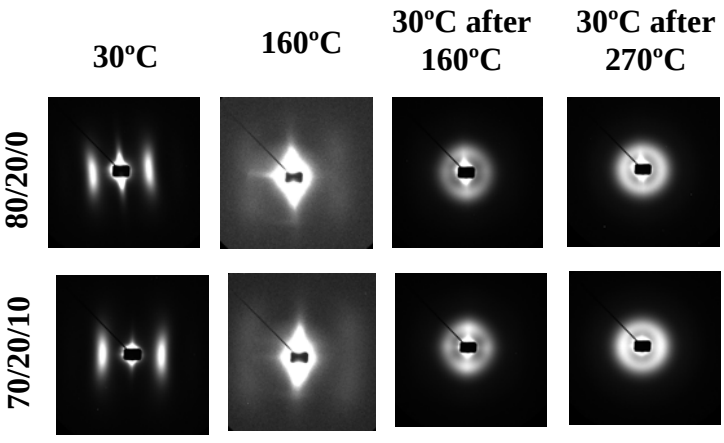

Figure 10.6 2D SAXS patterns of HDPE/PA12/YP oriented cables taken at various temperatures. DD is horizontal

The images at 30°C confirm the fiber symmetry of the two oriented cables without and with compatibilizer. The scattering of PA12 component can be observed directly only at 160°C after melting the matrix. At this temperature both patterns show four-point scattering suggesting the presence of stacks of tilted lamellae that were also observed in neat PA12 during its orientation (see Chapter 6, Figure 6.9). After cooling to 30°C, irrespective of the presence or absence of compatibilizer, a part of the matrix always tends to recrystallizes changing its original orientation by 90°. Contrary to the HDPE/PA6 systems (Chapter 7, Figure 7.5), the presence of compatibilizer is not enough to prevent the matrix reorientation. The reason for this should be related to the different molecular and crystallographic structures of the two polyamides. The patterns obtained after keeping the two samples while being irradiated for equal times at 270°C, and subsequently cooled to 30°C, were expected to be isotropic. However, as Figure 10.6 shows, in the presence of compatibilizer there is some residual orientation and the sample isotropization becomes more difficult.

Similar WAXS and SAXS measurements were performed with the respective 80/20/0 and 70/20/10 MFCs obtained under real processing conditions (Figures 10.7 and 10.8).

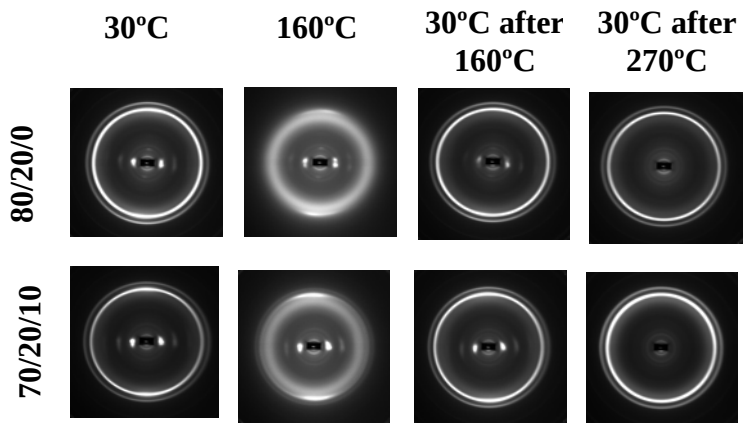

Figure 10.7 2D WAXS patterns of HDPE/PA12/YP microfibrilar composites taken at various temperatures. DD is horizontal.

The (0k0) meridional point reflections remain confirming that in the MFCs the PA12 is oriented and it is in γ-crystalline modification. The orientation is better seen at 160°C where all the reflections of PA12, including the equatorial ones, could be observed.

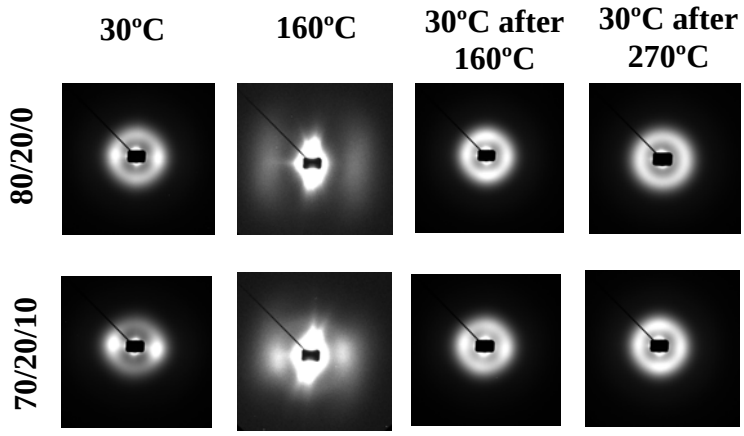

Figure 10.8 2D SAXS patterns of HDPE/PA12/YP microfibrilar composites taken at various temperatures. DD is horizontal.

The SAXS patterns of the two MFCs at 30°C (Figure 10.8) show that the visible reflections oriented along DD are with relatively large long spacings (of approximately 220 Å), which cannot be neat PA12 phase, whose typical L_B values are in the range of 100-110 Å (Chapter 5, Table 5.4). Therefore, at 30°C one observes the scattering of the HDPE material crystallized upon the oriented PA12 fibrils. The reflections of the latter are there but remain invisible due to the big difference in contrast and can be visualized only after the matrix melting. The two images at 160°C are different. While the one without compatibilizer is consistent with the neat PA12 (see Chapter 5, Figure 5.7), that of the sample containing 10% compatibilizer shows scattering of a material (L_B = 140-145 Å) which is not neat PA12, but most probably HDPE/PA12 copolymer still crystalline and oriented at 160°C. It is interesting to compare the SAXS patterns of the starting MFCs at 30°C and those obtained at 30°C after 160°C. The latter also represent MFCs but produced in the X-ray beam, *i.e.*, without pressure. In the first two we only observe equatorial oriented reflections. In the second two meridional spots also appear, better seen in the non-compatibilized sample. It can be concluded that under real processing conditions when pressure up to 20 bar is applied, a fraction of the HDPE matrix crystallizes epitaxially upon the PA12 fibrils without reorientation, irrespective of the fact whether there is or not compatibilizer. When there is no pressure during the matrix isotropization, in non-compatibilized MFCs the HDPE material can crystallize in a direction perpendicular to the PA12 fibril axis. Therefore, analogously to the PA6-reinforced MFCs, the PA12 reinforcing fibrils have a layered structure: a core of oriented PA12 and a shell of oriented HDPE whose orientation may vary. More results related to the influence of the processing conditions on the structure and mechanical properties of the PA12- based MFC will be presented in Chapter 12.

CHAPTER 11

MECHANICAL PROPERTIES OF PA12 REINFORCED *IN-SITU* COMPOSITES

This chapter is organized in the same way as Chapter 8 and considers the mechanical properties of the HDPE/PA12/YP MFCs, namely their tensile, flexural and impact behaviors. The variation of the blend composition as well as the type of the oriented precursors was similar to the PA6-reinforced MFCs. Thus, six HDPE/PA12/YP compositions were processed to obtain MFCs in the form of unidirectional ply (UDP) laminae, cross-ply laminates (CPC), and MFC obtained from middle length, randomly distributed bristles (MRB). Composites with non-oriented mixtures (NOM) were also prepared and studied to assess the influence of the precursors' length, diameters and arrangement of the PA12 reinforcing fibrils on the mechanical properties under study.

11.1 Tensile properties

11.1.1 HDPE/PA12/YP UDP lamina

Analogously to Chapter 8, orthotropic UDP laminae were used to investigate the tensile properties. Test samples were cut out along the axis of orientation, the respective modulus, E, yield stress, σ_y, and tensile strength, $\sigma_{\max}$, being denoted with index 1. Samples were also taken across the lamina and the respective characteristics indexed with 2.

Figure 11.1 shows typical stress-strain curves of HDPE/PA12/YP UDP MFCs samples with various compositions tested in the longitudinal direction. Generally, the failure of all composite samples occurs at stresses higher than the HDPE matrix. This increase is not so pronounced in the composites containing 10 and 30 wt. % PA12 (curves 1 and 6). The UDP MFCs containing 20% PA12, however (curves 2-5) show a considerable improvement of the tensile strength.

Young's modulus and tensile strength

The stress-strain curves in Figure 11.1 were used to determine the longitudinal Young's modulus, E_1, at 1% of strain and the data are given in Table 11.1.

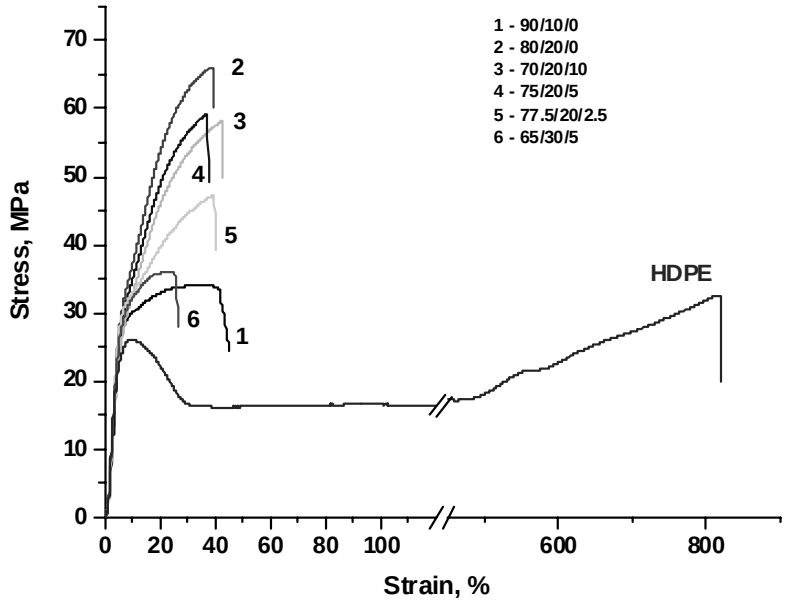

Figure 11.1 Representative stress-strain curves of UDP MFC with various HDPE/PA12/YP compositions. For comparison, the curve of the neat HDPE matrix is also shown.

Table 1.1 Longitudinal Tensile Properties of HDPE/PA12/YP UDP MFCs with various compositions.

Composition HDPE/PA12/YP Wt. %	**Vol. fract. of PA12, V_f**	E_1 MPa	ΔE_1 %	$\sigma_{1\max}$ MPa	$\Delta\sigma_{1\max}$ %	σ_{1y}, MPa
100/0/0	-	827 ± 47	0	26 ± 1	0	26 ± 1
90/10/0	0.094	902 ± 25	9.1	34 ± 1	30.8	34 ± 1
80/20/0	0.189	1054± 37	27.5	64 ± 3	146.2	64 ± 3
70/20/10	0.188	972 ± 47	17.5	55 ± 6	111.5	55 ± 6
75/20/5	0.189	1011 ± 12	22.2	56 ± 8	115.4	56 ± 9
77.5/20/2.5	0.189	1050 ± 29	27.0	47 ± 7	80.8	47 ± 8
65/30/5	0.285	1030 ± 43	24.5	33 ± 4	26.9	33 ± 4
0/100/0 or.	-	1519 ± 17	-	214 ± 2	-	207± 2

Notes: E_1 was determined as secant modulus at 1% strain; 0/100/0 or. = PA12 oriented cable.
$\Delta E_1 = (E_{1HDPE} - E_1)/E_{1HDPE}$, %; $\Delta\sigma_1 = (\sigma_{1HDPE} - \sigma_1)/\sigma_{1HDPE}$, %

Table 11.1 presents also data on the longitudinal tensile strength, $\sigma_{1\max}$, defined as the maximum stress the material can withstand, and on the longitudinal yield stress, σ_{1y}. Since none of the PA12 reinforced composites displays clear yield point, $\sigma_{1y} \equiv \sigma_{1\max}$.

All MFC compositions showed moduli higher than the HDPE, the increase being between 9 and 28% depending on the content of PA12, the presence and the amount of compatibilizer. The smallest improvement of 9% was registered with the 90/10/0 blend, which is related to the low concentration of reinforcing PA12. In the systems with 20% PA12 the improvement was in the range of 18-28%. A reduction was observed in association to the increase of the YP, as it was already observed in the case of the PA6 reinforcement. The Young's modulus of the 65/30/5 system was also improved but statistically it remained close to the values of the best MFCs with 20% of PA12 (80/20/0 and 77.5/20/2.5).

Concerning the tensile strength, in all UDP composites there was a significant growth from 27% for the 65/30/5 system to 146% for the 80/20/0 MFC composition. Contrary to E_1 , in this case the increase of the YP content did not result in a considerable decline of the tensile strength.

Prediction of the tensile properties

As in the case of the PA6 composites, the Young's moduli in longitudinal direction predicted using the rule of mixtures, $E_1{}^*$, were calculated according to equation 2.8 in Chapter 2. For the calculations the data of the matrix (HDPE), the fiber material (oriented PA12) and the volume fraction of the fibers were used. The tensile strength predicted, $\sigma^*_{1\max}$, was calculated according to equation 2.10 considering only the strength and the volume fraction of the fibers as suggested in [1].

Comparing the theoretical and experimental Young's moduli (Table 11.2 and Figure 11.2), it can be seen that the rule of the mixtures works well for all HDPE/PA12/YP UDP MFCs studied, since the experimental values are close to the predictions. It is remarkable that there are small positive deviations, reaching 10% in the 80/20/0 composite. This may be interpreted as in the case of the PA6 reinforcement, when it was observed that the lower the amount of compatibilizer, the bigger the deviation from the theoretical value. However, it is worth noting that with the PA12 reinforcement even the system containing 10% of YP displays an experimental Young's modulus close to the predicted one. In other words, in the PA12/HDPE systems the high compatibilizer content does not deteriorate so drastically the tensile behavior as it was in the case of PA6/HDPE systems.

Table 11.2 Longitudinal Tensile Properties of HDPE/PA12/YP UDP MFCs compared to theoretical values.

Composition HDPE/PA12/YP Wt. %	**Vol. fract. of PA12, V_f**	E_1 MPa	E_1* MPa	ΔE_1 %	$\sigma_{1\max}$ MPa	$\sigma_{1\max}$* MPa	$\Delta\sigma_{1\max}$ %
100/0/0	-	827 ± 47	-	0	26 ± 1	-	0
90/10/0	0.094	902 ± 25	892	1.1	34 ± 1	20	70.0
80/20/0	0.189	1054± 37	958	10.0	64 ± 3	40	60.0
70/20/10	0.188	972 ± 47	958	1.5	55 ± 4	40	37.5
75/20/5	0.189	1011 ± 12	958	5.5	56 ± 3	40	40.0
77.5/20/2.5	0.189	1050 ± 29	958	9.6	47 ± 4	40	17.5
65/30/5	0.285	1030 ± 43	1025	0.5	33 ± 4	61	-45.9
0/100/0 or.	-	1519 ± 17	-		214 ± 2	-	-

Note: E_1* and $\sigma_{1\max}$* are the theoretical values predicted using the rule of the mixtures; $\Delta E_1 = (E_1 - E_1^*)/E_1^*,\%$ and $\Delta\sigma = (\sigma_{1\max} - \sigma_{1\max}^*)/\sigma_{1\max}^*,\%$.

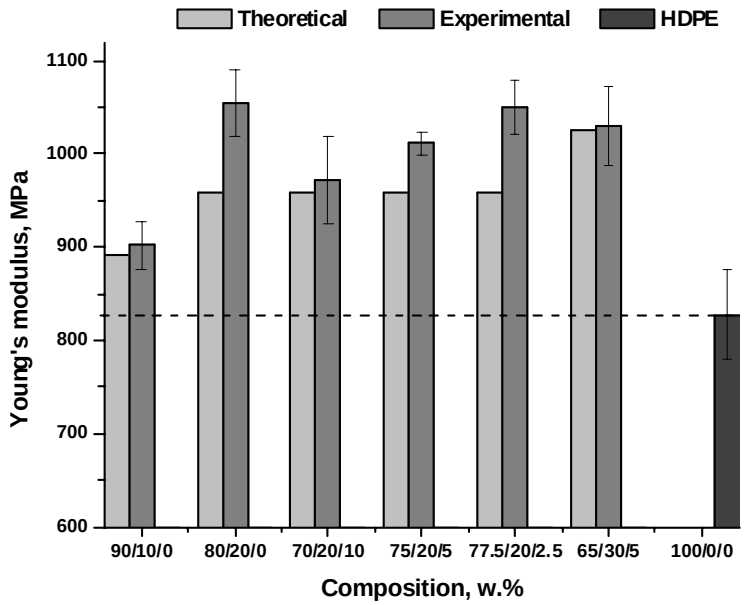

Figure 11.2 Longitudinal Young's moduli E_1 of HDPE/PA12/YP UDP MFCs compared to those predicted from the rule of the mixtures and to the HDPE matrix.

Figure 11.3 shows the comparison between the experimental tensile strength values, $\sigma_{1\max}$ and theoretical ones, $\sigma_{1\max}^*$.

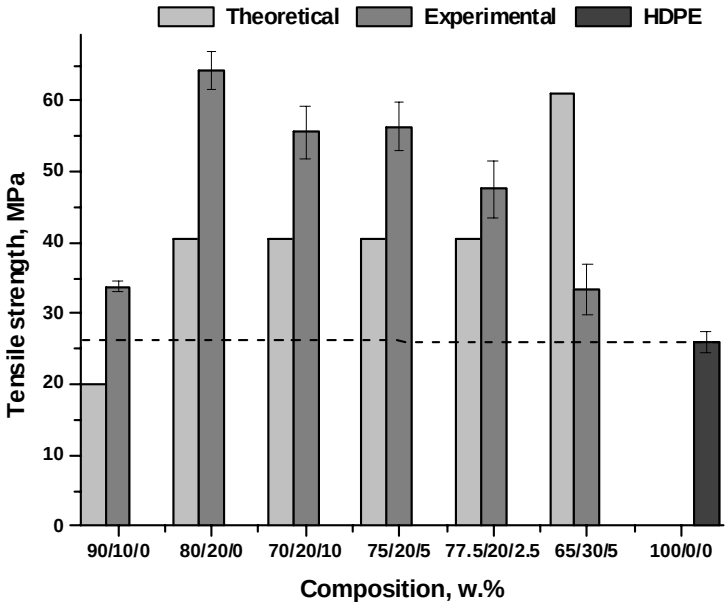

Figure 11.3 Longitudinal tensile strength, $\sigma_{1\max}$, of HDPE/PA12/YP UDP MFCs compared to those predicted from the rule of mixtures and to the HDPE matrix

Most composites in Fig. 11.3 display tensile strengths significantly higher than the HDPE and the predictions from the rule of mixtures. The 65/30/5 system is an exception with its $\sigma_{1\max}$ slightly higher than the matrix, remaining however below $\sigma^{*}_{1\max}$. It appears, as in the case of the PA6 reinforcement, that the optimum relationship between the PA12 and YP concentrations was not found.

Summarizing the results from the tensile properties in the longitudinal direction, one can conclude that with HDPE/PA12/YP UDP MFCs substantial improvements can be achieved with 20% of reinforcing component and small amounts of compatibilizer YP. The Young's moduli and tensile strengths are generally higher than the predicted ones. Most probably, this should be attributed to the mismatch in the diameters of the reinforcing PA12 fibrils in the composites and of the PA12 filaments used to calculate the theoretical moduli. As already mentioned in Chapter 10, the diameters of the PA12 fibrils were found to be between 0.5 and 1,25 μm, while their lengths varied in the 20 - 80 μm range, depending on the PA12 and YP concentrations. These dimensions correspond to aspect ratios from 80 to 150 for non-compatibilized composites and between 30 and 80 for compositions containing YP. It must be mentioned once again that the fibril diameter visible by SEM could be bigger than the real diameter of the PA12 reinforcement due to the formation of a transcrystalline layer of matrix material growing epitaxially upon the oriented polyamide phase. Hence, the aspect ratio of the PA12 fibrils could

be even bigger than the estimates on the basis of SEM data. The next chapter will try to shed more light on this issue.

Tensile properties in transverse direction

In agreement with the theory of the fiber reinforced composites [1], the tensile properties of the UDP lamina in the transverse direction should be very low and generally would not follow the rule of the mixtures. It is the matrix properties that govern the mechanical behavior of the composite, except at high volume fractions of fibers. The fibers in this case contribute very little to the stiffness, E_2, which usually has values close to those of the matrix. The tensile strength, $\sigma_{2\max}$, is also significantly reduced.

Table 11.3 shows the Young's moduli and tensile strength of HDPE/PA12/YP UDP MFCs in the transverse direction. To enable a comparison, the theoretical Young's moduli, E_2^*, were calculated according to equation 2.9 in Chapter 2.

Table 11.3 Transversal Tensile Properties of HDPE/PA12/YP UDP MFCs with various compositions.

Composition HDPE/PA12/YP wt. %	**Volume fract. of PA12, V_f**	E_2 MPa	E_2 * MPa	ΔE_2 %	$\sigma_{2\max}$ MPa
100/0/0	-	851 ± 32	-	-	27 ± 0.4
90/10/0	0.094	929 ± 35	864	7.5	25 ± 0.7
80/20/0	0.189	775 ± 33	905	-14.4	15 ± 1.2
70/20/10	0.188	831 ± 31	905	-8.2	20 ± 2.6
75/20/5	0.189	965 ± 55	905	6.6	21 ± 2.7
77.5/20/2.5	0.189	939 ± 57	905	3.8	24 ± 3.6
65/30/5	0.285	869 ± 59	951	8.6	19 ± 2.6

Notes: E_2 was determined as secant modulus at 1% strain; E_2 * is the theoretical value calculated according to Eq. 2.9, Chapter 2; $\Delta E_2 = (E_2 - E_2^*)/E_2^*$,%; $\sigma_{2\max}^* = 0.33 * \sigma_{p\max}$ = 8.91 MPa, wherein $\sigma_{p\max}$ is the tensile strength of HDPE in transverse direction.

Contrary to PA6 reinforced MFCs (Table 8.2 in Chapter 8), the E_2 data for PA12 reinforcement are close to or even higher than the theoretical values, as it happens with the 90/10/0, 75/20/5 and 77.5/20/2.5 compositions. The latter show $\sigma_{2\max}$ similar to the HDPE, *i.e.,* much higher than the expected strength, usually considered as 1/3 of the matrix value [1]. The 80/20/0, 70/20/10 and the

65/30/5 systems that performed best in the longitudinal direction, showed the lowest experimental tensile characteristics in the transverse direction. It appears that the PA12 reinforcement produces UDP laminae that are more uniform in the two mutually perpendicular directions than in the case of PA6 reinforcement. A possible reason could be the closer chemical similarity between HDPE and PA12 and/or a different composition and geometry of the transcrystalline layer.

11.1.2. Isotropic HDPE/PA12/YP composites - MRB and NOM

MRB Composites

In order to assess the influence of the fiber alignment on the tensile properties, composites with middle length randomly distributed bristles (MRB) were prepared in the same way as the PA6 MRB composites and subjected to tensile tests. Table 11.4 summarizes the data worked out from the stress-strain curves in both longitudinal and transverse directions.

Table 11.4 Longitudinal and Transversal Tensile Properties of HDPE/PA12/YP MRB MFCs

HDPE/PA12/YP wt. %	**Vol. fract. of PA12,** V_f	E_1 MPa	E_2 MPa	$\sigma_{1\max}$ MPa	$\sigma_{2\max}$ MPa
100/0/0	-	827 ± 47	851± 32	26 ± 1	27 ± 1
90/10/0	0.094	1028± 40	1033 ± 13	28.±.1	28 ± 1
80/20/0	0.189	1012 ±34	1032 ± 41	25 ± 1	24 ± 2
70/20/10	0.188	970 ± 43	970 ± 42	31 ± 3	38 ± 4
75/20/5	0.189	955 ± 29	976 ± 38	26 ± 1	26 ± 1
77.5/20/2.5	0.189	1001 ± 34	1005 ± 35	28 ± 1	25 ± 3
65/30/5	0.285	876 ± 42	876 ± 24	21 ± 3	20 ± 2
0/100/0 or.	-	1519± 17	-	214± 2	-

Note: 0/100/ or = PA 12 in oriented state

As expected for an isotropic lamina with random distribution of the reinforcing fibrils, the Young's modulus, E, and the tensile strength, σ, in both longitudinal and transverse directions are very close, in some cases even coinciding. All samples show significant improvement in both E_1 and E_2 values, as compared to the HDPE matrix. The tensile strength, however, remains similar to that of HDPE. It can be noted that the PA12 reinforcement in MRB MFCs is more efficient and gives rise to more homogeneous materials than in the PA6 MRB composites.

NOM Composites

Composites prepared from non-oriented mixtures (NOM) were also subjected to tensile tests to evaluate the reinforcing effect of the isotropic PA12 phase. The precursors for these composites are non-oriented HDPE/PA12/YP granulates obtained by extrusion and subsequent compression molding far below the melting point of the PA12. The tensile characteristics determined from the experimental stress-strain curves are presented in Table 11.5.

Table 11.5 Longitudinal and Transversal Tensile Properties of HDPE/PA12/YP NOM MFCs

HDPE/PA12/YP wt. %	Vol. fract. of PA12, V_f	E_1 MPa	E_2 MPa	$\sigma_{1\max}$ MPa	$\sigma_{2\max}$ MPa
100/0/0	-	827 ± 47	851 ± 32	26 ± 1	27 ± 1
90/10/0	0.094	931 ± 19	942 ± 15	28.±.1	29 ± 1
80/20/0	0.189	982 ± 39	989 ± 44	25 ± 1	24 ± 2
70/20/10	0.188	823 ± 7	857 ± 26	28 ± 4	28 ± 4
75/20/5	0.189	910 ± 36	883 ± 34	28 ± 2	28 ± 1
77.5/20/2.5	0.189	978 ± 42	984 ± 20	27 ± 2	25 ± 4
65/30/5	0.285	917 ± 34	975 ± 43	23 ± 2	31 ± 1
0/100/0 iso	-	1193 ± 15	1175 ± 20	36 ± 2	38±1

Note: 0/100/ iso = PA 12 in isotropic state.

All compositions show Young's moduli in the longitudinal and transverse directions statistically higher than those of the matrix. It is also observed that the lower the YP content, the larger the improvement of the modulus. This dependence was different in the NOM composites containing PA6, where the 70/20/10 composition with the highest concentration of compatibilizer performed in the best way.

A more detailed comparison and an additional analysis of the tensile properties of all HDPE/PA12/YP composites are made in the next subsection.

11.1.3. HDPE/PA12/YP UDP, MRB and NOM – A Comparison

The longitudinal Young's moduli of all PA12 reinforced composites discussed so far are presented in Figure 11.4. It can be seen that UDP or MRB MFCs that have a reinforcing fibrilar PA12 phase display

Young's moduli higher than the matrix. As to the composites with isotropic PA12 phase (NOM), their moduli are statistically identical to the HDPE and only the 80/20/0 composition does not follow this trend.

In all composites reinforced with 10 wt. % of PA12 the highest E_1 values were found with the MRB samples. At higher PA12 concentration, as in the 65/30/5 systems, it is the UDP that shows the best stiffness with values being among the highest in the whole range of compositions and composite types studied. At the intermediate PA12 concentration of 20%, what determines the stiffness is the compatibilizer content, since high moduli are observed either without or at low YP concentrations.

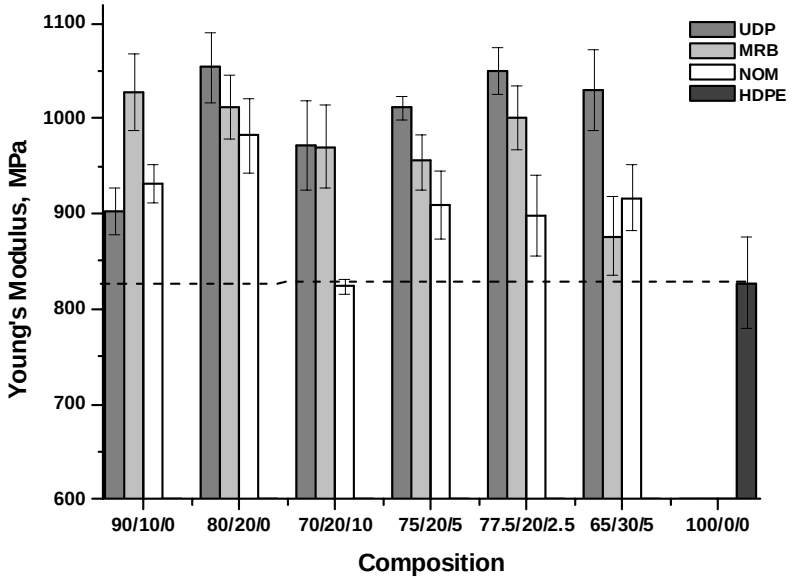

Figure 11.4 Longitudinal Young moduli, E_1, of HDPE/PA12/YP UDP, MRB

However, it should be noted that even with 10% of compatibilizer, the 70/20/10 UDP and MRB samples show an improvement of about 20% on the Young's moduli.

As far as the tensile strength is concerned (Fig. 11.5), all orthotropic UDP laminae display a clear increase of $\sigma_{1\max}$, this being more impressive in the compositions with 20% of PA12. The improvement of the tensile strength in this case is in the range of 30 – 150% (Table 11.1). The isotropic composites, either reinforced with fibrils (MRB), or non-oriented particles (NOM), have statistically identical tensile strengths close to the HDPE. It becomes clear that the fibrilar structure of

the PA12 reinforcing phase and its parallel alignment are of prime importance to obtain HDPE/PA12/YP MFCs with improved tensile strength.

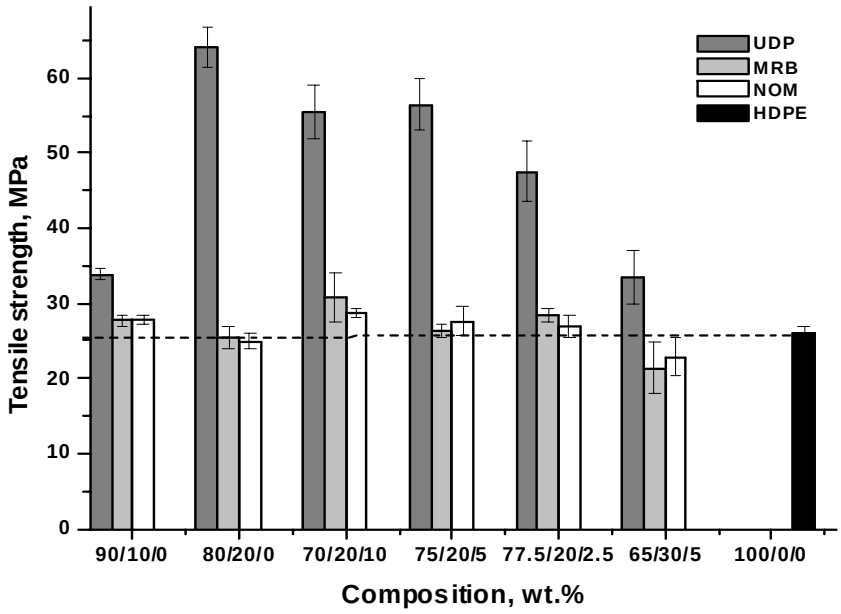

Figure 11.5 Longitudinal tensile strength $\sigma_{1\max}$ of HDPE/PA12/YP UDP, MRB and NOM composites, and the HDPE matrix

Summarizing, all anisotropic PA12 reinforced composites show quite similar tensile characteristics in both longitudinal and transverse directions, which was not the case with the PA6 composites of the same type. The structural studies in the next chapter will shed more light on this issue.

11.2. Flexural tests in plates

In order to assess the flexural stiffness, three-point support flexural tests were performed on plates with HDPE/PA12/YP MFCs as either cross-ply laminates (CPC) or composites produced from middle length randomly distributed bristles (MRB). For comparison, tests with NOM composites and HDPE were also performed. The flexural tests were carried out according to [2] and test details and data handling are given in Chapter 2. Analogously to the PA6 reinforcement, the test specimens were in the form of rectangular plates (100/155 mm) a shape already discussed in Chapter 8.

From the experimental load *vs.* displacement curves the slope S_p at 1 mm displacement was determined and the flexural stiffness, C_R, was estimated using the equation 2.12 in Chapter 2.

The improvement factor, IF, was calculated as the ratio between the difference in the flexural stiffness of the laminate and of the HDPE, with respect to the HDPE, in percentage.

CPC Laminate Composites

The data from flexural tests for HDPE/PA6/YP CPC are summarized in Table 11.6.

Table: 11.6. Three-point Support Flexural Test of HDPE/PA12/YP CPC MFCs

Composition HDPE/PA12/YP wt.%	**Slope** S_p N/mm	**Average thickness,** h mm	**Flexural stiffness,** C_R GPa	**Improvement factor,** IF %
100/0/0	11.361	2.002	1.478 ± 0.057	0
90/10/0	11.970	1.743	2.362 ± 0.067	59.8
80/20/0	21.599	1.915	3.214 ± 0.203	117.5
70/20/10	22.452	1.902	3.404 ± 0.591	130.3
75/20/5	23.369	2.012	2.980 ± 0.315	101.6
77.5/20/2.5	23.555	1.936	3.384 ± 0.287	129.0
65/30/5	33.595	2.034	4.185 ± 0.530	183.2

All CPC composites show improved flexural performance with the stiffness values in the range between 2.4 GPa, for the least concentration of reinforcing PA12 phase, and 4.2 GPa for the composition containing 30% PA12. The corresponding improvement factor, *IF,* varies between 60 and 180%. It can be noted that the best flexural performance is achieved by the composite with the highest amount of PA12. All systems containing 20% PA12 display similar flexural stiffness, revealing a low influence of the compatibilizer. Contrary to the PA6 reinforcement, the 70/20/10 CPC MFC with a PA 12 phase has the notable IF of 130%.

MRB Laminate Composites

Table 11.7 summarizes the flexural test data of the HDPE/PA12/YP MFCs prepared by middle length randomly distributed bristles (MRB).

Table 11.7 Three-point Support Flexural Test Data of HDPE/PA12/YP MRB MFCs

Composition **HDPE/PA12/YP** wt.%	**Slope** S_p N/mm	**Average thickness,** h mm	**Flexural stiffness,** C_R GPa	**Improvement factor,** IF %
100/0/0	11.361	2.002	1.478 ± 0.057	0
90/10/0	10.702	1.699	2.280 ± 0.140	54.3
80/20/0	21.727	1.956	3.019 ± 0.500	104.3
70/20/10	17.830	1.854	2.913 ± 0.497	97.1
75/20/5	16.990	1.728	3.447 ± 0.222	133.2
77.5/20/2.5	23.762	1.946	3.365 ± 0.368	127.7
65/30/5	16.781	1.814	2.933 ± 0.254	98.4

The following observations can be made in relation to these composites in which one can observe the effect of the alignment of the reinforcing phase. Generally, all these systems have flexural performance better than the matrix, the IF values, however, being lower than those of the respective CPC composites. Another observation is that the flexural stiffness in the case of MRB composites is not directly related to the PA12 content. Whereas there is a clear improvement of the flexural stiffnesses when the PA12 content is increased from 10 to 20%, the transition to 30% does not lead to any positive IF change. In the case of the 20% PA12-containing MRBs, the influence of the YP content becomes more pronounced, the highest IF values being displayed by the composites without any or with little amounts of compatibilizer.

NOM Laminate Composites

The flexural tests data for the HDPE/PA12/YP composites produced from NOM are summarized in Table 11.8. It gives an insight on how an isotropic PA12 reinforcing phase influences the flexural stiffness of the matrix. Unlike the CPC and MRB composites, the respective NOM composites do not show a significant difference when changing the PA12 concentration in the 10-30% range.

Apparently, when the reinforcing phase is not oriented and is randomly distributed within the matrix, factors such as chemical interactions between the HDPE and PA12 phases influence more the flexural behavior. In this case the content of compatibilizer becomes of prime importance, the higher the YP content, the lower the IF values.

Table: 11.8 Three-point Support Flexural Test of HDPE/PA12/YP NOM Composites

Composition HDPE/PA12/YP wt.%	**Flexural modulus,** S_p N/mm	**Average thickness,** h mm	**Flexural stiffness,** C_R GPa	**Improvement factor,** IF %
100/0/0	11.361	2.002	1.478 ± 0.057	0
90/10/0	15.546	1.743	3.056 ± 0.453	106.8
80/20/0	20.873	1.790	3.799 ± 0.339	157.0
70/20/10	12.666	1.749	2.475 ± 0.273	67.5
75/20/5	14.870	1.768	2.817 ± 0.312	90.6
77.5/20/2.5	17.875	1.737	3.553 ± 0.254	140.4
65/30/5	16.655	1.758	3.196 ± 0.232	116.2

A comparison between all types of HDPE/PA12/YP composites concerning their flexural stiffnesses is plotted in Fig. 11.6. It can be seen that PA12 is useful for reinforcement of HDPE since all HDPE/PA12/YP composites prepared as MFCs or NOMs possess flexural moduli better than HDPE. Even a small percentage of 10% PA12 improves the flexural stiffness of the matrix. In the compositions with 20% PA12, there is no significant difference between the flexural performance of the respective CPC, MRB or NOM composites, *i.e.*, it does not really matter if the reinforcement is distributed randomly or oriented. The alignment of the PA12 fibrils does not seem to be important, either.

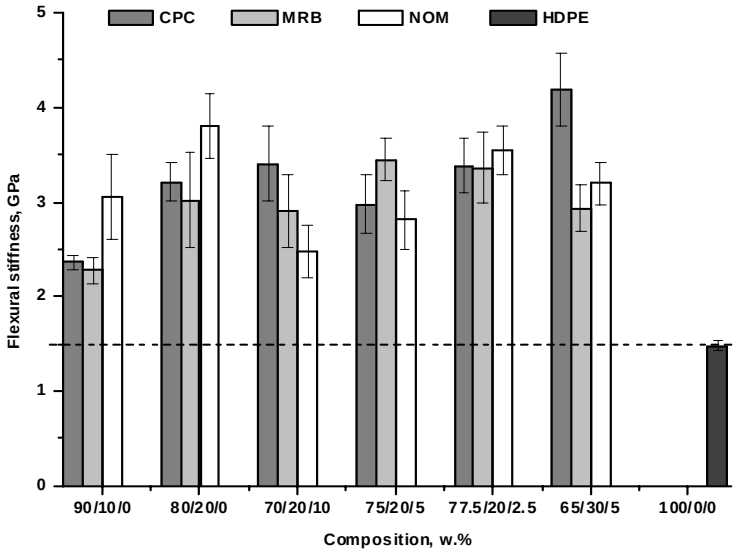

Figure 11.6 Comparative chart of the flexural stiffness of all HDPE/PA6/YP composites studied

It is noteworthy that increasing the PA12 amount to 30% (65/30/5 composites) resulted in superior flexural stiffness with the highest IF value only in the cross-ply laminates (CPC). The respective MRB and NOM composites showed improvement factors comparable to those of the samples with 20% reinforcement only.

11.3. Impact resistance tests of HDPE/PA12/YP composites

The next objective was to investigate the impact resistance of the HDPE/PA12/YP composites as a function of the composition and reinforcement type. As in the case of PA6, CPC laminates formed by compression molding of two mutually perpendicular unidirectional laminae were tested. For comparison, MRB and NOM composites as well as the HDPE matrix were also studied. Details about the test and data handling are given in Chapter 2, part 2.3.5. The impact performance was studied in the same way as for the PA6 reinforced composites already discussed in Chapter 8.

The peak and total energies per unit thickness of all PA12 reinforced samples are given in Figure 11.7 as a function of composition. Analyzing Figure 11.7 (a), it can be seen that in the PA12-reinforced CPC MFCs both peak and total impact energies are higher than those of the matrix, whereby the increase of the latter energy is more pronounced. This means that the composite has better toughness (higher peak energy) and is more ductile (higher total energy) that the plain HDPE plate. The best performance was registered with the 70/20/10 composition with total impact strength almost twice that of the matrix. Interestingly, even the 65/30/5 composition which was definitely inferior in the PA6 CPCs, in the case of PA12 reinforcement shows some improvement of the impact performance. As regards the compatibilizer amount, its influence is not so obvious. Nevertheless, large concentrations of compatibilizer seem to favor the impact behavior.

All MRB composites (Figure 11.7, b), display peak energies lower than that of the HDPE, while the total energy is equal or slightly higher than that of the matrix. This means that the sample failure starts with less energy but requires more energy to propagate. Apparently, the randomly distributed PA12 fibrils are less efficient for impact reinforcement than those aligned in the cross-ply laminates.

Most of the composites obtained from NOM precursors (Figure 11.7, c) show strong decline of the impact resistance since the peak and total energies are far below the HDPE matrix. Only two compositions - 90/10/0 and 70/20/10 – achieved an impact resistance close to that of HDPE.

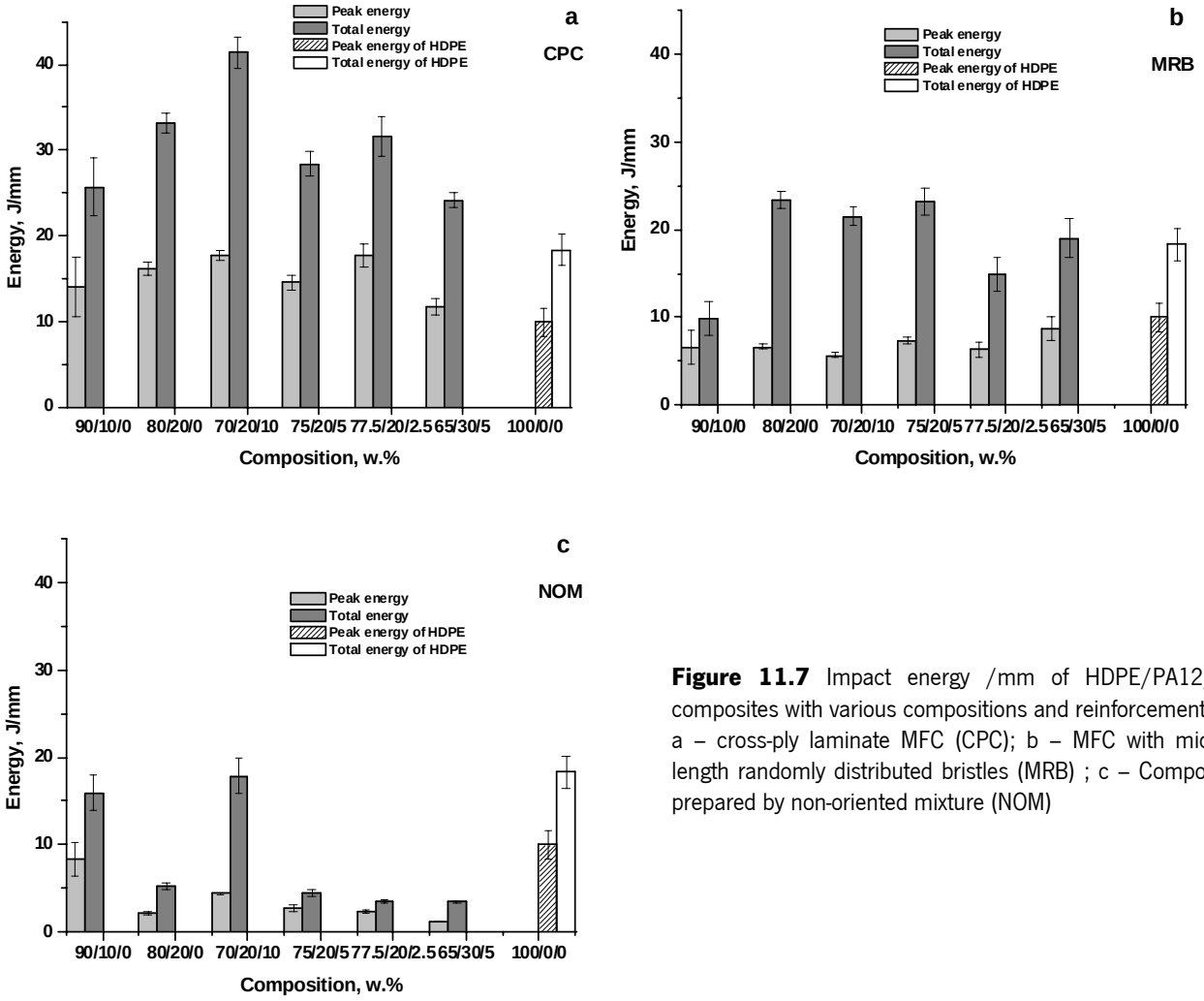

Figure 11.7 Impact energy /mm of HDPE/PA12/YP composites with various compositions and reinforcement: a – cross-ply laminate MFC (CPC); b – MFC with middle length randomly distributed bristles (MRB) ; c – Composite prepared by non-oriented mixture (NOM)

Consequently, the addition of the non-oriented PA12 phase in the studied concentration range does not lead to any improvement of the impact performance of the HDPE matrix.

The next two figures depict better the comparison between the impact characteristics of all HDPE/PA12/YP composites. It is shown in the Figure 11.8 that the improvement of the peak energy only occurs in the CPC composites within the entire range of PA12 and YP concentrations. All MRB compositions are worse than the HDPE. From the composites based on non-oriented precursors, only the 90/10/0 system displays a peak energy similar to HDPE. Apparently, the presence of the oriented and aligned PA12 phase is of decisive importance for impeding the start of the impact failure.

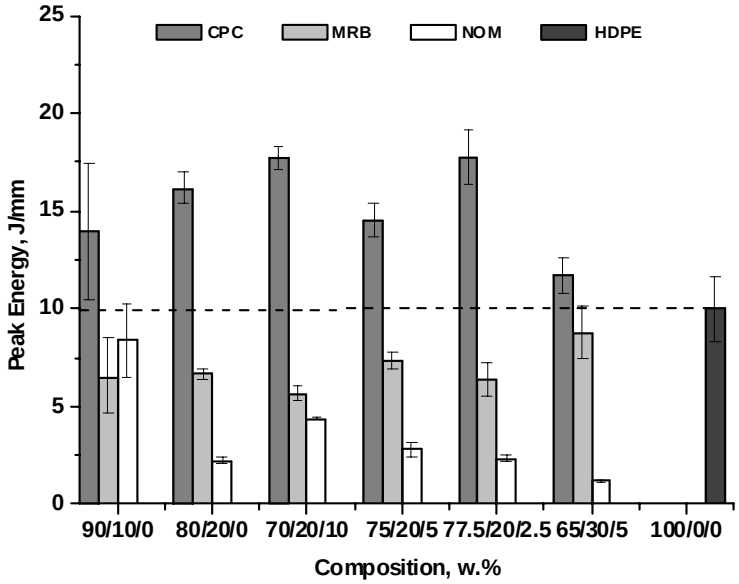

Figure 11.8 Peak energy per unit thickness of HDPE/PA12/YP composites with various compositions and reinforcement types

As far as the total energy is concerned (Figure 11.9), it is clearly superior in all CPC MFCs. The 80/20/0, 70/20/10 and 75/20/5 MRB compositions display statistically significant improvement in respect to the matrix. The rest of the MRB and NOM samples are either close or considerably worse than HDPE.

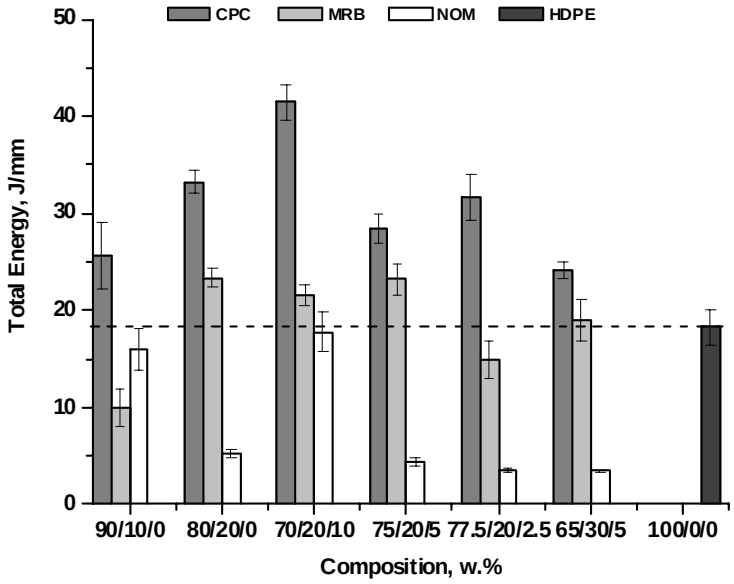

Figure 11.9 Total energy per unit thickness of HDPE/PA12/YP composites with various compositions and reinforcement types

In general, only the CPC laminates showed improved impact characteristics. Obviously, the orientation and the cross-ply alignment of the PA12 fibrils prevails over the other factors that influence the impact strength.

11.4. A Comparison of the Mechanical Properties of PA6 and PA12 Reinforced Composites

Despite the fact that when discussing the mechanical properties of PA12-reinforced composites references to the respective PA6 compositions were frequently made, a direct comparison is given below to help a better assessment of the reinforcing capability of the two polyamides.

Tensile properties

Figure 11.10 compares the longitudinal Young moduli E_1 of all composite types under investigation. Generally, all UDP MFCs are better than the MRB and NOM composites.

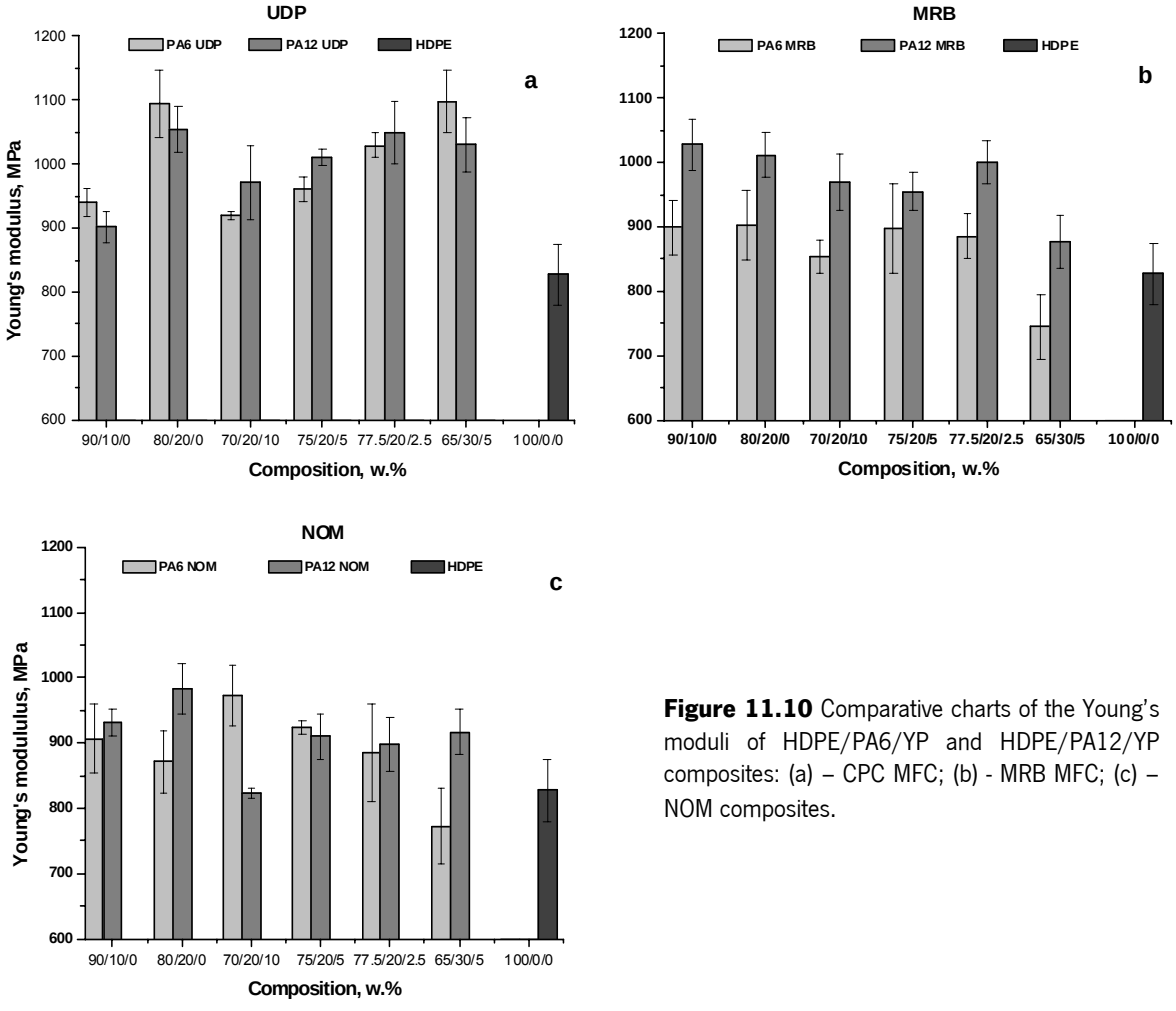

Figure 11.10 Comparative charts of the Young's moduli of HDPE/PA6/YP and HDPE/PA12/YP composites: (a) – CPC MFC; (b) - MRB MFC; (c) – NOM composites.

All UDP compositions (Fig. 11.10, (a)) are stiffer than the matrix. Both PA6 and PA12 UDP show a decrease of the Young's moduli when the YP concentration increases. As a whole, the stiffness of the PA6 and PA12 reinforced composites are quite similar.

This is not the case of the MRB composites (Fig. 11.10 (b)), where the PA12 reinforcement performs better. They have higher Young's moduli than HDPE and the respective PA6 compositions. The PA 6 reinforced composites are as stiff as the matrix or even worse as in the case of 65/30/5 system.

As seen in the Figure 11.10 (c), the NOM composites displayed the lowest E_1 moduli. This was to be expected having in mind the lack of orientation of the reinforcing phase. Two compositions are worth of special attention – the 80/20/0 and 70/20/10 where the influence of the two polyamides is completely different. The positive effect of PA12 is observed in the absence of compatibilizer, whereas the reinforcing action of PA6 is more effective at the highest YP concentrations. This difference is most probably caused by reasons related to the chemical structure.

Considering the tensile properties in general, another question about the influence of the structure arises. Based on the structure-properties investigations of the two polyamides in oriented state (Chapters 4 and 6), it would be expected a better performance of all PA6-reinforced composites, which was not confirmed in the experiments. The possible explanation will be looked for after X-ray structural studies.

Impact resistance

Figure 11.11 compares the peak and the total impact energies per unit thickness of PA6- and PA12 CPC, MRB and NOM composites. The data are quite heterogeneous and do not suggest clear trends. Nevertheless, as regards the CPC systems (Fig. 11.11 (a)), PA12 reinforcement leads to improvement of the peak energy values, which are higher than the HDPE and the similar PA6 compositions. This means that the PA12 reinforcement in the CPC laminates works better as far as the peak energy is concerned. However, in respect to the total energy (Fig.11.11 (b)) the comparison with PA6 is not so clearly in favor of PA12. The PA6 systems without (80/20/0) or with low YP concentrations (77.5/20/2.5) are better than the equivalent PA12 reinforced composites. The same considerations are valid also for the MRB composites with PA6 and PA12 (Figure 11.11 (c), (d)) although the peak and total energies here are lower than the respective CPC composites. In most of the MRB compositions the two energies are close or lower than HDPE marix.

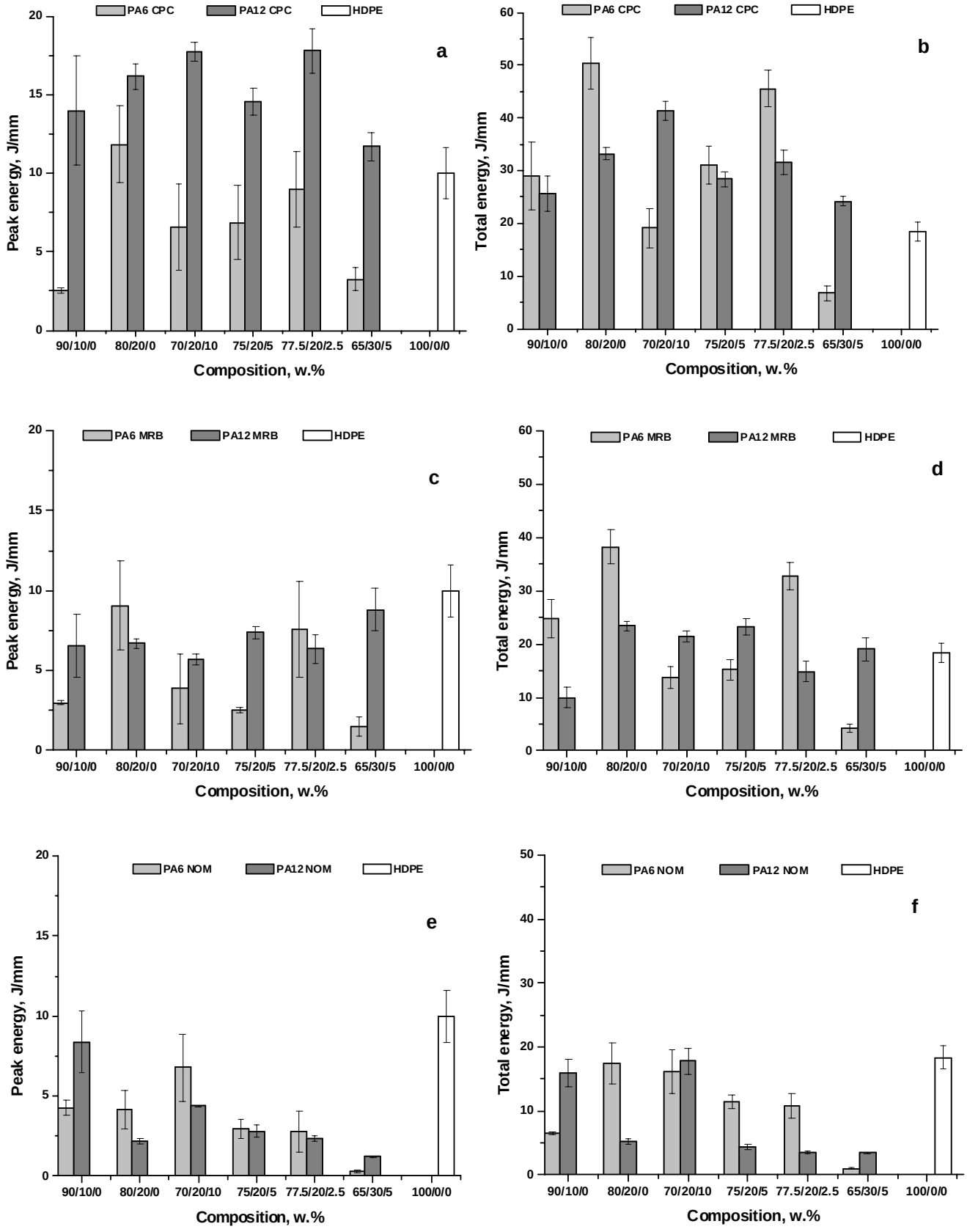

Figure 11.11 Comparative Impact test of HDPE/PA6/YP and HDPE/PA12/YP composites: (a);(b) – Peak and Total energies of CPC MFCs; (c);(d) – Peak and Total energies of MRB MFCs; (e);(f)– Peak and Total energies of NOM composites.

The absence of orientation of the reinforcing component (Figure 11.11 (e), (f)) leads to a considerable decline of the toughness in both PA6 and PA12 NOM systems.

A clear indication of these experiments is that the full potential of the PA6 and PA12-MFCs in impact is only reached when the material is used in laminates.

Flexural behavior

The three-point flexural test is perhaps the only one where both PA6- and PA12 composites undoubtedly showed better performance in all compositions under investigation in the form of CPC, MRB and NOM (Figure 11.12 (a)-(c)).

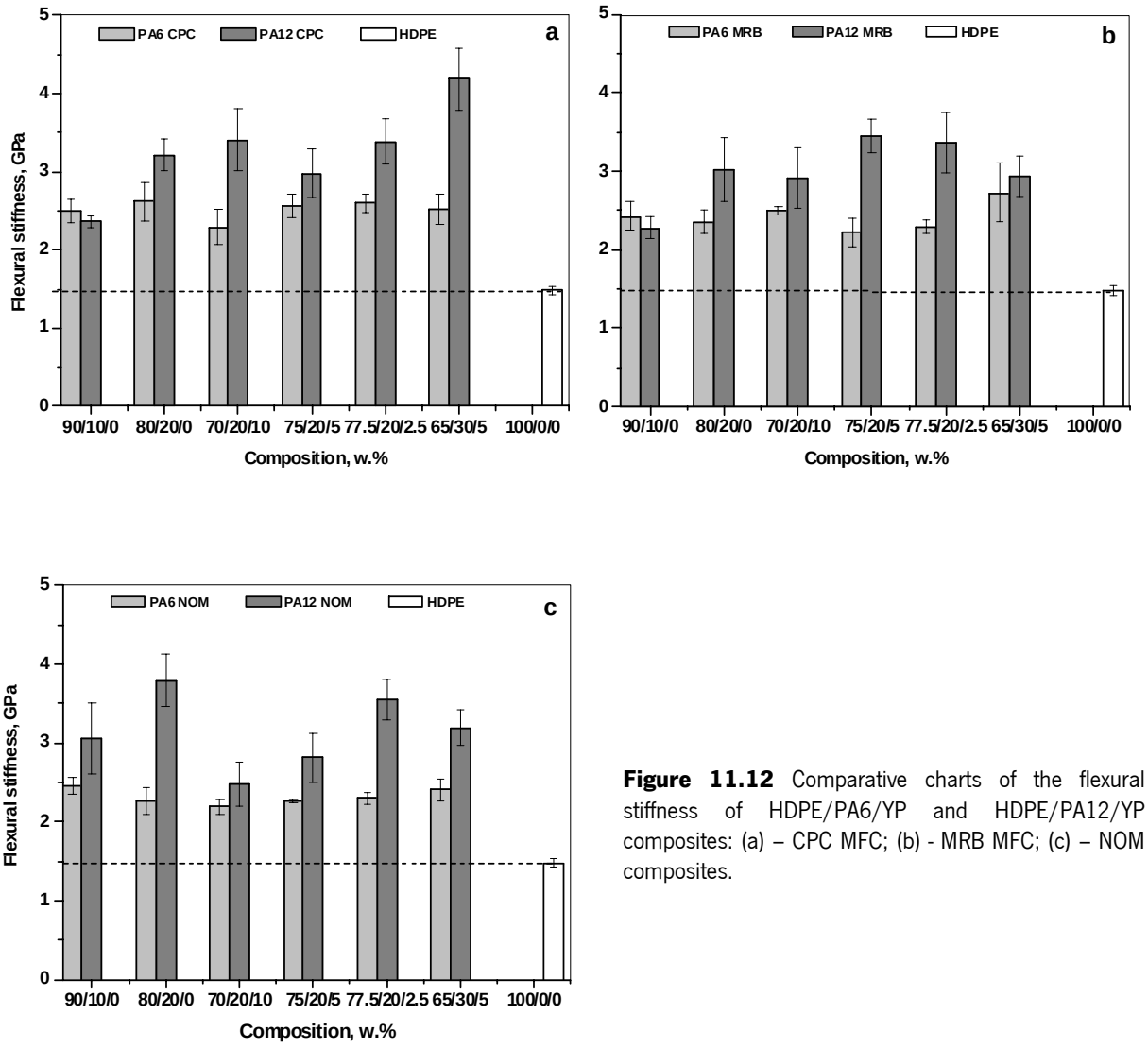

Figure 11.12 Comparative charts of the flexural stiffness of HDPE/PA6/YP and HDPE/PA12/YP composites: (a) – CPC MFC; (b) - MRB MFC; (c) – NOM composites.

Irrespective of the orientation and alignment of the reinforcing phase, all samples display notably better flexural stiffnesses, C_R, as compared to the HDPE, even with the lowest polyamide content. Although there is no big difference in the flexural behavior of the CPC, MRB and NOM composites, those with oriented polyamide phase, either PA6 or PA12, perform better.

As a whole, the PA12 containing composites showed better flexural behavior, keeping higher C_R values in all systems studied. The improvement varies in the range of 60-180% for the PA12 laminates and between 50 and 90 % for the PA6 laminates. From all compositions the best performing composite was based on PA12 65/30/5 CPC that displays a C_R of 4.2 GPa, which is 2.8 times higher than the respective HDPE value.

11.5 References

1. Powell PC, *Engineering with Fiber-Polymer Laminates,* Chapman & Hall, London, UK, p. 23 (1994).
2. Nunes JP, Pouzada, AS, Bernardo CA, *Polym Testing* **21**:27 (2002).

CHAPTER 12

RELATIONSHIP BETWEEN STRUCTURE AND MECHANICAL PROPERTIES IN PA12 REINFORCED NANOCOMPOSITES

12.1. Introduction

The main goal of this chapter is an in-depth investigation of the structure of the PA12 reinforced MFCs. This is necessary in order to understand better the nature of the reinforcing effect of the PA12 phase, to enable a comparison with the PA6 reinforcement and to relate the structure and the mechanical properties of the PA12 containing MFCs. The same approach was applied as in Chapter 9, using ^{13}C solid state NMR and synchrotron WAXS and SAXS methods to study UDP MFCs.

12.2 Crystalline Structure of the PA12 Reinforcing Phase

Solid state ^{13}C CP-MAS NMR spectroscopy was used to evaluate qualitatively two selected HDPE/PA12/YP MFC samples with 10 wt. % PA12 (no compatibilizer) and with 20 wt. % of PA12 (with compatibilizer), at 20°C. The extended aliphatic regions of the two samples are shown in Figure 12.1. To facilitate the analysis, the spectrum of HDPE in the same range is also presented, as well as that of PA12 in γ-isotropic and γ'-oriented crystalline forms. These forms were studied in detail in Chapters 5 and 6. As pointed out there, the α crystalline form is not very usual for PA12 at normal conditions (30°C, atmospheric pressure). Small amounts of α-fraction (4-15%) were discovered in PA12 samples obtained by either cold drawing or compression molding (Chapter 6, Table 6.3). As seen from Figure 12.1 (a) and (b), curve 5, the oriented polymer blend (OC) contain a weak signal at 42.5 ppm ascribed to the C nucleus next to the N atom (C_N). This resonance line is the most characteristic for the α PA12 and can be used for its identification. The αC_N resonance appears also in the spectra of the composites (Fig. 12.1, curves 4), being better expressed in the compatibilized sample (Fig. 12.1 (b)). The reason could be related either to the presence of compatibilizer YP, or due the fact that this sample contains twice as more PA12. By all means, one should expect the presence of α PA12 in the composites. The NMR traces reveal also the peaks characteristic of the oriented γ' PA12, whose detailed description could be found in Chapter 5.

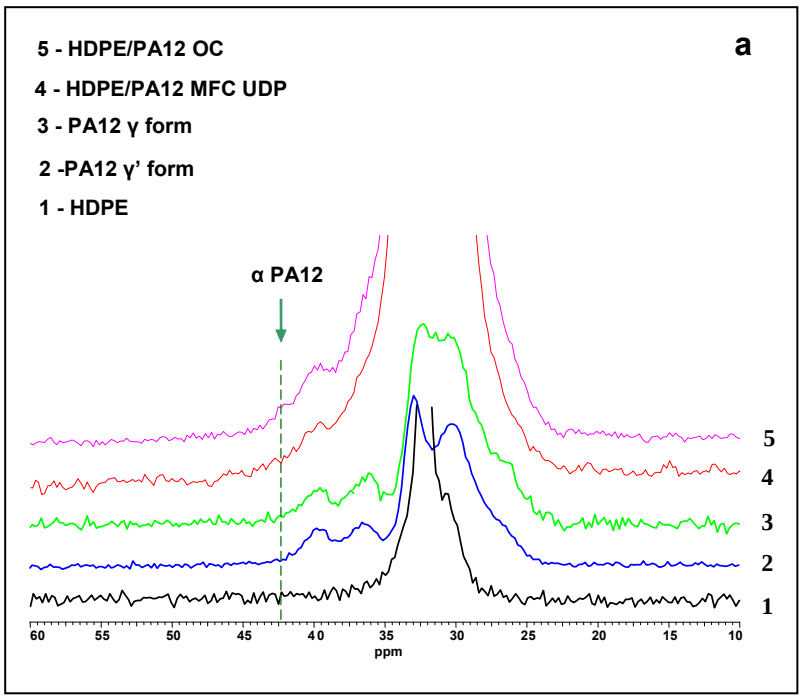

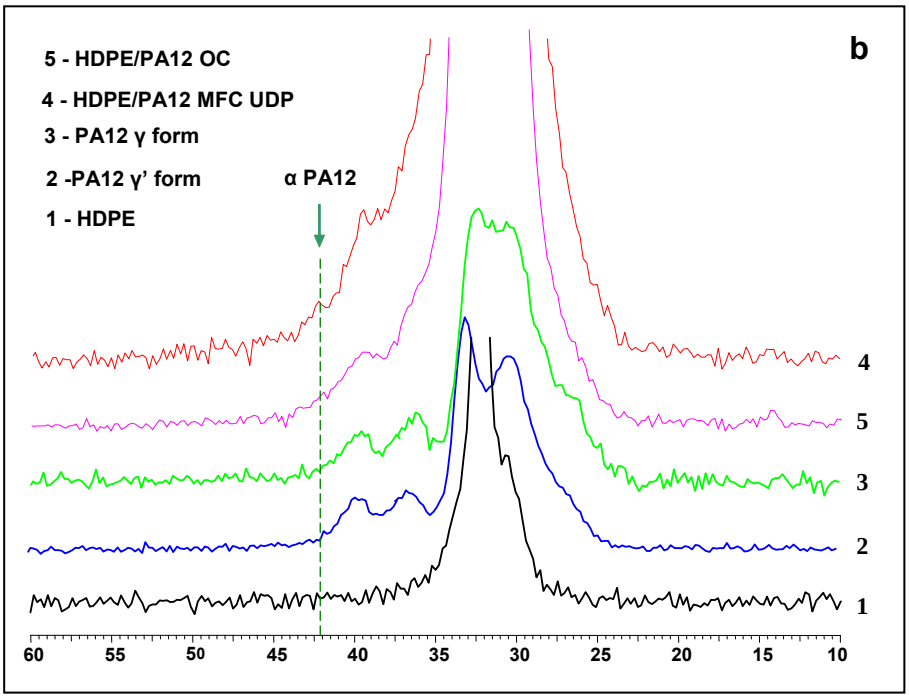

Figure 12.1 CP-MAS NMR spectra of two HDPE/PA12/YP UDP MFCs at 20°C: (a non-compatibilized 90/10/0 and b – compatibilized 70/20/10 system. To enable comparison, the figures contain also the traces of neat HDPE, γ PA12 (isotropic) and γ' PA12 (oriented) forms.

As in the case of the PA6-containing blends and composites, the solid state NMR does not allow for quantification of the polymorph amounts. This analysis was made by WAXS.

As was shown in Chapter 10, where the structure development in the HDPE/PA12/YP composites was discussed (Figure 10.7), the 2D WAXS patterns at 30°C show an almost complete overlapping of the crystalline reflections of PA12 and HDPE, which makes the assessment of the PA12 polymorph content at room temperature rather difficult. Hence, the patterns were studied at 160°C, *i.e.*, after melting of the HDPE matrix. These images were calibrated, background corrected and integrated over the whole range of scattering angles. The resulting curves are plotted in Figure 12.2. It can be seen that the (020) reflection (the arrow at 2θ of *ca.* 5°), which is characteristic of oriented γ PA12 form and appears at the meridian in the 2D WAXS patterns, is present in all compositions. In the case of 65/30/5, the shoulder appearing at *ca.* 11° is caused by the γ (040) reflection. The unresolved reflection at *ca.* 21° corresponds to the (002) reflection of the α polymorph.

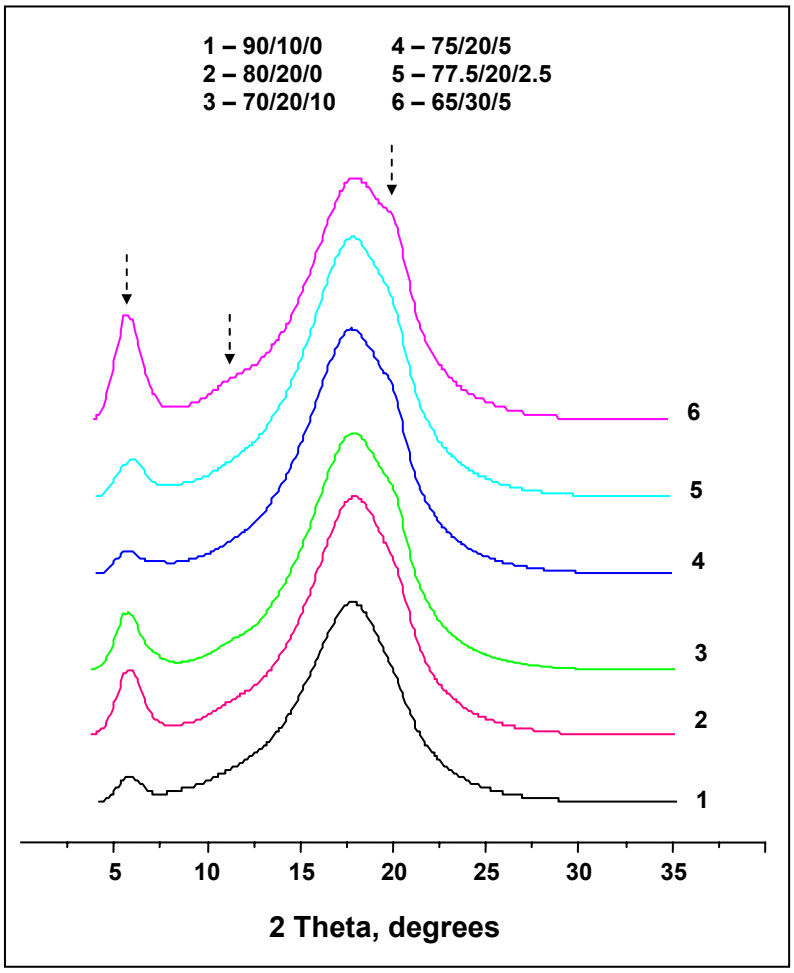

Figure 12.2 Stacked plot of 1D WAXS curves of HDPE/PA12/YP UDP MFCs at 160°C. The arrows point at specific reflections that change as a function of composition

The 1D WAXS curves were treated afterward with peak-fitting software as described in the Experimental part. Figure 12.3 exemplifies the fit of the 70/20/10 UDPE MFC at 160°C.

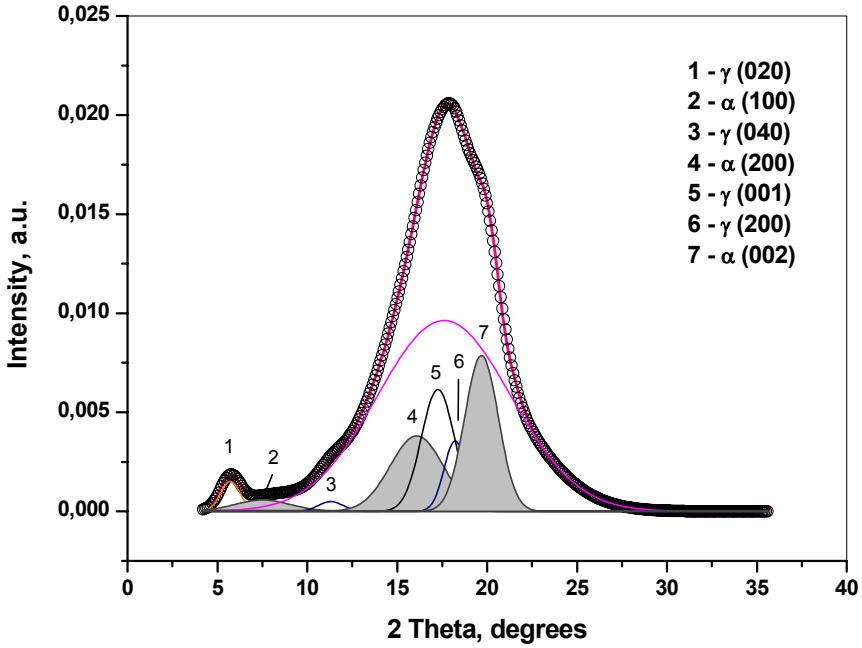

Figure 12.3 Peak fitting of 1D WAXS curve of the 70/20/10 UDP MFC at 160°C

There is overlapping of many reflections in the 2θ range studied, but with the help of the results obtained from the detailed investigation on neat PA12 (Chapters 5 and 6) their identification was possible in the composites. The deconvoluted reflections of the two PA12 polymorphs in the order of increasing 2θ are as follows: γ(020); α(100); γ(040); α(200); γ(001); γ(200); α(002). As seen from Fig. 12.3, there exist considerable amounts of α PA12 (the shaded peaks) in the 70/20/10 MFC. This observation is in good agreement with the solid state NMR studies. Table 12.1 summarizes the data extracted from the peak-fitting of the 1D WAXS curves of all HDPE/PA12/YP UDP MFCs at 160°C. The crystallinity index of the PA12 fibrils varies between 35-43%, which is slightly lower than the percentage in the neat oriented PA12 at the same temperature (48%, Chapter 5, Table 5.3). In all compositions, the PA12 is a mixture of two polymorphs – α and γ, in different proportions. The γ/α relation is the biggest (γ/α = 2.1) in the 90/10/0 composition. Within the samples containing 20% PA12, the γ polymorph is predominant in the 80/20/0 system (γ/α = 1.48), while the 70/20/10 composite containing the biggest YP concentration is richer in α form (γ/α = 0.65). Apparently, increasing the compatibilizer content favors the crystallization of PA12 in its α form.

Based on the angular 2θ positions, the d-spacings of the corresponding crystalline planes were calculated and are presented in Table 12.2. It can be noted that the d-spacings of the γ001 and γ200 planes in the PA12 reinforcing phase are slightly larger (by *ca.* 10%) than those found in the neat oriented PA12 at the same temperature, while of the γ020 almost coincide (Table 5.3., Chapter 5).

The d-spacings of the α-form displayed larger deviations between 15-20%, as compared to the neat oriented PA12.

Table 12.1 PA12 polymorph content in HDPE/PA12/YP MFCs at 160°C

Composition HDPE/PA12/YP wt. %	Vol. fract. of PA12, V_f	α form, %	γ form, %	γ/α	CI, %
90/10/0	0.094	11.3	23.8	2.10	35.1
80/20/0	0.189	16.9	25.0	1.48	41.9
70/20/10	0.188	23.7	15.4	0.65	39.1
75/20/5	0.189	19.6	23.7	1.20	43.3
77.5/20/2.5	0.189	20.0	21.2	1.06	41.2
65/30/5	0.285	20.5	20.7	1.01	41.2
0/100/0* or	-	-	48.4	-	48.4

Notes: CI = crystallinity index. CI = αCI + γCI; αCI = α(100) + α(200) + α(002); γCI = γ(020) + γ(040) + γ(001) + γ(100). *Value taken from Table 5.3. The neat oriented PA12 does not show any α form reflections.

Table 12.2 Angular positions and d-spacings of PA12 reflections in HDPE/PA12/YP MFCs at 160°C

WAXS	HDPE/PA12/YP UDP MFC Compositions											
	90/10/0		80/20/0		70/20/10		75/20/5		77.5/20/2.5		65/30/5	
	2θ, deg.	$d_{(hkl)}$ Å	2θ, deg.	$d_{(hkl)}$ Å	2θ, deg.	$d_{(hkl)}$ Å	2θ, deg.	$d_{(hkl)}$ Å	2θ, deg.	$d_{(hkl)}$ Å	2θ, deg.	$d_{(hkl)}$ Å
γ(020)	5.86	14.67	5.86	14.68	5.66	15.20	5.73	15.02	5.98	14.38	5.71	15.06
α(100)	-	-	-	-	6.68	12.88	7.57	11.36	-	-	7.78	11.05
γ(040)	-	-	11.09	7.76	11.40	7.55	11.30	7.62	-	-	11.27	7.64
α(200)	15.84	5.44	15.60	5.53	15.70	5.49	16.09	5.36	16.08	5.36	16.22	5.32
γ(001)	17.37	4.97	17.16	5.03	17.37	4.97	17.26	5.00	16.87	5.11	17.52	4.93
γ(200)	18.23	4.73	18.32	4.71	18.46	4.67	18.22	4.74	18.08	4.78	18.40	4.69
α(002)	19.93	4.33	19.83	4.36	19.91	4.34	19.69	4.39	19.83	4.36	19.79	4.36

As in the case of PA6 composites, the structure investigations continued by studying the polyethylene component of the MFC composite, particularly the oriented HDPE material found in the transcrystalline layer at the matrix-fibril interface.

12.3 Transcrystallization of HDPE in the presence of oriented PA12

The HDPE transcrystallization was studied in the UDP lamina where the reinforcing PA12 fibrils are unidirectionally aligned. Synchrotron WAXS and SAXS were employed as with the PA6-reinforced systems using the same image processing detailed in Chapter 9. The conditions common for all X-ray experiments are given in Chapter 2.

12.3.1 2D WAXS analysis

Based on the preliminary X-ray studies on the structure development during processing of HDPE/PA12/YP MFCs (Chapter 10, Figs. 10.7 and 10.8), shell-core morphology of the reinforcing PA12 fibrils was suggested. To separate the contribution of the isotropic and oriented crystalline fractions and to study their origin, the 2D WAXS patterns were processed with POLAR 2.7.1 X-ray software [1] after correcting for the incident beam and subtracting the empty chamber scattering. In this data handling, the total scattered intensity is separated into two contributions – isotropic and oriented [2]. The isotropic scattering originates from the amorphous domains and from the unoriented crystals. The oriented component is due to the all oriented scatterers calculated by subtracting the azimuthally independent component from the total scattered intensity. Figure 12.4 exemplifies this treatment for the 80/20/0 (a) and 70/20/10 (b) HDPE/PA12/YP systems.

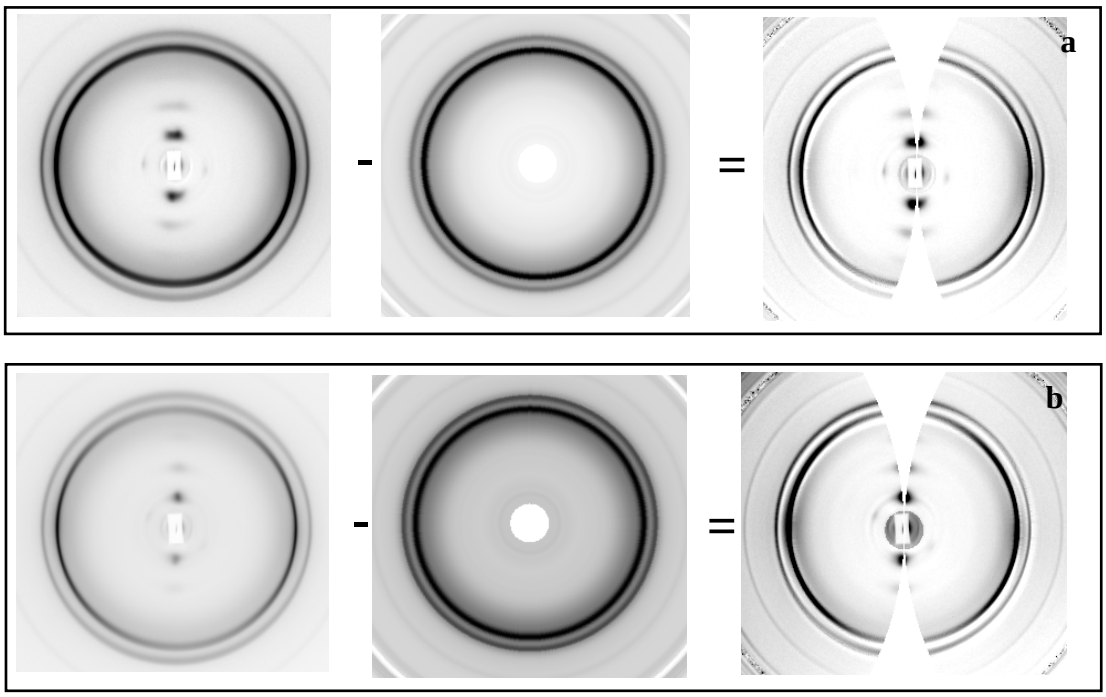

Figure 12.4 Example of the analysis of the WAXS patterns at 30°C of UDP MFCs: Left – total scattered intensity; Center: calculated isotropic intensity; Right: oriented scattered intensity. (a) 80/20/10 and (b) 70/20/10. The fiber axis is vertical; b-axis is the fiber axis.

The images on the left represent the total scattered intensity and, judging from the meridional point-like reflections characteristic of the (0k0) crystalline planes, they clearly show the presence of oriented γ PA12 fraction. Higher order reflections of this type suggest considerable orientation of the reinforcing fibrils (**b**-axis is the fiber axis). The two Debye rings that belong to the (110) and (200) reflections of the orthorhombic HDPE are not entirely isotropic – their intensity on the equator is stronger. However, in the same 2θ region appears the scattering from the (h00) and (00l) crystalline planes of the two PA12 polymorphs. Subtracting the computer generated isotropic scattering (central images) allows finding out if the HDPE phase gives some contribution to the equatorial anisotropy of the scattering. The right images in Figure 12.4, obtained after subtraction, clearly show the reflections of oriented HDPE. This is an indication for epitaxial crystallization of matrix material upon the reinforcing fiber, whereby the chain direction in the matrix crystals coincides with that in the reinforcing PA12 fibrils. This observation is valid for both type of samples – non-compatibilized (a) and compatibilized (b).

The results of the subtraction procedure are better seen in 3D (Figure 12.5), where two different projections of the same WAXS pattern of the 80/20/0 UDP MFC are presented. One can observe the anisotropy of the (110) and (200) HDPE reflections (left), as well as some of the oriented equatorial and meridional reflections of the PA12 phase (right). The numbers indicate some of the reflections of PA12: 1 – α(100); 2 – γ(020); 3 – γ(040); 4 – α(200). The remaining PA12 reflections coincide with those of HDPE and could be revealed only after deconvolution.

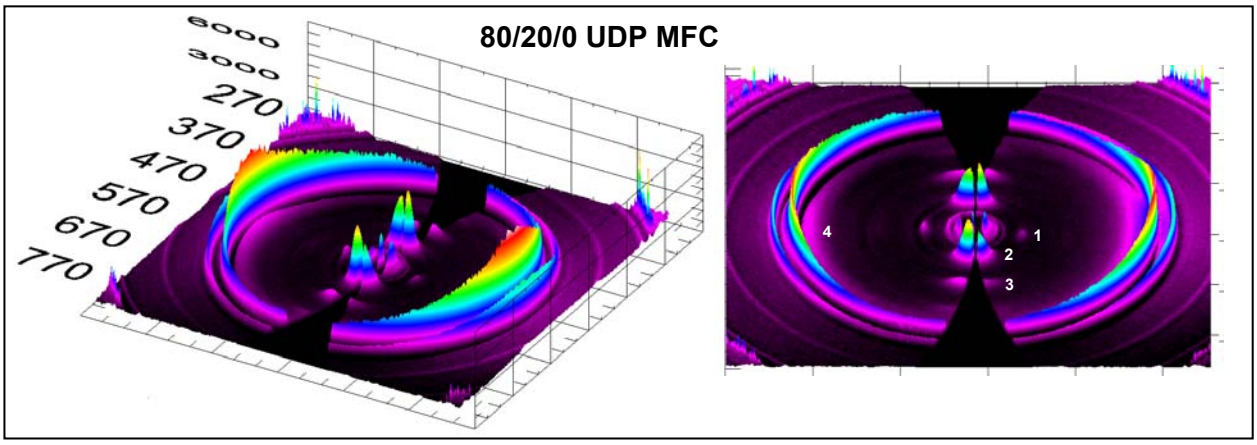

Figure 12.5 Different projections of the 3D WAXS pattern of the 80/20/0 sample after subtraction of the isotropic component from the total scattered intensity The numbers indicate the following PA12 crystalline planes: 1 – α(100); 2 – γ(020); 3 – γ(040); 4 – α(200).

Thus, the 2D WAXS patterns of both the oriented and the isotropic parts were integrated in the 0-180° range and the respective 1D WAXS profiles were treated afterwards by peak fitting software. The results from peak fitting for 70/20/10 sample are presented in Figure 12.6 (a) and (b).

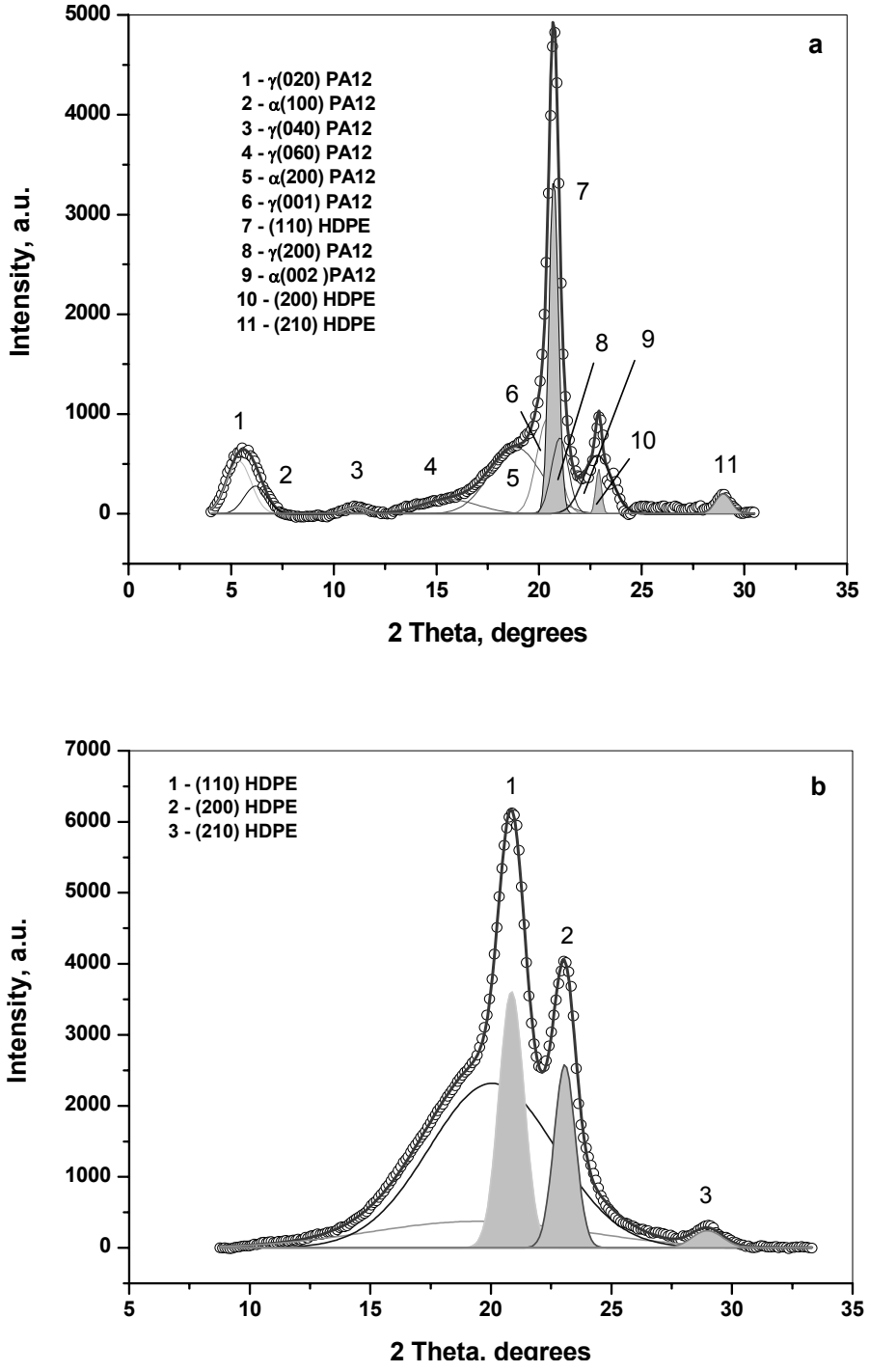

Figure 12.6 1D WAXS profiles of the 70/20/10 HDPE/PA12/YP UDP MFC depicting the peak-fitting of the oriented WAXS scattering (a) and of the isotropic WAXS scattering (b) after the subtraction of (b) from the initial WAXS pattern.

As seen from the deconvolution of the 1D profile of the oriented part (Fig 12.6 (a)), the main reflections of the HDPE (shaded peaks) overlap with those of the α PA12 (5 and 9) and γ PA12 (6 and 8). The following reflexes were identified (given in increasing 2θ order): γPA12(020); αPA12(100); γPA12(040); γPA12(060); αPA12(200); γPA12(001); HDPE(110); γPA12(200); αPA12(002); HDPE(200); HDPE(210). The peak-fitting of the isotropic part displayed crystalline reflections of the HDPE matrix only, indexed as (110), (200) and (210), and of the amorphous halos of PA6 and HDPE, respectively (Figure 12.6, (b)). A quantitative evaluation of the peak-fitting results for two samples, without (80/20/0) and with compatibilization (70/20/10), as well as the data for d-spacings are given in Table 12.3.

Table 12.3 Results from the deconvolution of the oriented and isotropic part of 2D WAXS patterns of selected HDPE/PA12/YP UDP MFC

WAXS Reflections	HDPE/PA12/YP					
	80/20/0			70/20/10		
	2θ, deg.	Content, %	d_{hkl}, Å	2θ, deg.	Content, %	d_{hkl}, Å
Oriented part of WAXS intensity						
(020) – γ PA12	5.22	11.7	16.48	5.39	8.6	15.96
(100) – α PA12	6.10	5.7	14.10	6.20	4.2	13.88
(040) – γ PA12	10.80	1.7	7.97	11.10	0.9	7.76
(060) – γ PA12	15.95	3.3	5.41	15.65	5.4	5.51
(200) – α PA12	18.80	23.1	4.59	18.87	23.0	4.58
(001) – γ PA12	20.29	11.2	4.26	20.41	13.7	4.24
(110) – **HDPE**	20.68	20.6	4.18	20.72	21.0	4.17
(200) – γ PA12	21.47	3.7	4.03	21.02	8.5	4.11
(002) – α PA12	22.78	13.4	3.80	22.84	1.7	3.79
(200) – **HDPE**	22.99	3.5	3.77	22.90	11.0	3.78
(210) – **HDPE**	28.90	2.0	3.01	28.97	2.0	3.00
PA12 oriented scattering, %		73.8			66.0	
HDPE oriented scattering, %		26.2			34.0	
HDPE or.scatt.: PA12 or.scatt.		0.355			0.515	
Isotropic part of WAXS intensity						
(110) – HDPE	20.790	22.4	4.16	20.855	17.2	4.15
(200) – HDPE	23.105	9.5	3.75	23.065	10.5	3.75
(210) – HDPE	28.945	1.0	3.00	28.981	1.4	3.00

Notes - In the isotropic part of the WAXS intensity only the crystalline reflections are included. The difference to 100% will give the content of the amorphous HDPE and PA12 material.

- d_{hkl} is the d-spacing of the respective crystalline plane.

Table 12.3 shows that a part of the HDPE matrix crystallizes oriented along the PA12 fiber thus forming a transcrystalline layer (TCL) in such a way that the chain directions of the two polymers coincide. It can be calculated that 26-34% of the oriented scattered intensity originates from this HDPE and the rest to 100% from oriented PA12 fibrilar material. Thus, the relation between the two intensity components was found to be 0.355 in the non-compatibilized 80/20/0 sample and 0.515 in compatibilized 70/20/10 sample. The d-spacings of PA12 α(200) and γ (001), *i.e.* the intra-sheet distances in the two polymorphs, are slightly larger as compared to the respective values found in the neat PA12 oriented cable. Diversely the inter-sheet distance (*i.e.* α(002) and γ(200)) determined by the planes that contain the H-H bounds almost coincide (Chapter 6, Table 6.4). As regards the HDPE unit cell vectors (Table 12.3), it can be seen that they are almost the same in the bulk and in the transcrystalline layer.

Similar treatment was performed with the 2D WAXS images of all PA12 reinforced UDP MFCs collected at 30°C. Table 12.4 shows the data obtained after peak fitting of the 1D WAXS profiles of the oriented scattering.

Table 12.4 Results from the deconvolution of the oriented part of 2D WAXS patterns of HDPE/PA12/YP UDP MFC

Composition HDPE/PA12/YP Wt. %	**α-PA12** %	**γ-PA12** %	**PA12 Total** %	**HDPE** (oriented) %	***f***	**[HDPE]*** (oriented) wt.%
90/10/0	21.7	43.6	65.3	34.7	0.531	5.31
80/20/0	42.2	31.6	73.8	26.2	0.355	7.10
70/20/10	28.9	37.1	66.0	34.0	0.515	10.30
75/20/5	13.2	54.2	67.4	32.6	0.484	9.68
77.5/20/2.5	19.9	49.0	68.9	31.1	0.451	9.02
65/30/5	23.8	47.3	71.1	28.9	0.406	12.19

Note: - The coefficient ***f*** is the relationship between the HDPE or. and PA12 components of the oriented scattering; The [HDPE] (oriented)***** represents the oriented part of the HDPE matrix material if the PA12 is assumed to be 100% fibrilar.

The α PA12 value corresponds to the overall area of all oriented reflections of PA12 in α form, the γ PA12 is the same for the γ polymorph and the PA12 Total is the sum of the two, respectively. The data show that in all compositions investigated there exist a part of HDPE that crystallizes orientated along the PA12 fibrils. The percentage of this part varies between 26% and 35% of the total oriented

scattering and depends on the PA12 concentration – it is the highest in the sample with 10% PA12 and the lowest in the 65/30/5 composition. If an assumption is made that PA12 phase is 100% fibrilar, the concentration of the oriented [HDPE]* included in the TCL could be calculated. It can be seen that the [HDPE]* increases as the PA12 content in the compositions grows from 10 to 30%. Another observation is that the YP concentration has also an influence – the bigger the YP content, the larger the [HDPE]* amount that crystallizes oriented along the PA12 fibrils.

Furthermore, having in mind the SEM micrographs (Figure 10.1, images 1c - 6c) and the WAXS data (Table 12.4), it is possible to determine the thickness of the layer formed by oriented HDPE crystallized along the PA12 fibrils. The calculations are based on the supposition that the fibrils are cylindrical and uniformly coated with a coaxial transcrystalline layer of HDPE. Table 12.5 encompasses the data of all PA12-reinforced composites whereby the same approach as in the case of PA6-reinforced composites was employed (Chapter 9.4). The idealized presentation of the fiber cross-section in Figure 12.7 explains the designations in the table.

Table 12.5 Fiber characteristics in HDPE/PA12/YP UDP MFCs based on SEM and 2D WAXS data

Composition HDPE/PA12/YP wt. %	$2R_2$ nm	R_2 nm	R_1 nm	TCL nm	$2R_1$ nm	L μm	Real aspect ratio
90/10/0	500	250	202	48	404	42	104
80/20/0	700	350	300	50	600	65	108
70/20/10	560	280	227	53	454	42	93
75/20/5	625	312	256	56	512	15	29
77.5/20/2.5	680	340	282	58	564	25	44
65/30/5	1025	512	432	80	864	54	63

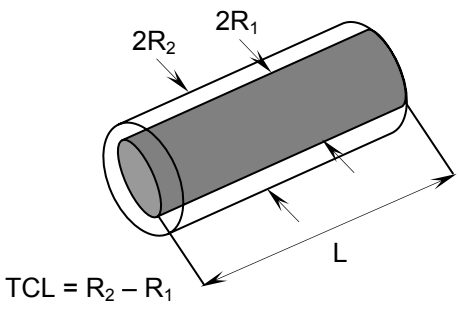

Figure 12.7 Idealized cross-section of the reinforcing fibril HDPE/PA12/YP UDP MFCs

$2R_2$ – average diameter of the fibrils visible by SEM;
R_1 – calculated average radius of the polyamide core of the fibril (Eq. 3)
TCL – average thickness of the transcrystalline HDPE layer;
L – Average length of the fibril calculated from SEM data;
Real Aspect Ratio = $L/2R_1$

As in the case of PA6 reinforcement, one can write:

$$V_f = \pi.R_1^2.L \quad (1)$$

$$V_{TCL} = \pi.L.(R_2^2 - R_1^2) \quad (2)$$

Here V_f is the volume fraction of the crystalline oriented PA6, V_{TCL} is the volume fraction of the crystalline oriented HDPE in the TCL, R_1 is the real PA6 fiber radius, R_2 the visible by SEM fiber radius (PA12 + TCL) and L is the fiber length. Combining Eq. 1 and Eq. 2 results in:

$$R_1 = R_2 \cdot \sqrt{\frac{1}{1+f}} \quad (3)$$

where the coefficient f is the relation between the intensities of the HDPE and PA12 components of the oriented scattering (Table 12.4).

The data from Table 12.5 indicate that the thickness of the HDPE transcrystalline layer is between 48 and 80 nm increasing proportionally to the PA12 content. It should be noted that the compatibilizer concentration does not influence the TCL thickness considerably, remaining in the range of 50-58 nm. As regards the real aspect ratio L estimated on the basis of SEM and WAXS data, the highest values were obtained for the non-compatibilized samples. No clear relationship between L and the YP content is noted. This can be attributed to the broad distribution in the size of the PA12 domains in the non-oriented extrudate (determined by SEM) leading to some error in the calculation of the average diameters and respective volumes.

12.3.2 2D SAXS analysis

Figure 12.8 represent the SAXS images of all of the HDPE/PA12/YP UDP MFCs at 30°C (a), heated in the beam at 160°C (b) and at 30°C after heating at 160°C (c). The initial images at 30°C show the presence of two scattering types: oriented and isotropic appearing at small scattering angles that are not typical of PA12. The PA12 scattering can be clearly observed at 160°C, being oriented along the equator, *i.e.*, in the fiber direction. It should be noted that in all compositions containing compatibilizer the oriented spots are shifting closer to the beamstop that corresponds to larger long spacings. Considering the images at 30°C after heating to 160°C, it can be noted that some oriented scattering also appears in the meridional direction. This is an indication of material with lamellar structure, crystallizing perpendicular to the fiber direction.

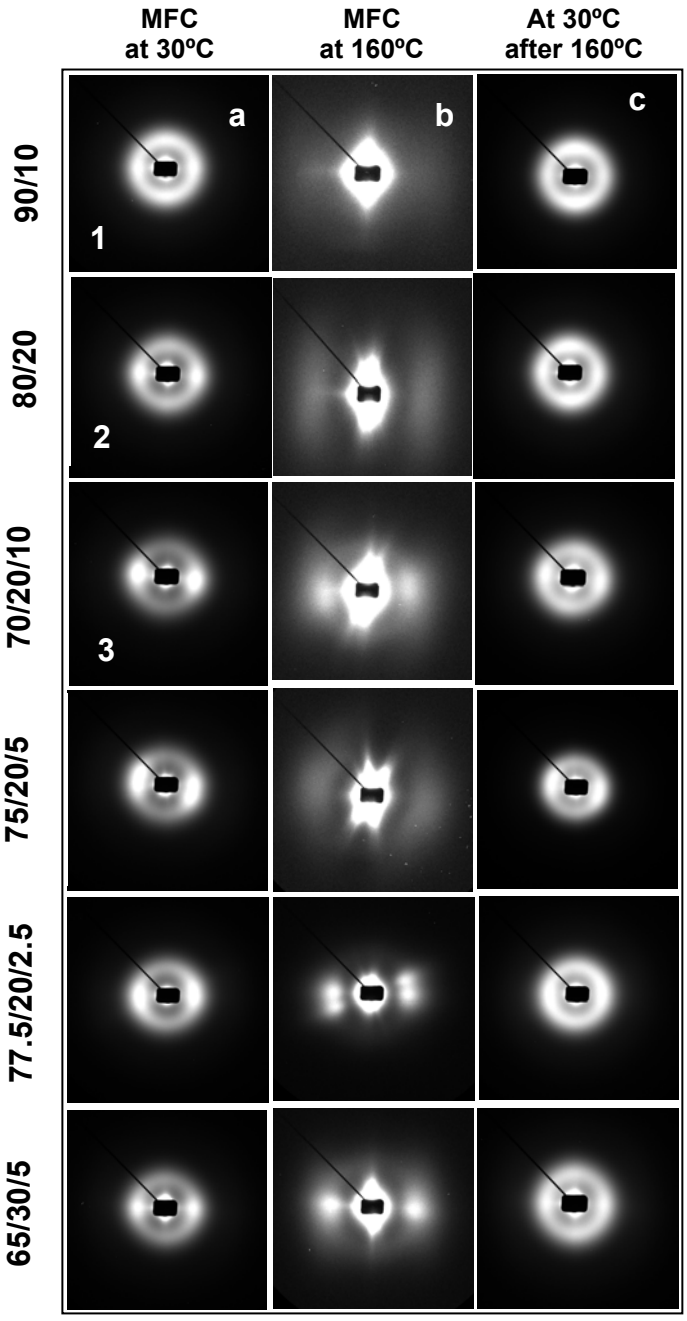

Figure 12.8 2D SAXS images of different HDPE/PA12/YP UDP MFC: column (a) – as prepared, at 30°C; column (b) – at 160°C, in-beam heating; column (c) – at 30°C after heating to 160°C.

The meridional scattering is also observed in the initial images of the non-compatibilized samples – 90/10/0 and 80/20/0. This effect can be better seen in Figure 12.9 that presents the azimuthal scans of the SAXS patterns of composite samples without and with compatibilization at two temperatures: (a) at 30°C (as-prepared composites) and (b) after the heating ramp to 160°C, cooled down to 30°C.

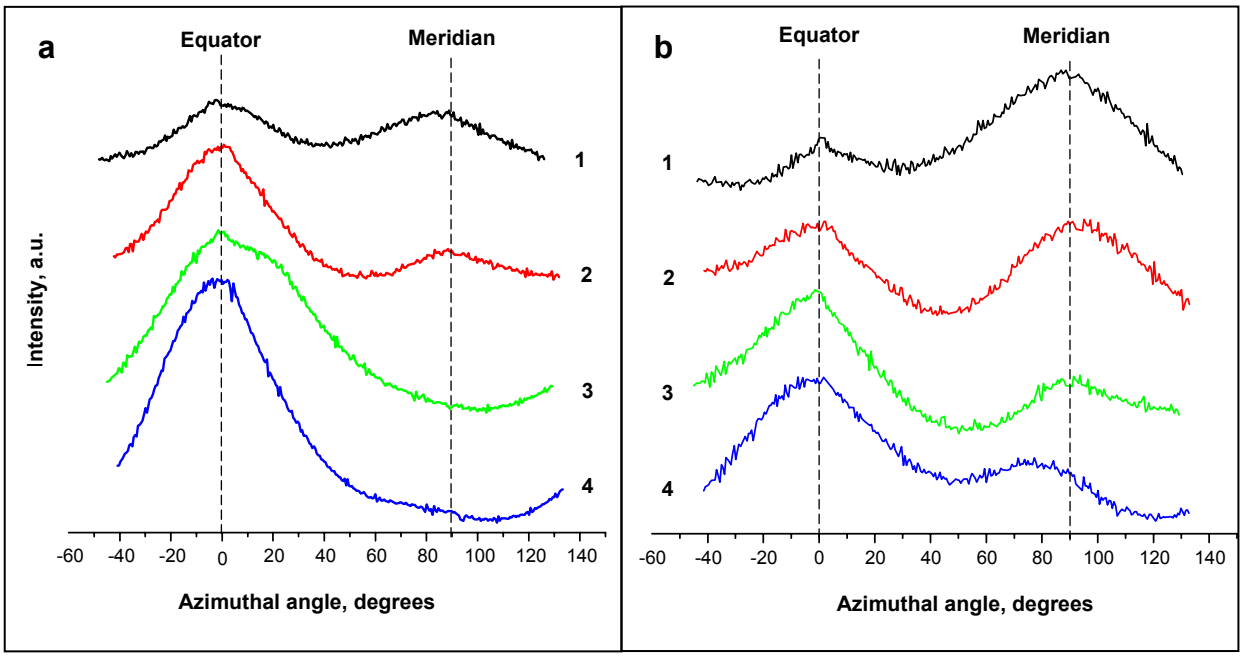

Figure 12.9 Azimuthal distribution of the scattered intensity in the 2D SAXS images of HDPE/PA12/YP MFCs obtained at: 30°C (a) and at 30°C after heating to 160°C (b). The compositions are as follows: 1 – 90/10/0; 2 – 80/20/0; 3 – 75/20/5; 4 – 70/20/10.

Figure 12.9 (a) clearly shows that the initial composites without compatibilizer (1 and 2), display both meridional and equatorial scattering, while those with compatibilizer (3 and 4) scatter in equatorial direction only. The result of the selective melting of the matrix at 160°C and its subsequent recrystallization (Fig. 12.9 (b)) is that all patterns show bimodal distribution of the scattered intensity. This means that two types of HDPE lamellae are formed: oriented along the fiber direction (equator) and oriented perpendicular to the fiber direction, *i.e.*, along the meridian of the SAXS pattern. Similar behaviour was observed with the PA6-reinforced composites without compatibilizer after matrix recrystallization in the beam (Figure 9.8 in Chapter 9). Figure 12.9 (b) shows that in the case of the PA12 reinforcement, reorientation of a fraction of the HDPE lamellae always occurs upon matrix recrystallization. Even the initial composites without YP display this effect (Figure 12.9 (a)). It should be noted that, as in the case of PA6-containing MFCs, this reorientation of the lamellae does not lead to chain direction reorientation in the crystallite, *i.e.*, the chain direction of PA12 and that of the oriented HDPE fraction continue to coincide. This is true for both compatibilized and non-compatibilized HDPE/PA12/YP samples as is well evidenced by the 3D WAXS images shown in Figure 12.10, displaying 80/20/0 (a) and a 70/20/10 (b) samples after matrix recrystallization. The isotropic part of the WAXS scattering was subtracted to reveal that the main crystalline planes of HDPE and PA12 are still along the equator, the images being identical to those of the initial composites (Figure 12.5).

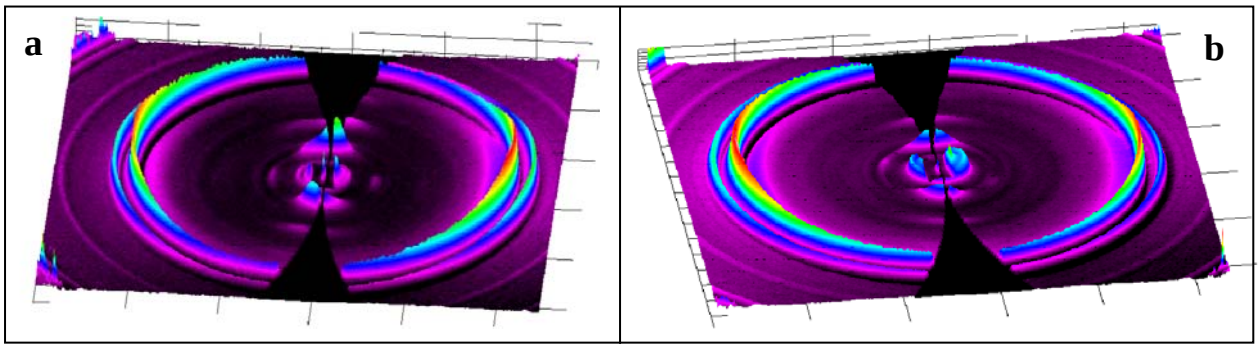

Figure 12.10 3D WAXS patterns (oriented scattering) at 30°C after heating to 160°C of: (a) - 80/20/0 MFC UDP; (b) – 70/20/10 MFC UDP. The isotropic component was subtracted. The fiber axis is vertical.

Furthermore, the SAXS patterns of the initial UDP MFCs were integrated in the range of $\boldsymbol{s}$ values between 0 and 0.15 nm^{-1}, $\boldsymbol{s}$ being the scattering vector, whose modulus is defined as $s = (s_{12}^2 + s_3^2)^{0.5} = (2/\lambda)\sin\theta$. The Bragg's long spacings L_B were calculated as the inverse value of s_{max} (Chapter 2, Eq. 2.1) and represent the sum of the average thicknesses of the crystalline lamellae and of the interlamellar amorphous regions. Figure 12.11 shows the 1D SAXS profiles of all HDPE/PA12/YP composites, whose maximums enabled the determination of the L_B values.

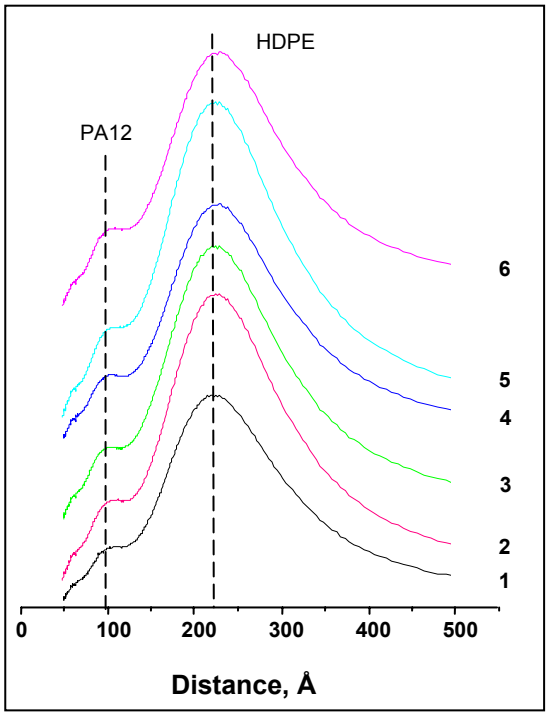

Figure 12.11 1D SAXS patterns of all HDPE/PA12/YP UDP MFCs at 30°C: 1 - 90/10/0; 2 – 80/20/0: 3 - 77.5/20/2.5; 4 - 75/20/5; 5 - 70/20/10 and 6 - 65/30/5.

In all curves there are two clear maximums, *i.e.*, two long spacings: one at about 100 Å attributed to the PA12 and other, larger (>200 Å) and more intense, belonging to the HDPE matrix. It can be noted that, irrespective of the amount of compatibilizer or PA12, the two L_B values remain basically unchanged.

This simple integration method can not reveal any possible differences in the long spacings of the oriented and isotropic HDPE fractions. To do that, the procedure of Somani et al [3] was applied as was done with the SAXS patterns of PA6-reinforced composites. Figure 12.12 (a) and (d) represent the initial SAXS patterns at 30°C of 80/20/0 and 70/20/10 composites, respectively. The computer generated 2D images of the isotropic intensity are presented in 12.12 (b) and (e). The resulting oriented scattering obtained for both samples after subtraction of the isotropic part from the total scattering is shown in the two right hand side images of the figure. This procedure clearly shows that if there is no compatibilizer (image (c)), two orientations of the HDPE lamellae exist: one coinciding with the horizontal fiber axis and other oriented in the perpendicular direction, along the meridian. In the presence of compatibilizer (image (f)), the oriented part of HDPE appears only on the equator, *i.e.* the HDPE lamellae crystallize only along the fiber direction.

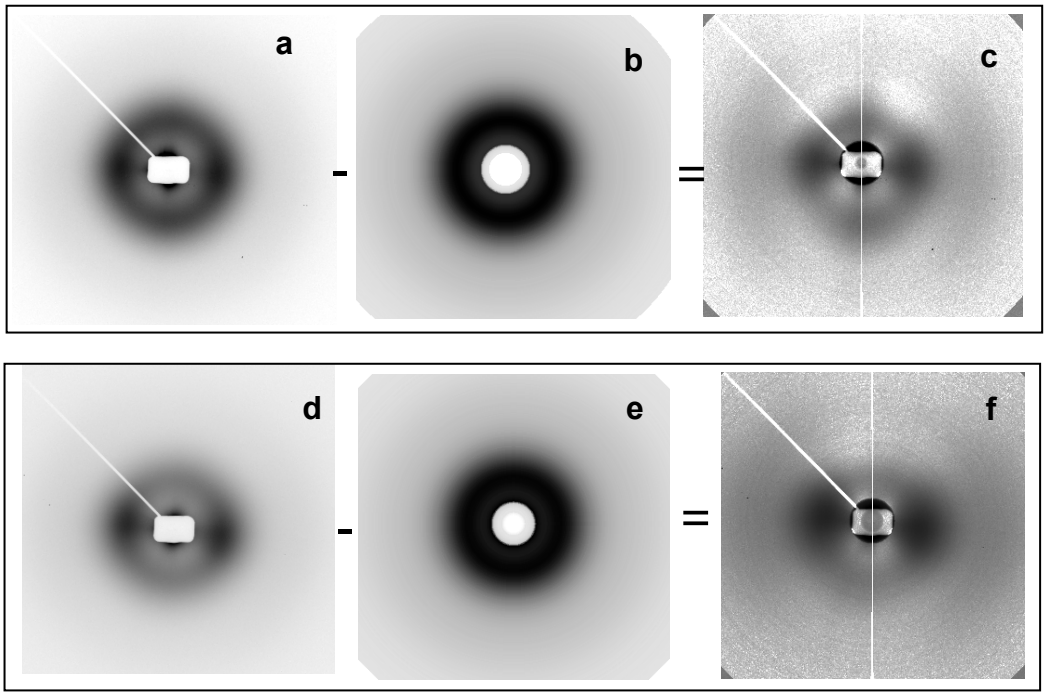

Figure 12.12 Deconvolution procedure with the SAXS pattern of the 80/20/0 UDP MFC (a-c) and 70/20/10 UDP MFC d-f): (a) and (d) – initial SAXS images; (b) and (e) – computer generated patterns of the isotropic scattering; (c) and (f) - intensity pattern of the oriented scatterers obtained by subtraction of the central images from the left ones. The fiber axis is horizontal.

Recrystallization of the matrix, by heating in the beam up to 160°C, and cooling down to 30°C was performed. Applying the same data processing revealed that all samples, even the compatibilized ones, contained meridional scattering similar to that in Figure 12.12 (c). The 3D images in Figure 12.13 display better the two types of oriented HDPE scattering – equatorial and meridional, the latter being indicated by horizontal white arrows. The meridional scattering clearly exists in both images (c) and (d) obtained after matrix recrystallization. The contribution of the PA12 phase along the equator is also seen (the vertical arrows).

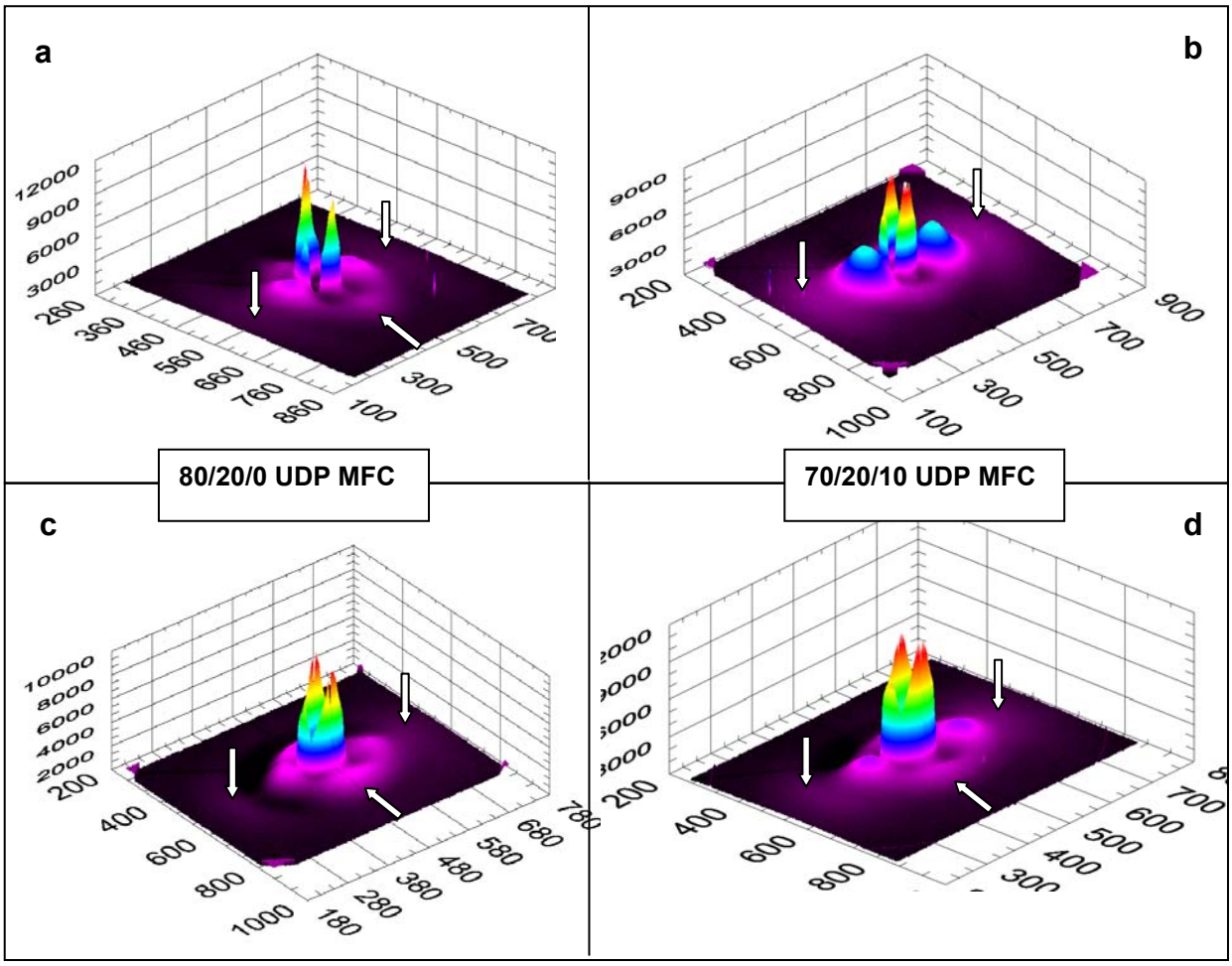

Figure 12.13 3D projections of the oriented SAXS scattering of two HDPE/PA12/YP composites. Initial composites at 30°C: (a) - 80/20/0 and (b) – 70/20/10. The same composites after selective matrix recrystallization (in beam heating) – images (c) and (d), respectively.

The isotropic part of the SAXS patterns was afterward integrated in the range of 0-180°. Two integrations were made of the oriented scattering – one along the equator and other along the meridian

so as to reveal possible differences in the long spacings values. The Bragg's long spacings L_B of the isotropic and oriented HDPE and PA12 scatterers were determined from the scattering intensities maxima. The data obtained are given in Table 12.6.

Table 12.6 Bragg's Long spacing values of HDPE/PA12/YP UDP MFC at 30°C and after matrix recrystallization (at 30°C after 160°C)

HDPE/PA12/YP MFC composition	**SAXS at 30°C**				**SAXS at 30° after 160°C**			
	Isotropic scattering	**Oriented scattering**			**Isotropic scattering**	**Oriented scattering**		
wt.%	L_B **HDPE** Å	L_B^{Eq} * **HDPE** Å	L_B^{Mer} * **HDPE** Å	L_B^{Eq} PA12 Å	L_B **HDPE** Å	L_B^{Eq} * **HDPE** Å	L_B^{Mer} * **HDPE** Å	L_B^{Eq} PA12 Å
90/10/0	220	229	251	91	229	235	251	108
80/20/0	216	235	256	101	218	253	268	112
77.5/20/2.5	215	220	-	100	218	248	255	120
75/20/5	213	229	-	97	244	242	244	118
70/20/10	208	233	-	96	225	215	229	124
65/30/5	218	229	-	99	218	250	265	118

Note: L_B^{Eq} * - long spacing of the HDPE lamellae oriented along the equator; L_B^{Mer} * - long spacing of the HDPE lamellae oriented along the meridian. The fibre direction (equator) is horizontal.

It can be seen that the oriented HDPE lamellae have bigger periodicities than the isotropic ones. It seems that the compatibilizer does not influence significantly the L_B values of either oriented or isotropic HDPE fractions. Changes toward increasing the periodicities occur upon matrix recrystallization. Generally, the HDPE lamellae along the meridian have bigger long spacings as compared to those of the HDPE crystallized along the fiber direction. As regards the PA12 L_B values, they are between 90 and 100 Å in the initial composites, which corresponds to the values of the neat oriented PA12. The increase of L_B of PA12 occurring after recrystallization of the matrix is similar to that observed with the neat PA12 subjected to the same temperature treatment (Chapter 5).

12.4 Structure of HDPE/PA12/YP MFCS – A Summary

The goal of this subsection is to summarize the structural data from the analysis of the HDPE/PA12/YP UDP MFC obtained by SEM, NMR, synchrotron WAXS and SAXS and to explain the mechanical properties of these materials.

As it was established by SEM, the reinforcing PA12 component maintains its orientation during the stage of selective matrix isotropization. The solid state NMR analysis revealed the presence of α-crystalline form which is not very typical of neat PA12. Furthermore, the synchrotron WAXS and SAXS disclosed that the HDPE lamellae of the matrix do not get completely random in either compatibilized or non-compatibilized MFCs but contains random and oriented fractions. The predominant fraction is of random lamellae. The minor fraction is of oriented HDPE material crystallized upon the PA12 fiber thus forming a trans-crystalline layer (TCL). Based on the WAXS data it was concluded that the HDPE lamellae in the TCL are oriented along the fibrils in such a way that the chain directions of the two materials coincide. When there is no compatibilizer meridional scattering in the SAXS pattern also appears, which is a proof of either the reorientation of some lamellae, or the presence of correlation between the lamellae in the direction perpendicular to the fiber axis. The last possibility is more probable because the long spacings determined in the meridian were bigger than those on the equator. Figure 12.14 gives an idealized model of HDPE/PA12/YP MFCs corresponding to the experimental data.

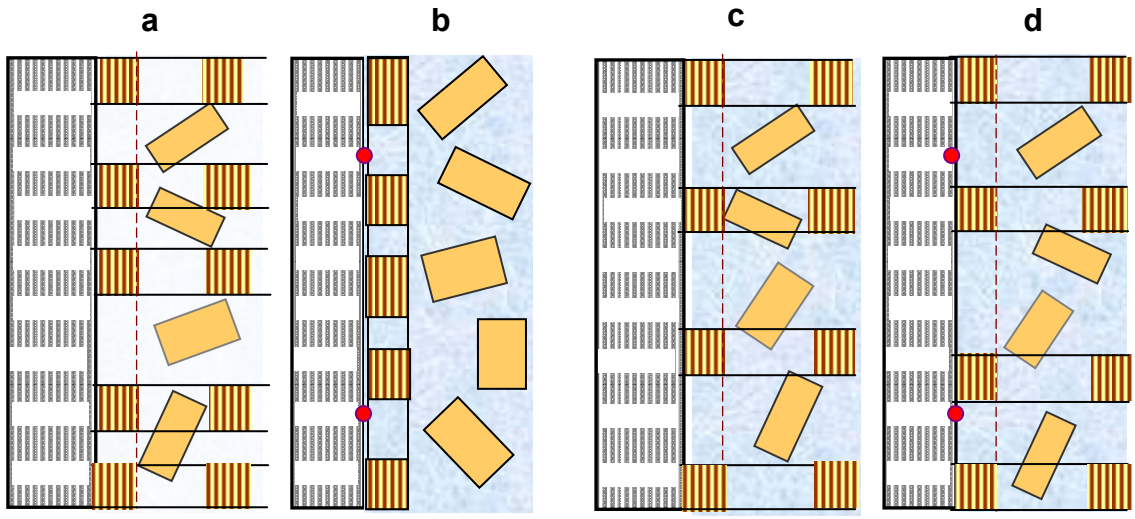

Figure 12.14 Structural models of non-compatibilized ((a) and (c)) and compatibilized ((b) and (d)) HDPE/PA12/YP UDP MFCs. (a) and (b) depict the structure of the as-prepared MFCs, (c) and (d) depicts the structure after the heating-cooling cycle in the absence of pressure. The red points represent the chemical bonds between the PA12 and Yparex. The vertical short solid lines indicate the chain direction in the lamellae. The dashed lines sketch out the maintenance of correlation of lamellae parallel and perpendicular to the PA12 fibers.

This model is similar to that shown in Chapter 9 depicting the PA6-reinforced MFCs, but there are some important differences: (i) the oriented part of HDPE is aligned along the PA12 fiber only in the compatibilized samples while in the non-compatibilized ones there exists correlation between the HDPE lamellae in both the fiber and in the perpendicular directions; (ii) during the matrix recrystallization, if no pressure is applied (*e.g.,* in the X-ray beam), even 10 % of compatibilizer are not enough to maintain the oriented HDPE part along the PA12 fiber. A possible explanation is the fact that PA12 has half of the concentration of amide groups as compared to PA6, *i.e.*, there are less possibilities of chemical bonds between YP and PA12; (iii) the thicknesses of the TCL containing the oriented HDPE part are quite different in the MFCs with PA6 and PA12 reinforcement. The next Figure 12.15 gives an idea of the fiber core/shell cross-section in PA6 and PA12 containing MFCs. To enable comparison, the models of two samples - without (80/20/0) and with compatibilizer (70/20/10) are presented in agreement with the SEM and WAXS data.

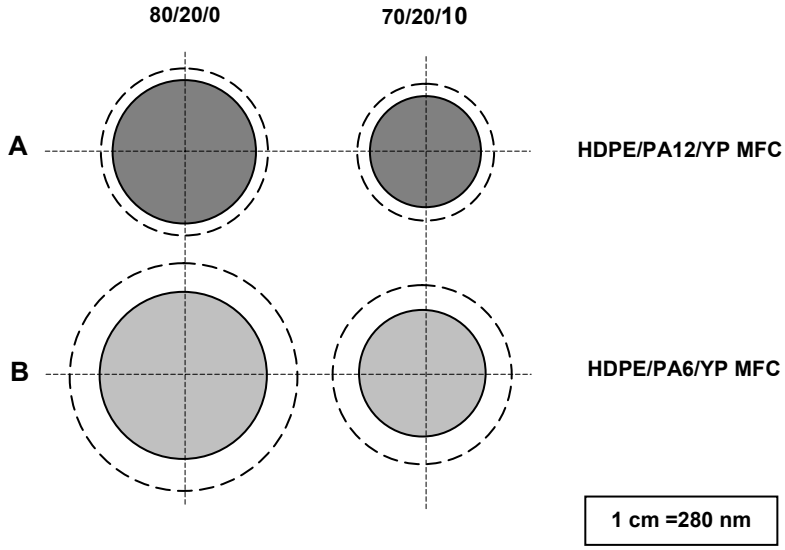

Figure 12.15 Idealized cross-section of the PA12 (A) and PA6 (B) reinforcing fibril in two HDPE/PA/YP MFCs: 80/20/0 and 70/20/10. The solid circles represent the polyamide fibers and the dashed circles – the trans-crystalline HDPE layer.

The models in Figs. 12.14 and 12.15 can be used to explain the differences in the mechanical properties of the PA6 and PA12-reinforced MFCs. As was confirmed by the tests of the neat materials, the oriented PA6 has superior tensile properties than the PA12. Consequently, it would be expected that the PA6-reinforced MFCs would be significantly better than the PA12 counterparts. However, as it was shown by the direct comparison of the tensile properties in Chapter 11.5, the Young's moduli of both composite types are close, in some cases the PA12 ones being even superior. As far as the

flexural properties are concerned, the improvement factors of the PA12 composites are clearly higher. A possible explanation of this behavior can be found in the structure and geometry of the transcrystalline layer in both composite types. As was depicted in Figure 12.15, the TCL is significantly thinner in the case of PA12 fiber – 50-60 nm as compared to 110-130 nm in the case of PA6-reinforcement. So far, there is still a dispute about the influence of TCL on the mechanical behavior of fiber composites [4]. In the case of the HDPE/polyamide MFCs the results evidence that a thicker TCL leads to a poorer reinforcement. With the PA12 composites, the addition of compatibilizer results in an insignificant increase of the TCL thickness while the real PA12 diameters decrease only slightly. This explains the small variation in the mechanical behavior of compatibilized and non-compatibilized PA12 samples. In the PA6 composites, as the YP content increases, the fibril diameters decrease although the TCL maintains almost the same thickness. This leads to a decrease in the real PA6 fiber diameter, and consequently to a drop in the tensile properties, particularly of the samples with the maximum amount of YP.

A deeper insight into the structure and morphology of the TCL in the HDPE/PA/YP composites will require new X-ray setups, testing techniques and software for data handling, *e.g.*, the newly developed scanning microbeam X-ray scattering tomography [5]. Such techniques will be very useful to provide a scientific basis for the best selection of matrix and reinforcing materials, as well as the temperature conditions for the matrix isotropization.

12.5. References:

1. Software developed by Stonybrook Technology and Applied Research Inc. NY, USA.
2. Nogales A, Hsiao BS, Somani RH, Srinivas S, Tsou AH, Balta-Calleja FJ, Ezquerra TA, *Polymer* 42 :5247 (2001).
3. Somani RH, Hsiao BS, Nogales A, Srinivas S, Tsou AH, Sics I, Baltá-Calleja FJ, Ezquerra, TA, *Macromolecules*, 33:9385 (2000).
4. Quan H, Li Z-M, Yang M-B, Huang R, *Comp Sci Technol* 65:999 (2005).
5. Stribeck N, Nöchel U, Almendárez-Camarillo, A, Macromol.Chem.Phys.2008 (in press).

CONCLUSIONS

Microfibrilar composites (MFC) based on HDPE as a matrix, PA6 or PA12 as reinforcing phases and maleic anhydride grafted polyethylene as a compatibilizer (YP), were produced. The composites' precursors were obtained by extrusion blending of the components followed by drawing of the blend to induce fibrillation of both phases. The MFC were obtained by hot plate compression molding at a temperature below the melting point of PA, thus maintaining its fibrilar morphology. The MFCs were studied to investigate the influence of the blend composition, length and alignment of the reinforcement, and processing conditions on the structure and mechanical behavior. The polyamide concentration was varied between 10 and 30 wt % and the compatibilizer in the range of 0-10 wt %. Composites with various geometry and alignment of the polyamide phase were obtained from each blend composition – unidirectional laminae (UDP), cross-ply laminates (CPC), composites with middle-length, randomly-oriented bristles (MRB) and composites with non-oriented polyamide phase (NOM).

To obtain MFCs with good mechanical properties, it was of prime importance that the polyamide reinforcements could be with best mechanical performance. For this reason, it was necessary to know the polymorphic transitions in PA6 and PA12 and their influence upon the mechanical properties. This information was used further for optimization of the conditions of the MFC preparation. All composites obtained in this work were mechanically tested and subjected to structural investigations by various methods including SEM, solid-state ^{13}C NMR, synchrotron WAXS and SAXS.

The following conclusions may be derived from this research program:

Preparation of PA6 and PA12-reinforced MFCs

- HDPE/PA6/YP or HDPE/PA12/YP oriented precursors were obtained by melt-blending and extrusion at 250 and 210°C respectively, followed by cold drawing at 95°C to draw ratios of *ca*. 16.
- Microfibrilar composites from HDPE/PA6/YP and HDPE/PA12/YP oriented precursors with various alignments were obtained by compression molding at 160°C and a pressure of 20 bar.
- Composites with non-oriented polyamide phase were prepared at the same conditions and used as control samples in all tests.

Structure and properties of PA6

- The structure of isotropic and oriented PA6 in the 30–240°C range, *i.e.* modeling the temperature conditions of the MFC preparation, was studied. It was established that in both isotropic and oriented PA6 samples there is a co-existence of α and γ crystalline forms. Close to 200°C, the α-polymorph was predominant. Annealing of oriented PA6 always causes γ- to α-form transition.
- The tensile modulus and the yield stress of both PA6 films and cables increased with the annealing temperature. This behavior was explained, on a crystallographic level, by a decrease in the d-spacing of the main crystal slip planes of the two polymorphs after annealing.
- The external stress applied led to additional γ-to-α form transitions in both the isotropic and oriented PA6 samples, whereby the higher the annealing temperature, the weaker the inclination to stress-induced transitions. This effect was attributed to a possible formation of a rigid fraction (isotropic PA6) or oriented fraction (oriented PA6) in the amorphous phase.

Structure and properties of PA12

- The PA12 presented a hexagonal crystalline lattice at room temperature, ascribed as γ-form or γ'-form modifications, depending on the polymer being isotropic or oriented, respectively. When heated, the two polymorphs showed different behaviors. Above 140°C the isotropic γ form partially transformed into α form. No such transition was observed with the oriented γ' phase, even after annealing at temperatures close to melting. Only after isotropization by melting, the oriented γ' form transformed into γ form.
- The Young's modulus and the yield stress increased with the annealing temperature, while the elongation at break decreased. This behavior was explained by a temperature induced γ-to-α form transition and by the decrease of the inter-sheet distances leading to denser macromolecule packing in the crystalline domains.
- Similarly to what was observed with PA6, additional stress-induced γ-to-α form transition occurred when external stress was applied. The structural data led to the supposition of formation of a rigid amorphous phase in the annealed samples.
- Deformation models were suggested for explaining the experimental results.

Structure and properties of HDPE/PA6/YP microfibrilar composites

- The microfibrilar structure of the PA6 phase in the MFCs was confirmed by SEM, WAXS and SAXS analyses. The diameter and the length of the fibrils decrease with the presence of compatibilizer in the blend. In the samples without compatibilizer, the average length is 120 μm and the diameter vary between 0.6 and 1.5 μm whereas in the compatibilized ones the length is *ca.* 40 μm and the diameter ranges from 0.5 to 1.0 μm.
- The solid state ^{13}C NMR and 2D WAXS methods revealed the co-existence of the two PA6 polymorphs (γ and α) in the fibrils. The γ/α ratio is influenced by the composition, being 1/2.5 for the non-compatibilized MFC and 1/1 for that with the highest Yparex compatibilizer concentration.
- The X-ray analysis revealed the presence of a transcrystalline layer of HDPE that crystallized upon the oriented PA6. This suggests a shell-core structure of the reinforcing fibrils. The lamellae of the transcrystalline layer are aligned epitaxially along the PA6 fibers in such a way that the chain directions of the two polymers coincide.
- Combining the data from WAXS and SEM analyses, the thickness of the HDPE transcrystalline layer was determined to be in the 110-130nm range. On this basis, the real aspect ratio of the PA6 fiber was found to be *ca.* 160 for the non-compatibilized samples and *ca.* 80 for the compatibilized samples.
- Crystallographic and lamellar characteristics, such as d-spacing and Bragg's long spacing for both PA6 and HDPE phases were determined. Idealized models of the structure of HDPE/PA6/YP MFCs were suggested.
- All HDPE/PA6/YP MFCs with uniaxially aligned PA6 reinforcing fibrils, compression molded as single laminae (UDP), showed better longitudinal tensile characteristics than the HDPE, the improvement being up to 33% for the Young's modulus and up to 120% for the tensile strength. The composites with the biggest concentration of compatibilizer showed the smallest enhancement of the tensile properties.
- The tensile properties of the UDP composites in the transversal direction were, at the best, similar to the HDPE matrix.
- The rule of mixtures can be used to predict the tensile behavior of HDPE/PA6/YP UDPs. The compositions without compatibilizer displayed positive deviations from the predicted values, *ca.* 10% for the Young's and up to 50% for the tensile strength. These deviations may have resulted

from the fact that the fibrils in the composites are much smaller and certainly stiffer than the PA6 oriented cable whose data were used for the predictions.

Structure and properties of HDPE/PA12/YP composites

- The fibrilar morphology of the PA12 reinforcements in the MFCs was proved by SEM and synchrotron X-ray methods. The better intrinsic compatibility of HDPE and PA12 caused a reduction of the length and diameter of the fibrils in the PA12 composites. Thus, the fibrils diameter varied between 500-800 nm and the length – between 20 and 80 μm being influenced by the YP content only slightly.
- Along with the usual for PA12 γ-polymorph, considerable amounts of the α-polymorph were detected in the reinforcing fibrils by solid state ^{13}C NMR and 2D WAXS methods. The γ/α form ratio was dependent on the compatibilizer concentration, being 1.5/1 in the non-compatibilized MFCs and 1/1.6 for that with the highest Yparex compatibilizer concentration.
- The presence of HDPE transcrystalline layer was proved at the fiber-matrix interface with the lamellae being aligned epitaxially along the PA12 fibers. When there was no compatibilizer, some HDPE lamellae perpendicular to the fiber axis were also observed. In all cases the chain directions of the oriented HDPE and PA12 coincided. Idealized models for the structure of the PA12-reinforced composites were proposed.
- Based on data from WAXS and SEM analyses, the thickness of the HDPE transcrystalline layer was calculated. It varied between 50 and 80 nm, depending on the PA12 content. The real aspect ratio of the PA12 fiber was found to be *ca.* 110 for the non-compatibilized samples and between 30 and 90 for the compatibilized ones.
- The improvement of the Young's modulus in the HDPE/PA12/YP UDP MFCs was in the range of 10-30 %, while the tensile strength grew up to 150% in respect to the HDPE matrix.
- The tensile properties of the UDP composites perpendicularly to the fiber direction were close to or even higher than HDPE.
- The composites with random distribution of the PA12 reinforcement showed statistically higher moduli in respect to HDPE in both longitudinal and transverse directions.

- The rule of mixtures was valid for all compositions. However, in the composites without compatibilizer the measured values were higher than the predicted: up to 10% for the Young's modulus and about 70% for the tensile strength.
- The better mechanical performance of the PA12 reinforced composites as compared to the PA6 may be related to the differences in the structure and geometry of the transcrystalline layer in the composites. It appears that the presence of the transcrystalline layer generally leads to the deterioration of the mechanical properties. Thus, the thicker this layer is, the poorer is the reinforcement.

Engineering applications of microfibrilar composites

- Cross-ply laminates (CPC) were obtained by compression molding using the HDPE/PA/YP oriented precursors developed in this work. These laminates can resist transversal loading and impacts.
- All microfibrilar laminates (CPC and MRB) showed better flexural behavior than the HDPE. The maximum improvement was 85% for the PA6 and 180% for the PA12, being the highest in the CPC laminates.
- The best flexural stiffness was achieved in the absence of or at low concentration of the compatibilizer. The PA6 compositions with the best flexural behavior were 80/20/0, 77.5/20/2.5 and 75/20/5 with improvement factors between 80 and 75%, respectively. The best PA12 compositions were: 65/30/5 (183%), 75/20/5 and 70/20/10 with 130% improvement factor.
- The PA12 fiber reinforcement led to impact properties better than of the HDPE matrix. The maximum improvement of the peak and of the total energy (70% and 135%, respectively) was obtained for the CPC laminates with the 70/20/10 composition.
- The reinforcement with PA6 fibers led only to an improvement of the total energy, being the highest for the 80/20/0 composition (180%). The peak energy, however, was generally similar to that of the HDPE matrix.
- Plates with isotropic PA phase (NOM) had better flexural stiffness than the HDPE. Under impact, however, the toughness of these composites showed a total energy comparable or lower than the matrix. This clearly shows the importance of the microfibrilar morphology of the PA reinforcement.

RECOMMENDATIONS FOR FUTURE WORK

Nowadays polymer composites are important commercial materials with a wide range of applications in many industries where highly resistant, lightweight materials are of prime importance. In recent years, however, optimizing the properties of traditional polymer composites containing micrometer-scale reinforcing entities has reached its limits. The nanostructured polymers composites, to which the MFCs also belong, open a large window of opportunities to overcome the inherent limitations of the conventional polymer composite materials. The results of this thesis confirm the concept that changing the size, shape, volume fraction, interface, and degree of dispersion or aggregation of the reinforcements is a way to understand, tailor, and optimize the composites' mechanical properties.

Additional reinforcing effect in the MFC systems can be achieved if layered, fibrilar or particulate nanosized inorganic fillers are introduced into either the reinforcing fibrils or in the matrix of NFC and dispersed to nanometre-scale entities. This can be one of the future lines of investigation in this area employing nanotubes, montmorillonite, *in-situ* produced nanoparticles of silica, TiO_2 *etc*. Different types of compatibilizers can be used in such hybrid (*i.e.*, organic-inorganic) materials. The hyperbranched or dendritic polymers possess a high content of functional groups, which could be modified arbitrarily in order to obtain additional effects on the physical properties or to change the reactivity for further chemical reactions. Due to their unique structure, dendritic polymers can entrap organic or inorganic phases thus serving as perfect compatibilizers. It is believed that the additional reinforcement by hyperbranched polymers entrapping nanosized inorganic fillers could make the MFCs even more versatile and capable of replacing metal parts, *i.e.*, in automotive and aerospace industries, where presently this is still impossible.

Very recently, a new trend toward *in-situ* polymer-polymer composites is observed, namely the molecular dispersion of one polymer in another. The synthetic principle is simple – the reinforcing polymer is dissolved in the monomer of the matrix and than the latter is polymerized by means of adequate initiators. In general, i*n-situ* polymerization seems to have a bright future as far as new polymer nanocomposites are concerned.

This thesis demonstrated also that synchrotron WAXS and SAXS studies can be very useful in studying the relation between the structure and the mechanical properties of the polymer composites. The

standard testing methods and software used for SAXS and WAXS data handling, however, show some limitations. In most of the instances, the WAXS and SAXS patterns are processed and interpreted, reflection by reflection, so as to extract indirectly the structural information. The latter can often be distorted or even damaged due to various reasons related either to the data collection or to the data treatment. The progress in the X-ray experiments during the last years has been tremendous and included development of new two-dimensional X-ray detectors, the use of high power X-ray microbeams, and the application of novel processing methodologies allowing for a direct transformation of the WAXS and SAXS 2D patterns into an image of the nanostructure. This is, in fact, microscopy at nano-level (nanoscopy) that provides structural information absolutely unavailable in other ways. With the advent of the nanotechnologies requiring a strict and rigorous control over the structures on the nanometer scale, nanoscopy becomes of crucial importance. The latest invention is a fast tomographic imaging method based on SAXS data from a scanning-microbeam experiment. By means of this method real time X-ray experiments using mechanical testers for slow or fast load-cycling test can be incorporated into the synchrotron beamline. In such a way fatigue and failure can be studied in MFC within reasonable intervals of time and the data related to microstructure variation inside the material.

These are only a few of the possible directions of the future work in the exciting and rapidly developing research area of the MFC nanocomposites.

"The exit is usually where the entrance was"
Stanisław Jerzy Lec